UNIVERSITY OF BELGRADE

FACYLTY OF TECHNOLOGY AND METALLURGY

Somaya Ahmed Ben Hassan

STRUCTURE AND THE PHYSICAL AND MECHANICAL PROPERTIES OF DENTAL HYBRID COMPOSITE MATERIALS

Doctoral Dissertation

Belgrade, 2014

UNIVERZITET U BEOGRADU

TEHNOLOŠKO-METALURŠKI FAKULTET

Somaya Ahmed Ben Hassan

STRUKTURA I FIZIČKO-MEHANIČKA SVOJSTVA STOMATOLOŠKIH HIBRIDNIH KOMPOZITNIH MATERIJALA

Doktorska Disertacija

Beograd, 2014

Supervisor

Dr Radoslav Aleksić, full professor, University of Belgrade, Faculty of Technology and Metallurgy

Member of Committee

Dr Petar Uskoković, full professor, University of Belgrade, Faculty of Technology and Metallurgy

Dr Vesna Radojević, associate professor, University of Belgrade, Faculty of Technology and Metallurgy

Dr Radmila Jancić-Hajnemann, associate professor, University of Belgrade, Faculty of Technology and Metallurgy

Dr Kosovka Obradović Đuričić, full professor, University of Belgrade, Faculty of Dentistry

Date:_____

ACKNOWLEDGEMENTS

It is a great pleasure for me to express my sincere gratitude to the people whose generous assistance and support this research.

First and foremost, I would like to express my sincere thanks and appreciation to my project supervisor Dr Radoslav Aleksic, for his patient guidance. His intellectual insight, work discipline and personal strengths have had a positive influence on my research life, for which I am grateful.

I would like to acknowledge Dr Petar Uskokovic, Dr Vesna Radojevic, Dr Radmila Jancic-Hajnemann and Dr Kosovka Obradovic Đuricic my thesis examiners for their insightful suggestions and comments on my thesis.

Special thanks to Dr Dusica Stojanovic for her encouragements in my research life and technical support in experiments.

STRUKTURA I FIZIČKO-MEHANIČKA SVOJSTVA STOMATOLOŠKIH HIBRIDNIH KOMPOZITNIH MATERIJALA

Rezime

Kompoziti sa dodatkom nanočestica pokazuju poboljšanje mehaničkih svojstava. PMMA polimer korišćen je kao matrica u kombinaciji sa dva različita ojačanja, koja imaju izrazito različite oblike, kada su dodati u kompozit. Ojačanja napravljena od aluminijum oksidnih čestica imaju sferičan oblik a viskersi imaju odnos dužina prema prečniku od 200. Uticaj veličine čestica, njihov oblik i udeo, na mehanička svojstva proučavani su pomoću nanoindentacionih merenja i dinamičko-mehaničke analize. Utvrdjeno je da i ćestice i viskersi poboljšavaju mehanićka svojstva, ali poboljšanje je mnogo više izraženo u slučaju viskersa. Koncentracija ojačavajućih čestica varira do 5 mas. %. Najbolja svojstva dobijena su sa dodatkom 3 mas. % viskersa u pogledu mehaničkih svojstava dobijenog kompozita.

U disertaciji su prikazani rezultati istraživanja uticaja procesnih parametara elektropredenja na uniformnost, morfologiju i sastav nanokompozitnih vlakana u obliku mata (PVB/Sep). Suspenzija sepiolita ima tiksotropna svojstva zbog svoje vlaknaste prirode, velike specifićne površine i prisustva silanolnih grupa na površini. Funkcionalizacija sepiolitnih vlakana uradjena je u vodenom tiksotropnom gel stanju korišćenjem silana kao vezivnog agensa. Ispitano je ponašanje pri elektropredenju suspenzije tri različite koncentracije sepiolita (3 mas. %, 30 mas. % i 59 mas. %) u rastvoru PVB u etanolu sa i bez modifikacije silanima vlakana sepiolita. Utvrdjeno je da pod istim uslovima kompozitna vlakna PVB/Sep imaju nižu vrednost srednjeg prečnika vlakana nego čista PVB vlakna. Optimalni uslovi dobijanja najravnomernijih nanokompozitnih vlakana se postižu pri protoku suspenzije od 0,5 mL/h, rastojanju dizne od kolektora 15 cm i naponu od 24 kV.

Ključne reči: polimerni kompoziti, oblik čestica, nanoindentacija, dinamičko – mehanička analiza

Naučna oblast: Hemija i hemijska tehnologija

Uža naućna oblast: Nauka o materijalima i inženjerstvo materijala

UDK: 66.014

STRUCTURE AND THE PHYSICAL AND MECHANICAL PROPERTIES OF DENTAL HYBRID COMPOSITE MATERIALS

ABSTRACT

Composites with the addition of alumina nanofillers show improvement in mechanical properties. The PMMA polymer was used as a matrix and two different types of nanofillers, added as reinforcement in the matrix, having extremely different shapes were added to form the composite. Reinforcements were made of alumina spherical nanoparticles having spherical shape and whiskers having the length to diameter ratio of 200. The influence of alumina fillers size, shape and fillers loading on mechanical properties of obtained composite were studied using the nanoindentation measurements and dynamic mechanical analysis. It was observed that both alumina whiskers and alumina spherical nanoparticles added in the PMMA matrix improved the mechanical properties of obtained composite samples but the improvement was significantly higher with alumina whisker reinforcement. The concentration of the reinforcing alumina spherical nanoparticles and alumina whiskers in PMMA matrix varied up to 5 wt. %. The best performance was obtained by the addition of 3 wt. % of alumina whiskers in the PMMA matrix with regard to mechanical properties of the obtained composite.

This study presents investigation of processing conditions on the uniformity, morphology and structure of patterned nanofibrous mats for poly (vinyl butyral)/sepiolite (PVB/Sep) nanocomposite fibers obtained by electrospinning process. Sepiolite aqueous suspensions show a thixotropic behavior because of their fibrous structure, porosity, large specific surface area and the presence of silanol groups on the surface. Functionalization of the sepiolite fibers in aqueous thixotropic gel was made on the surface of individual fibers using amino silanes as coupling agents. Different contents (3 wt. %, 30 wt. % and 50 wt. %) of neat and modified sepiolite fibers were dispersed by ultrasonic irradiation in the solution of PVB in ethanol and were used to obtain nanocomposite fibers by electrospinning. The PVB/Sep nanocomposite fibers showed lower mean fiber diameter than of the neat PVB fibers. Uniform nanofibers

were obtained using the lower flow rate (0.5 mL/h), high collector distance (15 cm) and a constant applied voltage of 24 kV.

Keywords: polymer composite, particle shape, nanoindentation, dynamic mechanical analysis,

Academic Expertise: Chemistry and Chemical Technology

Field of Academic Expertise: Materials Science and Engineering

UDK: 66.014

TABLE OF CONTENTS

1. INTRODUCTION

A composite material is a product which consists of at least two distinct phases normally formed by blending together components having different structures and properties. The purpose of this is to produce a material with properties which could not be achieved from any of the individual components alone. Resin-based filled composites are very complex mixtures containing many substances. These are usually classified into the following groups:

- Filler particles
- Matrix resins and corresponding catalyst systems
- Coupling agents between fillers and matrix resins, (Figure 1.1)

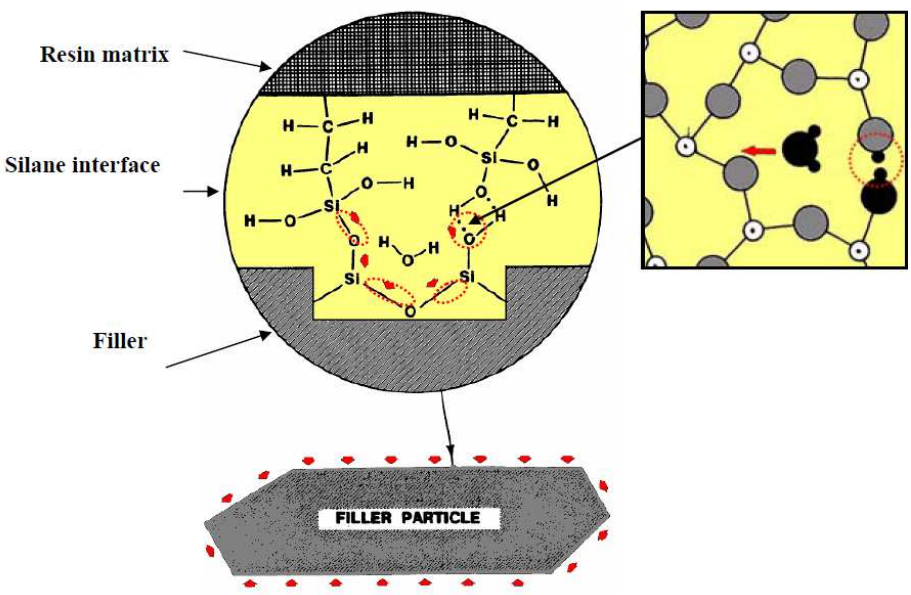

Figure 1.1 Diagram representing filler particles within the resin matrix[1].

Resin-based composites possess good esthetic properties, and are currently among the most popular dental restorative materials. They have increasingly replaced conventional dental amalgams containing mercury, a controversial component. However resin-based composites are inferior to mercury amalgams in several mechanical aspects: wear resistance, hardness, and shrinkage behavior. Hence, their application is still restricted to some extent. In order to improve the properties of resin-

based composites, previous studies have focused on the pretreatment of inorganic fillers and resin monomers and the development of curing methods. Heat-curing and post-curing heat treatments both increase the degree of polymerization, improving the composite strength to some extent. Microparticles and fibers can also be used to reinforce dental resin-based composites. It has been shown that adding a small amount of short or networked fiber-like fillers to the composite results in a modest increase in strength.

Although the composite materials based on PMMA have become vital for dental restorations due to their superior aesthetic quality, they experience a considerable mechanical challenge during function. Thus, improving the mechanical properties is one of the most important research tasks in this field. In recent years, the use of reinforcing inorganic fillers in various forms has been a major approach towards the development of improved dental composites. In general, the size, shape, amount, and hardness of the filler material, the nature and quality of the bond between the filler and the polymer matrix, and the distribution of filler particles in the polymer matrix - all have an influence on the wear and mechanical properties of the composite resins. Perhaps one of the most noticeable advances in composite filler technology has been the incorporation of fillers in the nanometer scale. One potential advantage of nanoparticles is the improvement in the optical properties of the epoxy resin composite because their diameter is a fraction of the wavelength of visible light resulting in the inability of the human eye to detect the particles. In addition, the high surface area associated with nanoparticles provides more interfacial interactions and improved properties in the composite samples. The positive effect of nano-sized silica and silicate-based fillers on flexural strength, surface hardness, fracture toughness, and optical properties has already been reported in the literature [2,3,4,5]. In view of the importance of the size of the fillers, the main purpose of this study was to determine the effect of nano-sized Al_2O_3 particles as reinforcing filler, on the mechanical properties of dental composite samples. Nano and micrometer size whiskers containing dental restorative samples have been compared. The use of nano-sized Al_2O_3 filler particles proved to be quite effective in improving the mechanical properties. One other advantage of nano-size reinforcing agents compared to micro-sized particles was certainly the possibility of using lower loading contents. The improved mechanical property exhibited by nanoparticle

reinforced composites is most likely due to better filler/polymer interaction. A more efficient nanoparticle dispersion combined with higher loadings may lead to even more improved composite dental restorative materials. Further investigations are needed to improve the interaction between the nano-sized fillers and the matrix phase and also to increase the loading capacity of nano filler particles into the polymer matrix.

As a candidate inorganic filler, natural sepiolite has many excellent properties: it is nontoxic while chemically stable, and exhibits a highly efficient effect. Up to the available literature, the natural sepiolite nanofibers were not reported as fillers in dental composites. In this study, natural sepiolite nanoparticles were coated with an organosilane and blended into dental resin-based composites. The general nature of the surface modification is showed. The purpose of this treatment is to help the particles form a homogeneous surface along with the PVB matrix. The mechanical properties of specimens containing the modified natural sepiolite nanoparticles were tested.

Recently, indentation tests are becoming most commonly applied means of testing the mechanical properties. Nanoindentation usage for dental hard tissue studies began in 1992; since then several studies have been published using this technique. The instrumented nanoindentation systems enable the measurement of the mechanical properties, hardness and elastic modulus, on the surface of dental materials. The nanoindentation technique is a much simpler procedure compared with other micro and macroscale mechanical tests such as compressive, tensile, bending, and punch shear tests, particularly on small complex-shaped samples such as enamel and dentine. Nanoindentation tests are relatively nondestructive, and the specimen preparation is less time consuming than regular tests. Of particular importance, it allows probing the mechanical properties of a very small concise selected region of the specimen, the dimension of which may arrange between several nano - to micrometers, which is of crucial importance for measuring the local properties of non homogenous structures such as dental calcified tissues. The objective of this study is to investigate the mechanical properties and wear resistance of the different natural dental materials and dental filling materials using the nanoindentation and nanoscratch techniques, and dynamic mechanical analysis, respectively.

2. DENTAL COMPOSITE FORMULATION

The composition of resin-based dental composites has evolved significantly since the materials were first introduced to dentistry more than 50 years ago, (Figure 2.1). Until recently, the most important changes have involved the reinforcing filler, which has been purposely reduced in size to produce materials that are more easily and effectively polished and which demonstrated greater wear resistance. The latter was especially necessary for materials used in posterior applications, but the former has been important for restorations in all areas of the mouth.

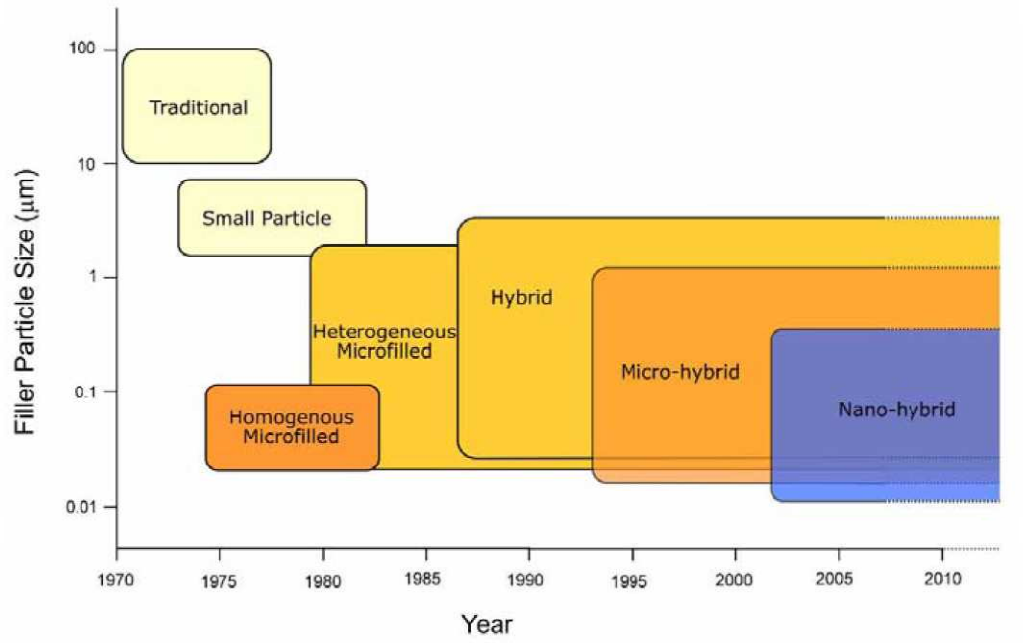

Figure 2.1 A perspective on the evolution of dental composites[6]

Current changes are more focused on the polymeric matrix of the material, principally to develop systems with reduced polymerization shrinkage, and perhaps more importantly, reduced polymerization shrinkage stress, and to make them self adhesive to tooth structure. Several articles recently have reviewed the current technology of dental composites[7,8] and described future developments, such as self-repairing and stimuli-responsive materials[9]. The current review will provide a brief historical perspective on dental resin composites to serve as a framework for a treatise

on the current state of the art, primarily concentrating on work published in the past 5 years. Resin composites are used for a variety of applications in dentistry, including but not limited to restorative materials, cavity liners, pit and fissure sealants, cores and buildups, inlays, on lays, crowns, provisional restorations, cements for single or multiple tooth prostheses and orthodontic devices, endodontic sealers, and root canal posts. It is likely that the use of these materials will continue to grow both in frequency and application due to their versatility. The rapidity by which the materials have evolved suggests a constantly changing state of the art.

Dental composites can be distinguished by differences in formulation tailored to their particular requirements as restoratives, sealants, cements, provisional materials, etc. These materials are similar in that they are all composed of a polymeric matrix, typically a dimethacrylate, reinforcing fillers, typically made from radiopaque glass, a silane coupling agent for binding the filler to the matrix, and chemicals that promote or modulate the polymerization reaction. The many types of fillers in use recently have been reviewed.

The predominant base monomer used in commercial dental composites has been bis-GMA, which due to its high viscosity is mixed with other dimethacrylates, such as TEGDMA, UDMA or other monomers[10]. Some of these monomers, or modified versions of them, also serve as base monomers in many commercial materials. While there have been attempts to develop different polymerization promoting systems, most composites are light-activated, either as the sole polymerization initiator or in a dual cure formulation containing a chemically cured component. The most common photoinitiator system is camphoroquinone, accelerated by a tertiary amine, typically an aromatic one[11]. Some commercial formulations have included other photoinitiators, such as PPD (1-phenyl-1,2-propanedione)[12], Lucirin TPO (monoacylphosphine oxide), and Irgacure 819 (bisacylphosphine oxide)[13], which are less yellow than CQ and thus potentially more color stable. Additional photoinitiators, such as OPPI (p-octyloxyphenyl-phenyl iodonium hexafluoroantimonate) have been proposed based on encouraging experimental results[14].

The different types of composite materials are distinguished by their consistency. The universal restorative capable of being placed with a syringe or instrument may have a variety of consistencies depending upon its formulation. These

materials are distinguished from the flowable composites, designed to be dispensed from very fine bore syringes into tight spaces for enhanced adaptation, and from the packable composites, designed to provide significant resistance to an amalgam condenser or other instrument in order to avoid slumping and to enhance the formation of tight interproximal contacts. Flowable composites are typically produced with a lower viscosity by reducing the filler content of the mixture, or by adding other modifying agents, such as surfactants, which enhance the fluidity while avoiding a large reduction in filler content that would significantly reduce mechanical properties and increase shrinkage[15]. Packable composites achieve their thicker consistency through modification of the filler size distributions or through the addition of other types of particles, such as fibers, but generally not by increasing overall filler level[16].

Within each type of composite, the materials are further distinguished by the characteristics of their reinforcing fillers, and in particular their size (Figure 2.2).

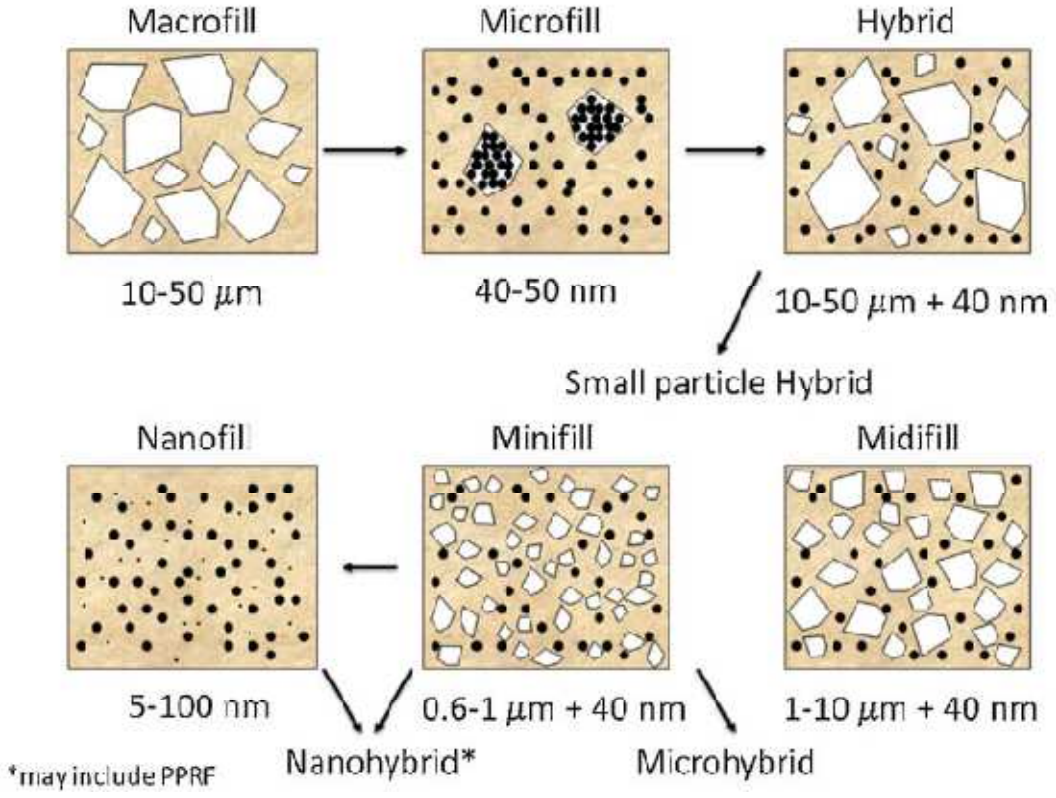

Figure 2.2 The chronological development of the state of the art of dental composite formulations based on filler particle modifications[17].

Conventional dental composites had average particle sizes that far exceeded 1μm, and typically had fillers close to or exceeding the diameter of a human hair (~50 μm). These "macrofill" materials were very strong, but difficult to polish and impossible to retain surface smoothness. To address the important issue of long-term esthetics, manufacturers began to formulate "microfill" composites, admittedly inappropriately named at the time, but probably done to emphasize the fact that the particles were "microscopic". In truth, these materials were truly nanocomposites, as the average size of the amorphous spherical silica reinforcing particles was approximately 40 nm. The field of nanotechnology is defined at the nanoscale, and includes the 1–100 nm size range. Thus, the original "microfills" would have more accurately been called "nanofills", but likely were not due to the lack of recognition of the concept of "nano" at the time. The filler level in these materials was low, but could be increased by incorporating highly filled, pre-polymerized resin fillers (PPRF) within the matrix to which additional "microfill" particles were added.

The "microfill composites were polishable but generally weak due to their relatively low filler content, and a compromise was needed to produce adequate strength with enhanced polishability and esthetics. Therefore, the particle size of the conventional composites was reduced through further grinding to produce what was ultimately called "small particle hybrid" composites. These were further distinguished as "midifills," with average particle sizes slightly greater than 1 μm but also containing a portion of the 40 nm-sized fumed silica "microfillers." Further refinements in the particle size through enhanced milling and grinding techniques resulted in composites with particles that were sub-micron, typically averaging about 0.4–1.0 μm, which initially were called "minifills"[18] and ultimately came to be referred to as "microhybrids." These materials are generally considered to be universal composites as they can be used for most anterior and posterior applications based on their combination of strength and polishability. The most recent innovation has been the development of the "nanofill" composites, containing only nanoscale particles. Most manufacturers have modified the formulations of their microhybrids to include more nanoparticles, and possibly pre-polymerized resin fillers, similar to those found in the microfill composites, and have named this group "nanohybrids." In general, it is difficult to distinguish nanohybrids from microhybrids. Their properties, such as flexure strength

and modulus, tend to be similar, with the nanohybrids as a group being in the lower range of the microhybrids, and both being greater than microfills[19]. While some have shown evidence for reduced stability during water storage for nano-hybrid or nano-fill composites vs. microhybrids[20], others have shown an opposite trend[21] or fairly similar susceptibility to aging[22]. It has been suggested that the slightly lower properties of some nanohybrid composites may be due to the incorporation of pre-polymerized resin fillers[23]. Regarding clinical evaluations, two recent studies over 2 and 4 years, respectively, showed similar excellent results in class II cavities for a nanofill vs. a microhybrid[24] and nanohybrid vs. a microhybrid, with slight evidence for better marginal integrity for the micro-hybrid in the latter study[25].

The state of the art of the composition of dental composites has been changing rapidly in the past few years. The nanofill and nanohybrid materials represent the state of the art in terms of filler formulation. Comprehensive electron microscopy and elemental analysis has been performed on many current composites to verify the significant differences in filler composition, particle size and shape[26]. New options for reinforcing fillers generally have focused on nanosized materials and hybrid organic-inorganic fillers. Years ago, novel organically modified ceramics (ORMOCERS) were developed[27] and have been used in commercial products. However, significant progress has been made in the development of new monomers for composite formulations with reduced polymerization shrinkage or shrinkage stress, as well as those with self-adhesive properties.

A recent review noted that efforts to modify fillers have been aimed at improving the properties of composites by the addition of polymer nanofibers, glass fibers, alumina and titania nanoparticles. There is also very interesting work incorporating silsesquioxane nanocomposites which are essentially an organic–inorganic hybrid molecule that reduce shrinkage, but also reduce mechanical properties if used in too high concentrations[28]. Perhaps the most promising work in composites with modified fillers for both enhanced mechanical properties and remineralizing potential by virtue of calcium and phosphate release has been the work with fused silica whiskers and dicalcium or tetracalcium phosphate nanoparticles[29]. These composites may be stronger and tougher, but the optical properties are not ideal and their opacity requires them to be self-cured or heat-processed at this point. Calcium fluoride

containing fillers also have been added to filled dental resins and have shown high fluoride release and good mechanical properties[30]. There are other monomers that are in various stages of development for potential use in dental composites, such as the (meth)acrylate vinyl ester hybrid polymerization system which exhibits phase separation during curing[31].

Other areas of development have included the incorporation of anti-bacterial agents and remineralizing agents into composites. Examples of compounds that have been added to resin composites to kill bacteria or inhibit biofilm formation include fluoride, chlorhexidine[32], zinc oxide nanoparticles[33], quaternary ammonium polyethyleneimine nanoparticles[34], and MDPB monomer[35]. The effectiveness of the various fluoride-releasing restorative materials have been critically reviewed, and it was concluded that the clinical results are not conclusive for dental restorative materials, including composites[36]. Remineralization may be promoted by the slow release of calcium and phosphate ions followed by the precipitation of new calcium-phosphate mineral. Years ago a material was developed which was purported to exhibit "smart release" of these ions as a result of an acidic challenge, as occurs during caries formation. This material, Ariston pHc, was not ultimately successful, in large part due to the fact that it absorbed too much water which affected its dimension and properties. But the idea of a "smart" material that reacts to its environment to release remineralizing ions or anti-microbial agents is attractive and stills a focal point of research.

A large number of different materials are used in dentistry for a wide spectrum of applications.

Dental amalgams are filling composites that consist of silver/tin powder mixed with mercury/gallium. The mercury free amalgam is referred to as Galloy. The gallium dissolves the outside layers of the metal powder particles forming a matrix of silver-tin-gallium that hardens to form the finished amalgam composite. The advantages of amalgam restorations over other direct-placement materials include resistance to wear, tolerance to wide range of clinical placement conditions such as wet fields, and excellent load-bearing properties. However, amalgams have been reported to be capable of sealing tooth-restoration margins with corrosion products. Also, due to its metallic

nature it is unable to mimic the translucency of natural teeth and its silver-grey colour limits its use to anterior teeth.

Dental cements are made from a nonmetallic powder that dissolves partially in a liquid that serves as glue that is used to cement crowns and posts. Silicate cement is made by mixing a powder of Alumino-Flouro-Silicate glass with phosphoric acid. This acid dissolves the glass and chemically combines with it creating a hard and brittle matrix. Due to its brittleness and lack of translucency and weak wear resistance this material is not used as restorative in stress bearing areas. Its usage mainly is limited to front teeth. The advantage of this cement is the prevention of further decay due to its rich content of fluoride.

The *glass ionomer cements* consist of a mixture of polyacrylic acid and Alumino-Flouro-Silicate glass. The acid-base reaction between these two ingredients results in the formation of metallic-polykenoate salt which precipitates and begins to gel until the cement sets hard. Unlike the silicate cement, this matrix is reasonably translucent allowing the colour of the glass particles to dominate the aesthetics. Also it is less brittle making it less prone to chipping and crasing. The strong ionic interaction with the dental hard tissues will yield an ion-enriched layer of cement that is firmly attached to the tooth. The glass powder has a natural rich fluoride content that has been credited with providing a cavity–inhibiting environment to protect the tooth from decay. On the negative side, the glass ionomer cements are less hard than the silicate cements so the restorations wear faster. They also lack fracture resistance, hence, they are excellent fillings on the surfaces of front teeth, but should not be used to rebuild the top edges of the teeth due to their weakness.

Resin cements are composed of powder glass filler in a hard matrix (mostly acrylic) which binds together. The hard matrix is composed of a refined form of acrylic known as BIS-GMA (bisphenol-A-glycidyl dimethacrylate). These fillings are usually cured through hardening the acrylic by adding a hardening catalyst or photoinitialiser that will harden the acrylic when illuminated under a strong light. The acrylic cannot be used by itself because it tends to shrink while it is setting. This shrinkage will lead to generation of stresses that might either break the tooth or create spaces between the filling and the walls of the cavity in the tooth. Moreover, acrylic on its own has low wear resistance. Therefore, the addition of rigid glass particles prevents most of the

shrinkage associated with the resin, and enhances the wear resistance significantly. The size of the glass particles determines the overall properties of resin-filled composites. Using macro particles such as crystalline glass (8–12 microns in diameter, 70–80% by weight) will make the macrofill not very polishable. Large particles are also easily dislodged from the surface of the restoration. This tendency to abrade away makes macrofills unsuitable for posterior restorations.

Microfill composites use particles very small in size (about 0.04 microns in diameter, 35–50% by weight). This type is usually used in front teeth because it is fairly polishable. However, having that many small particles might make the composite stiffer to work with. In order to overcome the limitations of the micro and macrofilled composites, it is better to use a layer of microfilled composite over a bulk of macrofill in order to spatially increase the strength of the structure and provide a more polishable restoration and a translucent enamel-like appearance. Another approach utilises 'Hybrid' composites that are cross between microfilled and macrofilled composites. Hybrid composites contain particles between 0.6–1 microns in diameter and 70–75% by weight. Hybrid composites are formulated to be layered. Often, hybrid composites are formulated with more resin than fillers (flowable composites), to form a loose mix that can be delivered to cavities using a syringe. Flowable composites are used to seal the dentine of a tooth prior to placing the filling material. Due to the low level of fillers, they are more prone to shrinkage, so they are not recommended by themselves to fill large cavities. Nanocomposites can be considered solid structures with nanometer-scale dimensional repeat distances between the different phases that constitute the structure. These materials typically consist of an inorganic (host) solid containing an organic component or vice versa. Or they can consist of two or more inorganic/organic phases in some combinatorial form with the constraint that at least one of the phases or features is of nanosize.

Hybrids nanocomposites fillers were synthesised by sol-gel processing of hydrolytically condensable silica (silicon oxides). However, the particles size was in average of 50–100 nm, and the authors did not characterise the improvement in the mechanical properties or the biocompatibility. The study showed that nanofillers outperform the micro and hybrid fillers in compressive strength, wear resistance and polish retention. However, the investigators relied on macroscale techniques to quantify

the mechanical behaviour of the nanofillers, and that usually leads to underestimating the actual mechanical behaviour of the nanofiller.

Recently, so-called nanofiller particles have been added to resin based composites, with particle sizes from 100 nm down to 5 nm (0.005 μm). Nanoparticles and microfiller particles are used in clusters/complexes (older formulations) or dispersed forms (newer formulation). Classification of resin-based composites is usually based on the type and size of the fillers (Figure 2.3).

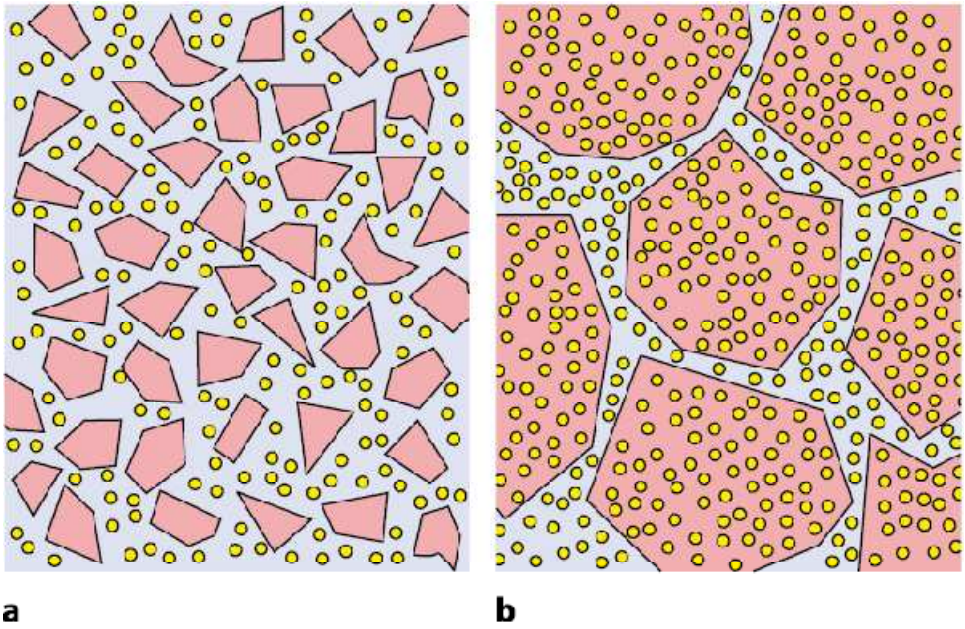

Figure 2.3 Schematic composition of a resin-based composite. a) fine particle hybrid, b) prepolymer filler resin[37]

Modern fine-particle hybrid-type resin-based composites should contain particles with a size between 0.6 μm and 1 μm, which are combined with microfillers and partly nanofillers/nanofiller complexes. Some resin-based composites contain fluoridated filler particles (for instance, based on YbF3), which release varying amounts of fluoride depending on the product. Composites with prepolymer fillers are also available. These consist of finely ground filler-containing resin-based composite (prepolymerized). The size and distribution of filler particles are decisive for the physical and mechanical characteristics of resin-based composites So-called flowable

composites reveal an improved flow capacity, which is generally caused by reduced filler content.

Because of the major influence of the fillers on the physical properties, the classification of dental filling composites is based on the type and the particle size of fillers used in them (Figure 2.4).

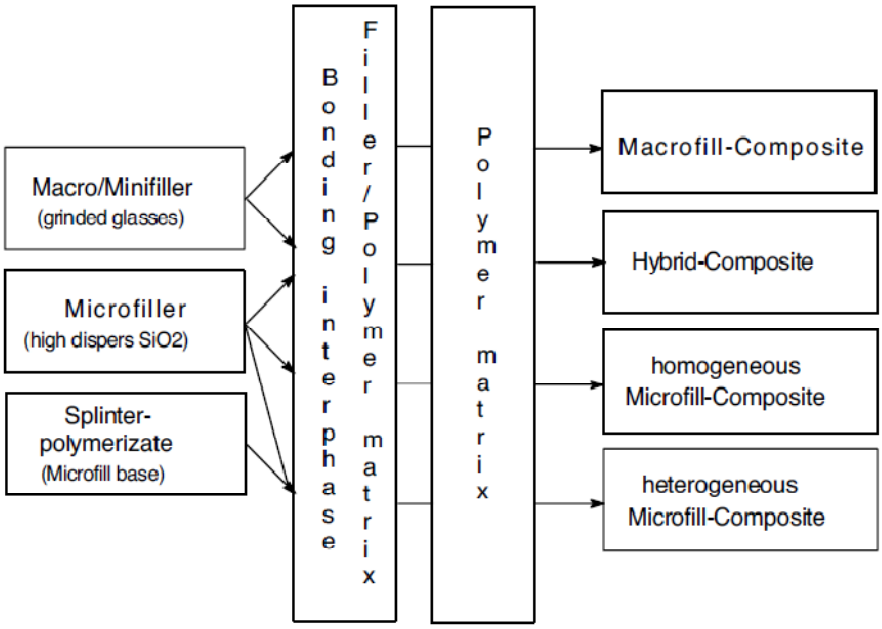

Figure 2.4 ***C****lassification of composite filing materials*[38].

In general, two types of composites are available on the market: microfill and hybrid composite filling materials. Microfill composites are based on nanofillers with a particle size in the range of 10–250 nm. Furthermore, a differentiation between homogenous and heterogeneous micro fills is made. To enhance their handling properties and achieve a higher load, heterogeneous microfill composites contain prepolymer particles that are based on a homogeneous microfill material. The inorganic part of hybrid composites consists of about 70–80% glass fillers and 20–30% nanofillers.

The fillers used in dental composites directly influence the radiopacity, abrasion

resistance, flexural modulus, and thermal coefficient of expansion. Polymerization shrinkage largely correlates with the volumetric amount of the filler in the composite. Many modern dental composites use the fillers listed in Table 2.1. In general, dental filling composites contain a mixture of at least two different fillers. Ytterbiumtrifluoride serves mainly as radiopacifier, yttrium fluoride, fluorosilicate glasses, or sparingly soluble fluoride salts are added to composites for fluoride release.

Table 2.1 Type of Fillers and Filler Size used in Dental Composites

Filler composition	Particle size
Highly dispersed silicon dioxide	10–40 nm
Radiopaque, finely ground barium or strontium silicate glasses	0.7, 1.0,1.5 μm, or larger
Radiopaque, finely grinded Ba-/Sr-fluoro silicate glasses	1.0, 1.5 μm or larger
Ground quartz glass	1.0–1.5 μm
Ytterbiumtrifluoride, yttriumtrifluoride	100–3000 nm
Si-/Zr-mixed oxide	250–500 nm (3.5 μm)
Titanium-, zirconium-, and aluminum oxides used as opacifier	250–500 nm
Splinter polymerizate mainly based on silicon dioxide	10–100 μm

To improve the clinical performance of composite filling materials, a large number of investigations are currently being conducted. The main topics are as follows:

- Reduction of the polymerization shrinkage to improve marginal adaptation and avoid recurrent caries
- Release of fluoride or other substances to reduce recurrent caries
- Improvement of mechanical properties
- Improvement of biocompatibility by reducing the elution of components

The introduction of ‘nano-hybrid’ fibre-reinforced composite was an approach chosen by several manufactures to produce what have been described as low shrinkage and high wear resistant. An alternative novel approach to the clinical application of

'nanofill' technology in dental restorative materials has been an fibre-reinforced composite containing a combination of individually dispersed filler particles of 0.005-0.075 μm (5-75 nm) and agglomerated nanosized particles of 1.3μm, described as 'nanoclusters' [Filtek Supreme; 3M ESPE, St. Paul, MN, US] (Figure 2.5).

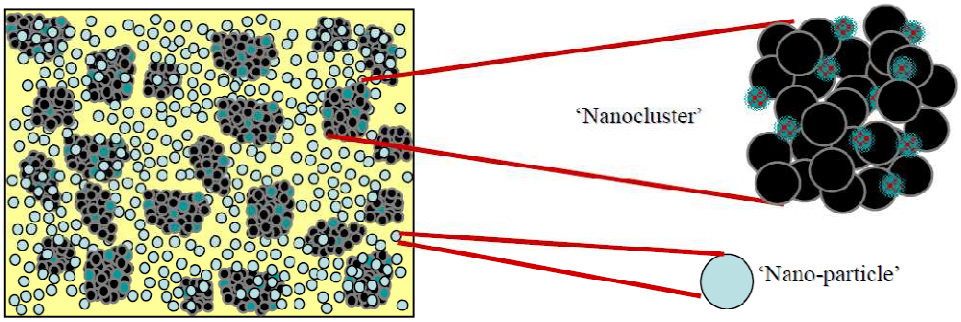

Figure 2.5 Schematic representation of silica-zirconia nanoclusters and individually dispersed nano-sized filler particles embedded in the methacrylate resin matrix of Filtek Supreme (3M ESPE, St Paul, MN, US).

The agglomerated porous clusters are partially calcined and infiltrated with a dilute silane coupling agent to ensure infiltration of the silane into the cluster interstices, a second undilute silane coupling agent was then admixed with the 'nanoclusters' prior to incorporation into the resin matrix. The presence of nanosized filler particles in RBC materials have been identified to produce distinct improvements to the material, such as increased filler loading in hybrid-type materials as nano-sized particles pack more efficiently between larger particles and also a subsequent reduction in polymerization shrinkage.

3. HYBRID MATERIALS FOR DENTAL APPLICATIONS

Inorganic–organic hybrid materials can be used as filling composites in dental applications. As schematized in Figure 3.1 these composites feature tooth-like properties (appropriate hardness, elasticity and thermal expansion behavior) and are easy to use by the dentist as they easily penetrate into the cavity and harden quickly under the effect of blue light. Moreover, these materials feature minimum shrinkage, are non-toxic and sufficiently non-transparent to X-rays. However, the composition of the hybrid material and the chemistry behind it depends strongly on its later application: as filler/particles, as matrix materials, as composites, as glass ionomer cements or as bonding.

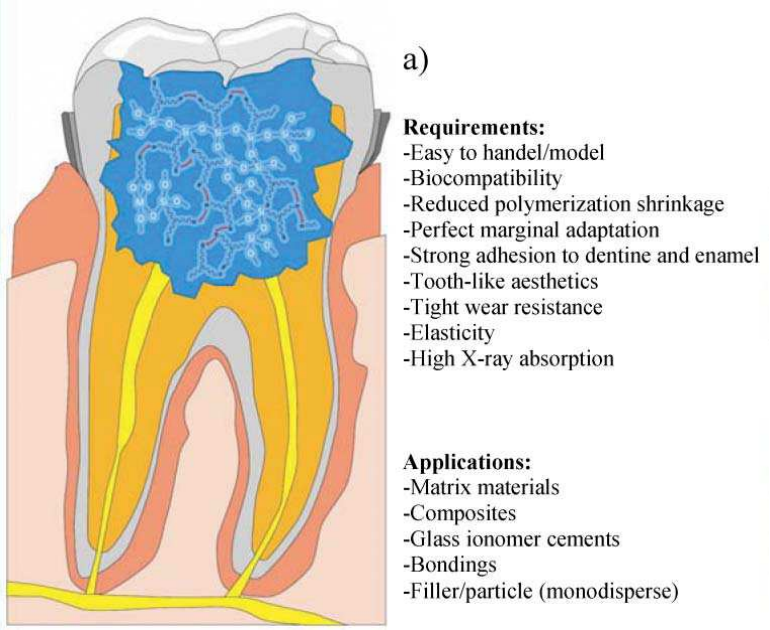

Figure 3.1 Requirements and possibilities of dental applications of ORMOCER®s.[39]

Traditional plastic filling composites had long-term adhesion problems and a high degree of polymerization shrinkage resulting in marginal fissures. The dual character of the ORMOCER®s as inorganic–organic copolymers is the key for improving the properties of filling composites. The organic, reactive monomers are

bound in the sol–gel process by the formation of an inorganic network. Thus, in the subsequent curing process, polymerization takes place with less shrinkage. Furthermore, abrasion resistance, in particular, is significantly enhanced by the existing inorganic Si–O–Si network. For example, in dental fillers organic functionalities including ring-opening reactions, such as functionalized spyrosilanes, are commonly included in the hybrid network. Other systems are based on multiacrylate silanes, offering a high organic density. In addition, mechanical properties of the composite can be tuned through variation of the spacer between the silicon atom and the reactive functionality. All these possibilities are already taken into account, and most of these hybrids include various fillers in their composition. As examples of available commercial filling composites based on dental ORMOCER®s from Fraunhofer ISC one can appoint ‘‘Definite1’’ and ‘‘Admira1’’. In the case of the Admira1 product, a specifically designed dentine-enamel bonding, an adhesive ORMOCER®s developed in cooperation with VOCO GmbH, is used to make this product especially advantageous. In glass ionomer cement based dental composites blue light polymerisable carboxyl functionalised ORMOCER®s have been developed. In this case, the cement forming reaction compensates the shrinkage resulting from organic crosslinking reaction of e.g. methacryl functionality.

Ormocer stands for organically modified ceramic. The aim was to improve the composites by improving marginal adaptation, abrasion resistance, and biocompatibility. In vitro studies confirmed that ormocers demonstrate favorable abrasion resistance[40]. Their marginal adaptation is comparable with that of conventional composites in conjunction with the adhesive technology[41,42] Improvement in biocompatibility can only be achieved if no diluting monomer, such as TEGDMA, is used to reduce the viscosity of the corresponding condensate. Ormocers can be prepared by sol–gel processing of organofunctional metal alkoxides such as chloro or alkoxy silanes, which contain polymerizable groups P or functional groups R (Figure 3.2).

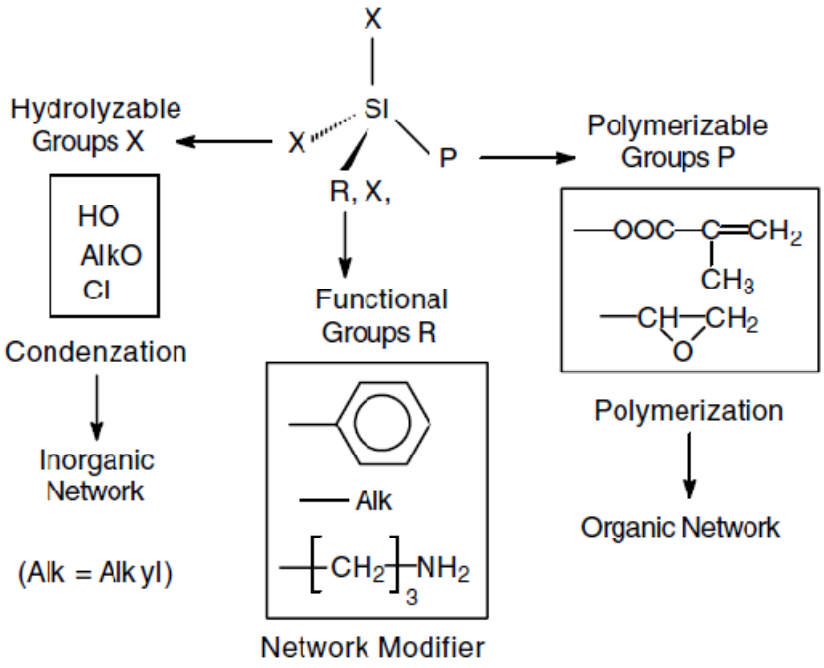

Figure 3.2 Chemical structure variations of ormocer silanes. [43]

These oligomers may replace the conventional monomers in the dental composites. The composite in a second stage is hardened by linking the polymerizable groups and forming a three-dimensional network (Figure 3.3).

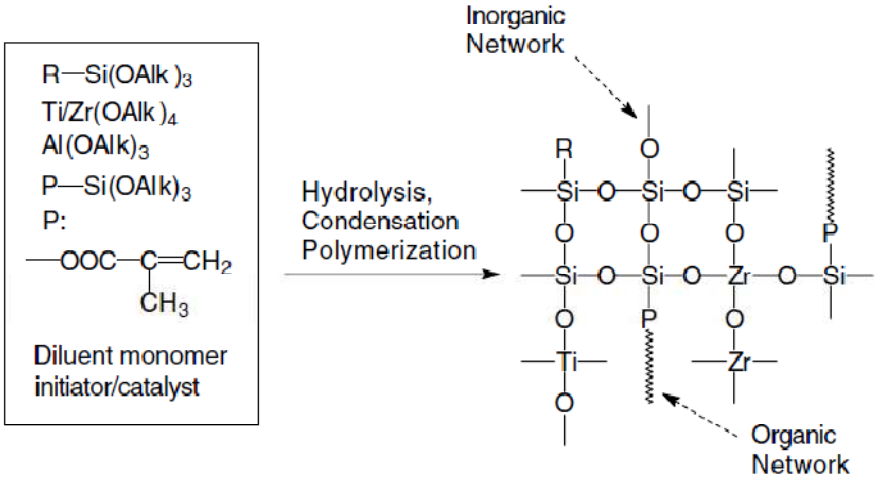

Figure 3.3 Formation of an organic-inorganic hybrid material by hydrolytic condensation and polymerization of functionalized alkoxy silanes[44].

The hybrids formed are composites in which the organic and inorganic components are combined on a nanoscopic or molecular scale. Therefore, these materials not only show the properties of both pure organic and inorganic components, but they also have the potential of providing properties that have been unknown to date and that make these materials very attractive for use in dental materials.

When bonded interfaces are imposed on a polymerizing sample of a composite, as is necessary with a dental restoration, the resultant restriction in free shrinkage induces significant internal and external stress (Figure 3.4).

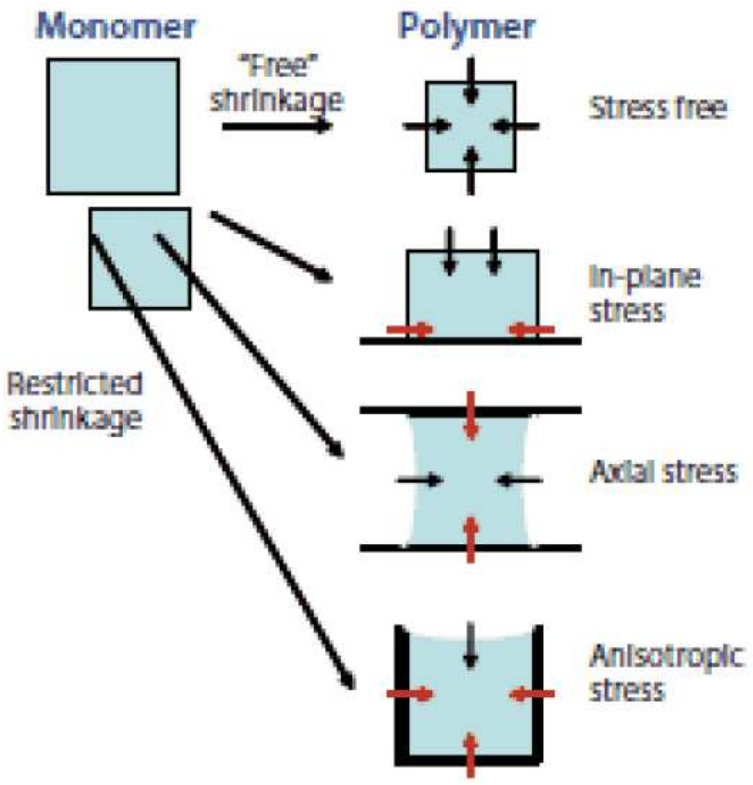

Figure 3.4 Restricted shrinkage associated with bonded surfaces during polymerization leads to significant stress development within a polymerizing sample[45].

This stress can cause a series of problems including: (a) deflection of the tooth, (b) failure of sections of the adhesive bond, and (c) defect formation within the polymer matrix at the filler-matrix interface, or in the adjacent enamel substrate[46]. Reliable, long-term stability of the tooth-restoration interface has remained elusive, prompting substantial new materials research and development projects in both industrial and academic laboratories. The concerns with polymerization shrinkage and stress are not

unique to dental polymers, and the research can also be applied to other industrial polymer applications including coatings, adhesives, encapsulants, aspheric lenses and photolithography. Stress development during the formation of glassy polymers in a polymerizing composite is a major concern. Therefore a basic understanding of the evolution of shrinkage strain and elastic modulus is critical to begin solving the stress/strain problems. The values of the shrinkage strain and modulus are dependent on the polymerization degree, along with temperature change in the non-isothermal composite photo polymerizations. Dimethacrylate monomers are capable of forming polymer networks with glass transition temperatures above the curing temperature, but this usually means that a significant percentage of the methacrylate functionality remains un-reacted in the fully cured polymer[47].

Nanoparticles or nanofibers have been used as fillers in both polymeric nanocomposites[48,49,50] to improve the mechanical, electric and optical properties, and in metallic nanocomposites[51,52] to control the electrodeposition. As compared with other nanomaterials such as carbon nanotubes, alumina is cheaper and has the ability to be functionalized for nanocomposite fabrication. Vinyl ester resin was chosen due to the fact that the cured resins are thermosetting with a network structure possessing high resistance to chemicals. Upon incorporation of the alumina nanoparticles into the vinyl ester resin matrix, the obtained nanocomposite has potential applications in fabrication and building materials such as electrodeposition tank and marine vessels which require high resistance to acid or base and superior mechanical properties. The existing challenge in composite fabrication is to provide a high tensile strength due to local stress within the nanocomposite. In other words, the response of a material to an applied stress is strongly dependent on the nature of the bonds. Poor linkage between the filler and the polymer matrix such as in composites made by simple mixing[53,54,55] will introduce artificial defects, which consequently result in a deleterious effect on the mechanical properties of the nanocomposite[56]. However, an appropriately engineered interphase could both improve the strength and toughness of composites, and make the nanocomposites stable in harsh environments as well[57]. The interfacial interaction between the nanoparticle and the polymer matrix plays a crucial role in determining the quality and properties of the nanocomposite, please see recent reviews on the classification of organic–inorganic materials by Sanchez et al.[58] Surface

functionalization of the nanoparticles with a surfactant is subsequently important not only to stabilize the nanoparticle[59] but also to render the nanoparticle compatible with the polymer.

3.1 ALUMINA NANOPARTICLES AND ALUMINA WHISKERS

Alumina has received considerable attention and has been historically well accepted as biomaterials for dental and medical applications. Alumina (Al_2O_3) in particular possesses a variety of commercial and industrial uses and has become one of the most important commercial ceramic materials. As a widely studied nanomaterial, Al_2O_3 nanoparticles have been applied in catalysis, nanocomposites, polymer modification, functionalization of textiles, heat transfer fluids, and waste water treatment. In addition, Al_2O_3 nanoparticles have featured in biological applications such as biosensors, biofiltration and drug delivery, antigen delivery for immunization purposes and bactericides. Particle aggregation and settling are important in many of these applications and require further exploration.

Solid-liquid separation of particles has its own importance in a range of industrial and natural processes such as waste-water treatment, mineral separation, and deposition of sediments in rivers and lakes. Very often these processes involve suspensions that are flocculated and not colloidally stable. Moreover most industrial slurries contain a wide variety of particle sizes and shapes. For the case of a single particle in a static fluid (unhindered settling), the settling rate has been found to depend on the density and viscosity of the fluid as well as the density, size, shape, roundness, and surface texture of the particle. For the multi-particle case the situation is more complicated. The spherical particles tend to settle more faster, than non-spherical particles, and larger spheres were found to settle faster than smaller ones. At high concentrations (> 40 wt. %), the polydisperse spheres (of diameter ~100 μm) attained the theoretical settling rate expected from monodisperse spheres (unhindered settling). Knowledge of the particle shape is crucial in order to use this formula accurately.

More recently, alumina is also used as filler for reinforcing the dental restorative composite. Alumina filler with higher elastic modulus (370 GPa) is favorable reinforcement of dental composites. The elastic modulus and strength of composites can

be increased with relatively low volume fractions compared to the counterparts reinforced with silica glass. Therefore, uses of ultra-stiff filler materials such as alumina, especially in nanoscale size, appear to be a viable strategy in improving the elastic properties of dental composites[60].

Alumina nanoparticles[61,62,63,64] and (3-methacryloxypropyl) trimethoxysilane (MPS)[65,66] have been used as filler and surfactant, respectively, for nanocomposite fabrication. The functionalization of the alumina nanoparticles is normally carried out in a pH = 4 acidic alcoholic solution. However, from the Pourbaix diagram[67], alumina will get dissolved and form aluminium ions in solutions with pH values lower than 4.25 or higher than 10.25. After treatment with a normal acidic solution, the more reactive alumina nanoparticles will dissolve and reshape into agglomerated bulk form existing in the possible salt form rather than alumina any more. The other reported method used a high temperature reaction at the silane toluene refluxing point to functionalize the nanoparticles with MPS[68].

Alumina whiskers are extremely strong micro-crystals, which have an a-alumina crystalline structure. Because of the high strength and excellent high temperature stability of a-alumina, these whiskers are highly desirable as the reinforcing constituent of composite structures.

3.2 SEPIOLITE

Sepiolite is a hydrous magnesium silicate ($Si_{12}O_{30}Mg_8(OH)_4(H2O)_4 \cdot 8H_2O$) characterized by its fibrous morphology and intra crystalline channels, (Figure 3.5). Due to its sorptive, rheological and catalytic properties, sepiolite is widely used in a variety of industrial applications. Sepiolite is used as a catalyst and catalyst support, as a filler in polymer composites[69], and as membrane for ultra filtration and as molecular sieves. Sepiolite is an effective and economical sorbent material, a bleaching and clarifying agent, a filter aid, an industrial sorbent and the spectrum of its utilization ranges from cosmetics to paints and fertilizers.

Sepiolite, is a non-swelling, lightweight, porous clay with a large specific surface area. Unlike other clays, the individual particles of sepiolite have a needle-like morphology. The high surface area and porosity, as well as the unusual particle shape of

this clay account for its outstanding sorption capacity and colloidal properties that make it a valuable material for a wide range of applications.

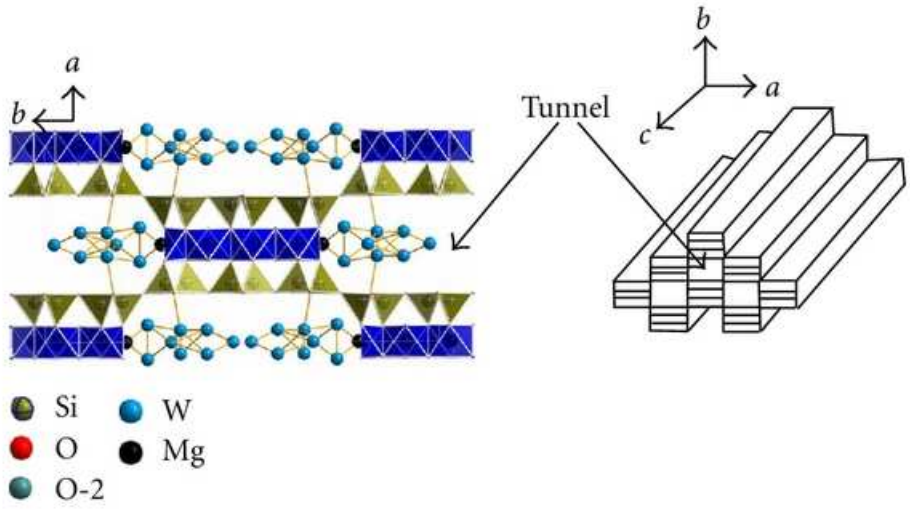

Figure 3.5 Crystal structure of sepiolite proposed by Brauner and Preisinger[70]

Sepiolite is very uncommon clay because of both its peculiar characteristics and scarce occurrence. There are very few commercial deposits in the world. Sepiolite, unlike other clays, is not a layered phyllosilicate. Its structure can be described as a quincunx (an arrangement of five objects, so placed that four occupy the corners and the fifth the centre of a square or rectangle) of talc-type sheets separated by parallel channels. This chain-like structure produces needle-like particles instead of plate-like particles like other clays.

Sepiolite has the highest surface area (BET, N_2) of all the clay minerals, about 300 m^2/g, with a high density of silanol groups (-Si-OH) which explains the marked hydrophilicity of this clay. The silicate lattice has not a significant negative charge and therefore the cation exchange capacity of this clay is very low. The tiny elongated particles of sepiolite have an average length of 1μm to 2 μm, a width of 0.01 μm; and contain open channels with dimensions of 3.6 Å x 10.6 Å running along the axis of the particle. These particles are arranged forming loosely packed and porous aggregates with an extensive capillary network which explains the high porosity of sepiolite and its light weight because of the large void space

The high surface area and porosity of sepiolite account for the remarkable adsorptive and absorptive properties of this type of clay. It adsorbs vapours and odours and can absorb approximately its own weight of water and other liquids.

Sepiolite is a non-swelling clay and its granules do not disintegrate even when saturated with liquids. Colloidal grades of sepiolite must be dispersed into water or other liquid systems using high-shear mixers. Once dispersed in the liquid, it forms a structure of randomly intermeshed elongated particles, which is maintained by physical interference and hydrogen bonding, and entraps the liquid, increasing the viscosity of the suspension. This structure is stable even in systems with high salt concentrations, conditions that produce the flocculation of other clay's suspensions, as bentonite.

The random network of sepiolite particles holds coarser particles in the liquid preventing their settling by gravity, acting as a suspending agent. Sepiolite provides to its suspensions a pseudoplastic and thixotropic behaviour which make it a valuable material in multiple applications to improve processability, application or handling of the final product.

Sepiolite, structurally similar to palygorskite, intersilite, amphibole, and ratite, is one of the most important industrial magnesium-rich in 2:1 phyllosilicate clay minerals, i.e. octahedral layer is bound above and below by a silica tetrahedral sheet [71]. Since the discontinuous octahedral sheets extend only in one dimension, the tetrahedral sheets are divided into ribbons by a periodic inversion of rows of tetrahedrons. The very large channels or tunnels are located between these ribbon strips and formed chain-layer molecular structure of sepiolite mineral as well as its unique fibrous structure (Figure 3.5). Chain-layer molecular structure exactly determines the hydrophobicity and anisotropic character of sepiolite within the half-cell. While hydrogen bonding sides of silanol groups (Si-OH) are presented on the external surface; owing to discontinuities and chain-layer molecular structure, Mg^{2+} ions located at the edges of octahedral sheets exert more influence on the hydrophobicity of sepiolite[72]. In other words; the breakage of Si-O and MgO bonds provides many hydrogen bonding sites on the sepiolite edge surfaces similar to the natural hydrophobic talc mineral which edge surfaces facilitate the formation of strong hydrogen bonds with water dipoles[73]. The interest in sepiolite is more about its high adsorptive capacity, catalytic performance, and rheology. The extent of hydrophobicity or wettability is important in such applications.

The use of sepiolite fillers improve processing, dimensional stability, mechanical strength and thermal resistance.

Considering the studies on the nanocomposites with sepiolite, it is seen that polyurethane,[74] poly (hydroxyethyl acrylate),[75] and poly(sodium acrylate)[76] for in situ polymerization method; chitosan[77], epoxy resin[78,79] poly(dimetylsiloxane)[80,81] poly (ethyl methacrylate), and poly(2-hydroxyethyl methacrylate) for solution dispersion; Nylon-6,[82] polypropylene[83] for melt intercalation and polypropylene[84] for supercritical CO_2- assisted mixing have been used in the relevant experiments.

Nanofibers of sepiolite have proved to yield substantial improvement for the mechanical properties and thermal stability of these polymers even at low filler levels.

Poly (vinyl alcohol) (PVA) is a water-soluble polymer extensively used in paper coating, textile sizing, flexible water-soluble packaging films, etc. As both the sepiolite and PVA are very hydrophilic, sepiolite can be incorporated into PVA without need for pretreatment by simply dispersing the two components in water.

4. PERFORMANCE ENHANCEMENT OF DENTAL COMPOSITES USING ELECTROSPUN NANOFIBERS

The objective of the present chapter is to investigate the effect of electrospun nanofiber reinforcement on the properties of commercially available, and hyperbranched polymer modified dental formulations. The emergence of functionalized nanoscale reinforcements having large surface area (hundreds of square meters/gram) has enabled the design of novel nanocomposites with new and complex structures leading to enhanced mechanical and physical properties. Electrospun nanofibers from a range of polymer chemistries have been investigated as a reinforcing phase with and without a silane coupling agent surface treatment.

A main challenge for centuries has been the development and selection of biocompatible, long-lasting, direct-filling tooth restoratives and prosthetic materials that can withstand the adverse conditions of the oral environment. Polymer matrix composites, comprised of silica-filled UV curable acrylate resins, have emerged as desirable materials for these applications.

Key properties of dental composites include low viscosity prior to cure, biocompatibility, low polymerization shrinkage (both to insure good prosthesis adhesion and to eliminate unfilled space for infection or other contamination), high mechanical properties (especially fracture toughness, compressive strength, and fatigue), surface hardness, abrasion resistance, low moisture uptake, low coefficient of thermal expansion (in the range of body temperature), ease of handling in the oral environment, and the ability to match the esthetics of the patient's teeth[85,86,87,88].

The current state-of-the-art dental composites contain modified acrylate resin matrices filled with micro-/nanoscaled ceramic particles. It has been shown that the performance of dental composites can be improved through the use of nanotechnology[89,90,91,], including the use of covalently anchored nanoscaled organic moieties to an inorganic network[92], and the incorporation of nanoscaled monomethacrylate functionalized polyhedral oligomeric silsesquioxanes (POSSs) into an acrylate resin system[93]. Novel polymeric dental restorative composites have been explored, in which polyhedral oligomeric silsesquioxane methacrylate (POSS-MA) monomers were used to partially (or completely) replace the commonly used base

monomer, Bis-GMA. Fang[101] explored the use of polyamide nanofibers as a toughening agent in dental acrylate resins. The best performance reported up to date for acrylate-based dental composites was achieved by the Dodiuk-Kenig group through the modification of acrylate resin by the incorporation of hyperbranched moieties into the matrix resin[94]. It has been hypothesized that these hyperbranched moieties assemble to form nanophases that retard motions in the acrylate backbone, leading to improved mechanical performance and reduced polymerization shrinkage. This improved resin system has been commercialized by BJM Ltd. and distributed worldwide by the Premier Dental Company.

Many groups have worked extensively in the area of electrospinning[95,96,97,98], focusing on both process understanding and nanofiber applications. The objective of this chapter is to investigate the impact of nanofiber reinforcement on the performance of state-of-the-art dental composites.

Electrospinning uses an electrical charge to draw very fine (typically on the micro or nano scale) fibres from a liquid. Electrospinning shares characteristics of both electrospraying and conventional solution dry spinning of fibers[99]. The process does not require the use of coagulation chemistry or high temperatures to produce solid threads from solution. This makes the process particularly suited to the production of fibers using large and complex molecules. Electrospinning from molten precursors is also practiced; this method ensures that no solvent can be carried over into the final product.

In the electrospinning process a high voltage is used to create an electrically charged jet of polymer solution or melt, which dries or solidifies to leave a polymer fiber[100,101]. One electrode is placed into the spinning solution/melt and the other attached to a collector. Electric field is subjected to the end of a capillary tube that contains the polymer fluid held by its surface tension. This induces a charge on the surface of the liquid. Mutual charge repulsion causes a force directly opposite to the surface tension[102]. As the intensity of the electric field increases, the hemispherical surface of the fluid at the tip of the capillary tube elongates to form a conical shape known as the Taylor cone[103]. With increasing field, a critical value is attained when the repulsive electrostatic force overcomes the surface tension and a charged jet of fluid is ejected from the tip of the Taylor cone. The discharged polymer solution jet undergoes a whipping process[104] wherein the solvent evaporates, leaving behind a charged polymer

fiber, which lays itself randomly on a grounded collecting metal screen. In the case of the melt the discharged jet solidifies when it travels in the air and is collected on the grounded metal screen.

These preliminary results indicate that the introduction of hydroxyl-rich nanophases with specific composite architecture (need to differentiate from 150 nm PVOH) into acrylate matrix dental composites can lead to significant and unexpected improvement in clinically important dental material performance. In the case of acrylate resin modified by hyperbranched polyesteramide, the improvement is attributed to crack blunting by the nanophase inclusion, coupled with increased system cross linking through the hydroxy-rich chemistry. The addition of the hydroxyl-rich PVOH nanofiber phase further increases crosslinking density, while improving overall system toughness by allowing cracks to run and dissipate energy along the fiber-matrix interface. These results are consistent with the complex mechanisms suggested for the toughening of polymers, polymer blends, and fiber-reinforced composites[105]. While a detailed mechanism is beyond the scope of the present work, it is clear that composite performance is a function of matrix chemistry, fiber diameter, fiber dispersion, and fiber matrix interaction. In a more general sense, this work shows that significant improvement to the performance of simple polymer systems, in this case acrylates, can be effected by the introduction of small weight percentage (<1 wt. %) of nanoscale reinforcements. The introduction of more than one such phase can, as illustrated here by the inclusion of both hyperbranch (0.3 wt. %) resin modification and PVOH nanofiber (250 nm diameter, 0.05 wt. %), be synergistic and lead to even greater improvement of key performance properties. Future work will concentrate on the definition of detailed mechanisms of property enhancement and the extension of these concepts to new chemistries.

Electrospinning is a process by which a charged liquid polymer solution is introduced into an electric field. The liquid polymer solution is dispensed via a needle attached to a syringe at a voltage between 10-20 kV and is deposited on a conductive material at ground (0V) located between 10-30 cm from the needle location. The polymer is ejected from a needle with an inner diameter (ID) between 0.5-1.5 mm. The ejected polymer solution forms a continuous nanofiber when the electrical force (due to the high voltage potential of the polymer solution) overcomes the surface tension. At

this point the pendant droplet of the polymer solution at the tip of the needle is deformed into conical shape, typically referred to as Taylor cone. If the voltage surpasses a critical value (depends on the chemical makeup of the polymer solution), the electrostatic force overcomes the surface tension and a fine charged jet is ejected. The formation of the Taylor cone is shown in Figure 4.1. After the jet flows away from the droplet in a nearly straight line, it bends into a complex path and other changes in shape occur, during which electrical forces stretch and thin it by very large ratios. After the solvent evaporates solid nanofibers are left[106]

Figure 4.1 Formation of the Taylor cone. Voltage increases with each stage until equilibrium between surface tension and the electrostatic force is achieved in stage 3[107]

There are several experimental setups that have been developed to produce nanofibers. Each setup attempts to produce scaffolds that are either woven or non-woven. A method to create a woven scaffold is displayed in Figure 4.2. This method utilizes a disk that rotates as it collects the continuous nanofiber. The nanofiber is highly attracted to the large electric field created on the sharp end of the disk.

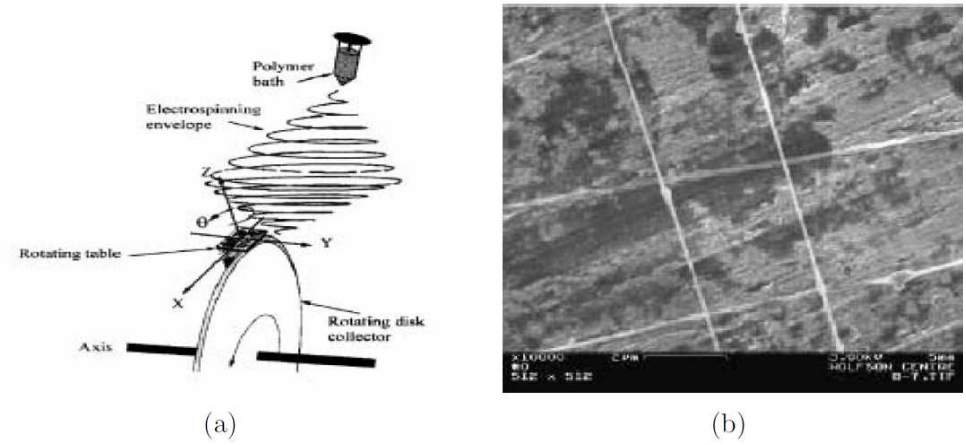

Figure 4.2 An effective method to produce aligned electrospun fibers (a) rotating disk collector (b) resulting woven scaffold[108]

Another method to produce aligned fibers is shown in Figure 4.3. This method forces the fibers to ”straighten” themselves in the region between the two plates. Due to the collection of the fibers within the air gap, the collection of aligned nanofibers is achieved without the possibility of contamination from the ground electrode. This is an ideal collection method for producing scaffolds for tissue engineering.

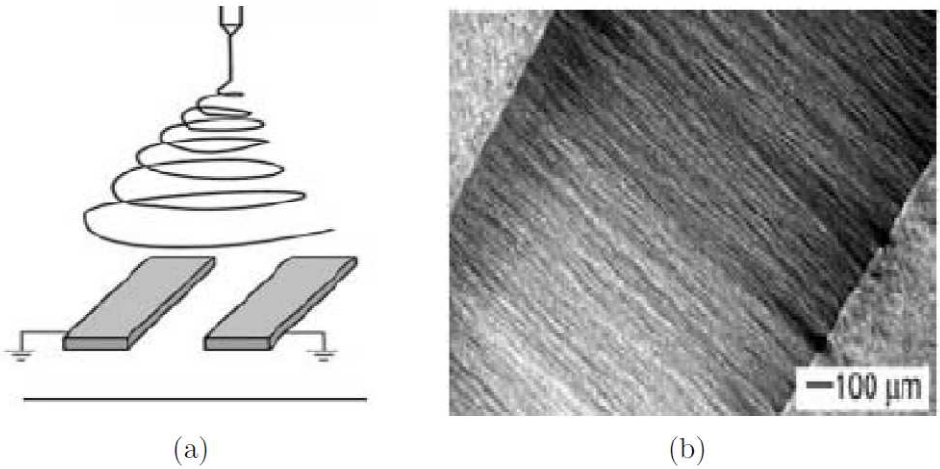

Figure 4.3 Another effective method to produce aligned electrospun fibers (a) double ground collector (b) resulting aligned fibers. Image reproduced from[109]

Methods have also been developed to create non-woven scaffolds. This type of collection involves the same basic setup already described. Non-woven scaffolds are made with randomly oriented nanofibers. This type of collection is typically made using a flat electrode. Using this type of electrode produces a highly uniform electric field. This means that there is no preferred location for the nanofiber to orient itself and is thus random. Two basic methods, a vertical orientation and a horizontal orientation, are presented in Figures 4.4 and 4.5, respectively.

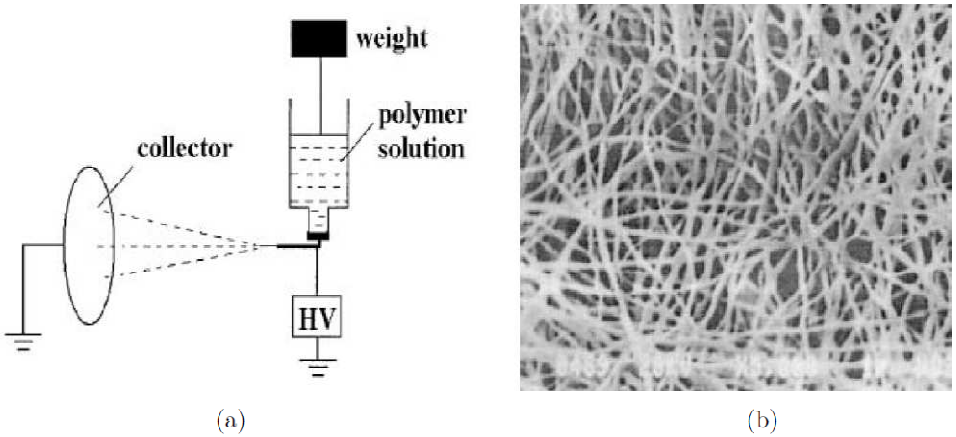

Figure 4.4 Horizontal flat ground collector for random nanofiber collection (a) Horizontal setup with weight as syringe driver and (b) Resulting nanofiber structure[110]

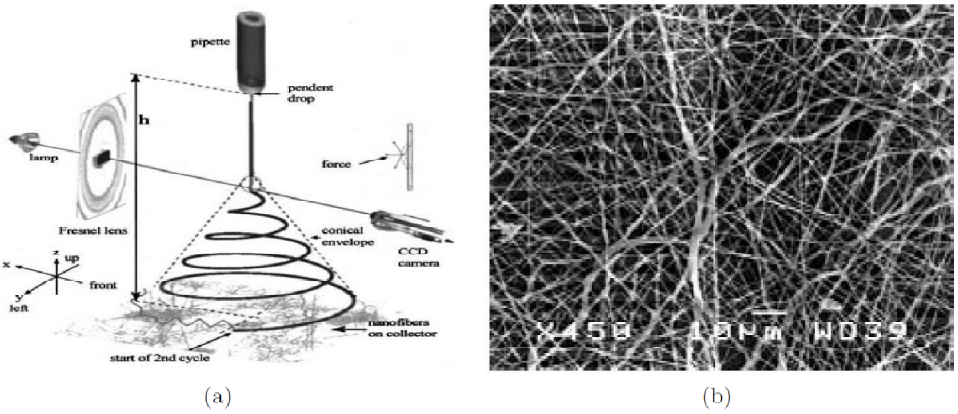

Figure 4.5 Vertical flat ground collector for random nanofiber collection (a) Vertical setup (b) Resulting nanofibers[111]

An important characteristic of electrospinning is the ability to make fibers with diameters in the range of nanometers to a few microns scale. Consequently these fibers have a large surface area per unit mass so that nanowoven fabrics of these nanofibers collected on a screen can be used for example, for filtration of submicron particles in separation industries and biomedical applications, such as wound dressing in medical industry, tissue engineering scaffolds and artificial blood vessels. The use of electrospun fibers at critical places in advanced composites to improve crack resistance is also promising.

The electrical forces on free charges residing on the surface of a polymeric liquid are primarily responsible for driving the electrospinning process. In conventional spinning processes like melt or solution spinning, the fiber is subjected to tensile, rheological, gravitational, inertial and aerodynamic forces. The action of these forces has been described in detail b y Ziabicki[112] (Figure 4.6).

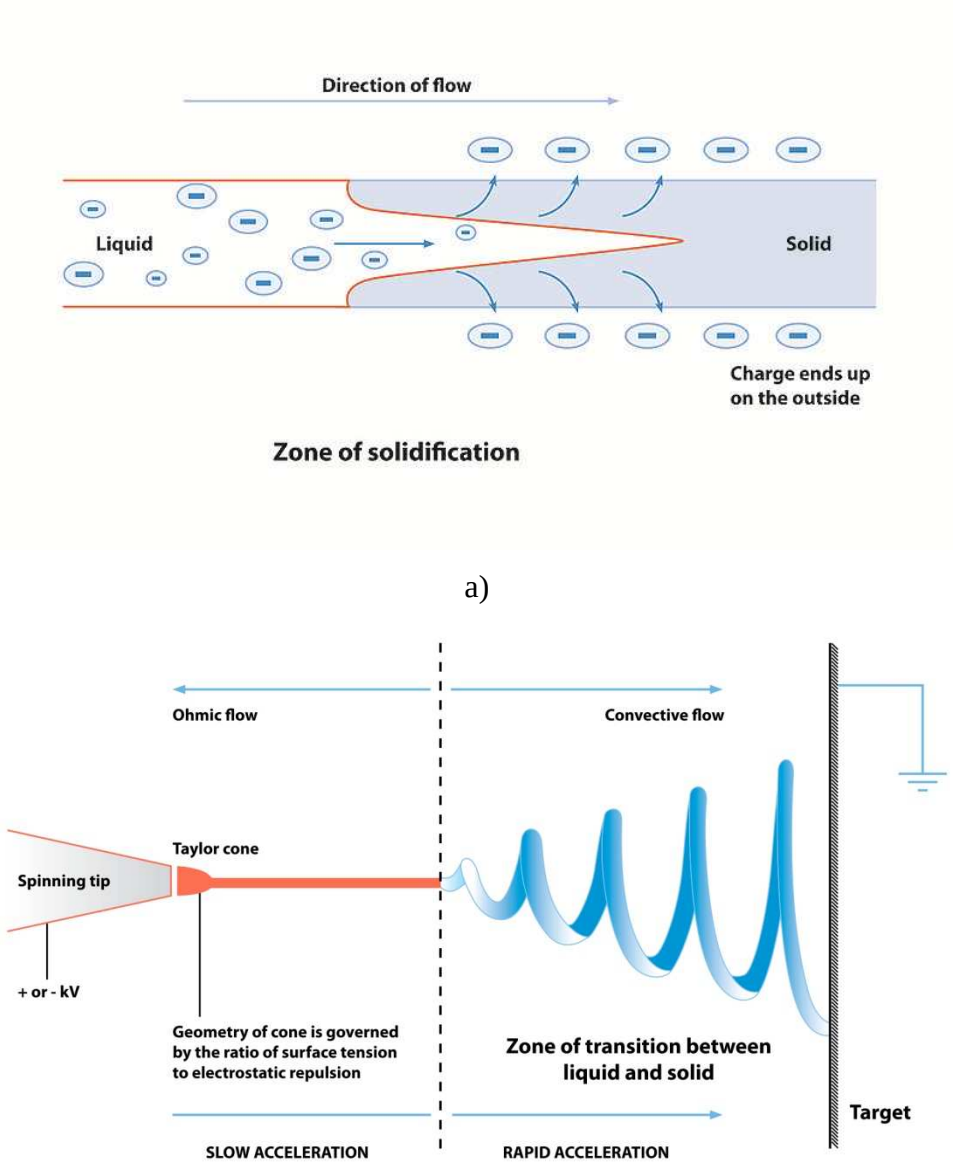

Figure 4.6 a) How the distribution of charge in the fibre changes as the fibre dries during flight, b) Diagram showing fibre formation by electrospinning[113]

When a sufficiently high voltage is applied to a liquid droplet, the body of the liquid becomes charged, and electrostatic repulsion counteracts the surface tension and the droplet is stretched; at a critical point a stream of liquid erupts from the surface. This point of eruption is known as the Taylor cone. If the molecular cohesion of the liquid is sufficiently high, stream breakup does not occur (if it does, droplets are electrosprayed) and a charged liquid jet is formed. As the jet dries in flight, the mode of current flow changes from ohmic to convective as the charge migrates to the surface of the fiber. The jet is then elongated by a whipping process, which is caused by electrostatic repulsion initiated at small bends in the fiber, until it is finally deposited on the grounded collector. The elongation and thinning of the fiber resulting from this bending instability leads to the formation of uniform fibers with nanometer-scale diameters. The electrospinning process has three stages: a) initiation of the jet and the extension of the jet along a straight line; b) the growth of a bending instability and further elongation or drawing of the jet that allows it to move in a looping and spiraling path; c) solidification of the jet into nanofibers. In the next three sections, these three stages will be described following with various mathematical models that have offered to quantify the jet behavior will be briefly outlined.

Initiation of the jet. In a typical electrospinning apparatus, the polymer solution is contained in a syringe or a glass capillary. One of the electrodes is dipped in the polymer solution whereas the other acts as the collector target that is kept at a certain distance from the syringe (hence, not immersed in the solution). When an electric field is applied to a polymer solution, ions in the solution aggregate around the electrode of opposite polarity. This results in the build-up of an excess of ions of oppositely charged polarity near an electrode. For instance, if a positive electrode is dipped in the polymer solution, then the negative ions migrate towards the anode but the positive ions aggregate at the tip of the capillary leading to a charge build-up. Thus, the region of interest is the solution near the tip of the capillary where these excess charges aggregate at the surface of the suspended liquid/solution drop. The shape of the meniscus of the suspended polymer droplet is defined by the balance of hydrostatic pressure, electrical forces and, surface tension[35]. In weak fields, the polymer solution is held at the end of the capillary by surface tension. When the electrical field increases, the meniscus elongates to form a conical configuration (Taylor Cone), until at some critical value of

the electrical field, surface tension can no longer balance the hydrostatic and electric forces and a thin jet is ejected from the surface of this meniscus. This ejected jet travels toward the nearest electrode of opposite polarity, or electrical ground. It is believed that excess charge is essentially static with respect to the moving coordinate system of the jet[36].This means that the electrospinning jet can be essentially thought of as a string of charged elements connected by a visco-elastic medium, with one end fixed at a point of origin and the other end free.

Growth of the Bending Instability and Further Elongation of the Jet. After initiation, the jet traveled in a straight line for some distance (typically 2-3 cm). It was hypothesized that an electrically driven instability triggered by the perturbations of the lateral position and lateral velocity of the jet caused it to follow a bending, winding, spiraling and looping path in three dimensions.

Solidification of the Jet into a Polymer Filament. As the rapidly 'whipping' jet moved towards the target maintained at an attractive potential, it continued to expand into a spiraling and looping path. This process continued until the jet became fairly thin and was intercepted by the target. As can be premised, the greater the distance the jet travels, the thinner it becomes. Thus, the distance between the capillary-end and the target is one process parameter that has direct implications on the fiber diameter. In fact, other process parameters include the flow rate, concentration, and electric field strength, to name a few.

Effect of System and Process Parameters on Electrospun Fiber Diameter. The following system and process parameters have been noted to affect the fiber diameter:

System Parameters:

- Viscosity
- Concentration
- Net charge density (conductivity)
- Surface tension of the polymer fluid.
- Molecular weight
- Molecular weight distribution
- Topology (branched, linear etc.) of the polymer.

Process Parameters:

- Electric potential
- Flow rate of the polymer solution
- Distance between the capillary-end and target/collection screen
- Ambient parameters (temperature, humidity and air velocity in the chamber)
- Motion of target screen
- Internal diameter of the nozzle/capillary

These parameters have been summarized in Figure 4.7, where generalized trends are shown. For continuous and uniform fiber formation it is imperative that the concentration of the polymer solution be above the critical chain overlap concentration. The critical entanglement concentration marks the transition of solution concentration from the semidilute unentangled to semidilute entangled regimes. The physical concept as well as the procedure to estimate will be outlined in chapter 8, where the author further investigates the effect of concentration, viscosity and molecular weight on fiber formation during electrospinning.

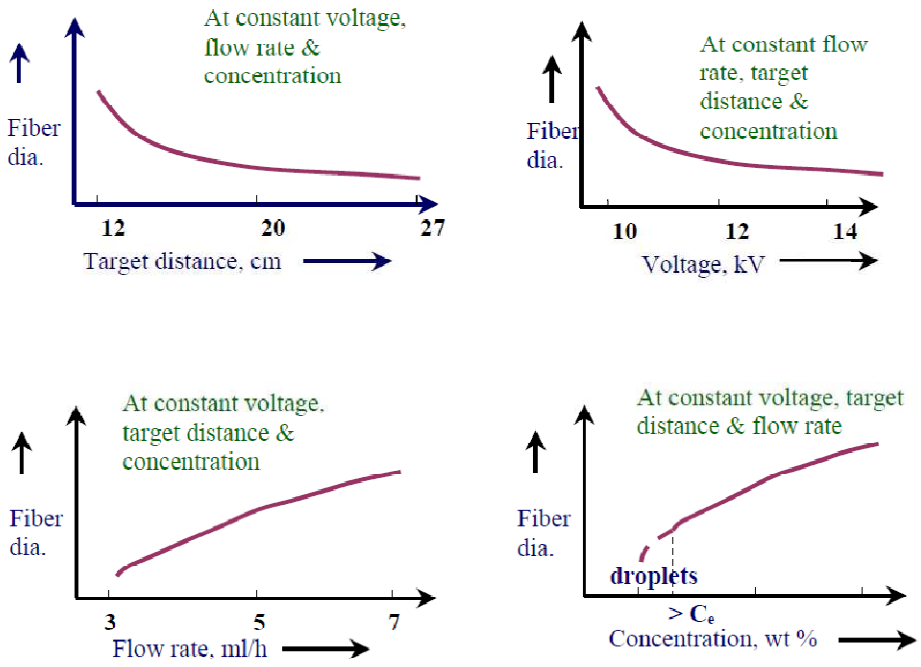

Figure 4.7 Effect of process parametars on fiber diameter produced by electrospinning[114]

With increasing flow rate and concentration, the fiber diameter was observed to increase as more mass of the solution (per unit time and volume respectively) was forced through the capillary end. The fiber diameter decreased with increasing target distance and electric potential. With increasing rotational speeds, the electrospun filaments were observed to become increasingly aligned in the rotating direction of the target. Furthermore, the diameter of the electrospun fibers that were collected on the rotating target was significantly smaller (ca. 5 times) than those collected under identical processing conditions on a stationary target.

Having described the effects of some of the system and process parameters on fiber formation and fiber diameter, the morphology of the electrospun fibers in terms of the surface characteristics and cross sectional shape will be discussed in the following sections.

5. USE OF NANO-INDENTATION AND NANO-SCRATCH TECHNIQUES TO INVESTIGATE NEAR SURFACE DENTAL MATERIAL PROPERTIES

In this chapter, the application of instrumented indentation devices to the measurement of the elastic modulus of polymeric materials is reviewed[115]. This review includes a summary of traditional analyses of load-penetration data and a discussion of associated uncertainties. Also, the use of scanning probe microscopes to measure the nanoscale surface roughness of tested polymers is discussed, particularly with regard to the associated limitations. The application of these methods to polymers often leads to measurements of elastic modulus that are somewhat higher in comparison to bulk measurements with potentially artificial trends in modulus as a function of penetration depth. Also, power law fits to indentation unloading curves are often a poor representation of the actual data, and the power law exponents tend to fall outside the theoretical range. These problems are likely caused by visco-elasticity, the effects of which have only been studied recently. Advancement of nanoindentation testing toward quantitative characterization of dental polymer composites properties will require material independent calibration procedures, polymer reference materials, advances in instrumentation, and new testing and analysis procedures that account for viscoelastic and viscoplastic polymer behavior.

Depth-sensing indentation (DSI) devices allow the amount of penetration of an indenter tip into a material to be measured often using either a constant loading rate or a constant displacement rate. Further, these devices are often capable of producing contact areas and penetration depths characterized by sub-micrometer or even nanometer dimensions for hard materials (e.g., single-crystal silicon, hardness = 14 GPa). One objective of using DSI methods is to produce quantitative, absolute measurements of elastic modulus, E. Producing such measurements with nanoscale spatial resolution can be a key to understanding mechanical behavior of technologically important material systems. However, polymeric materials create significant challenges to measuring E accurately using indentation testing.

First, many polymers are so soft that the material response cannot be measured at all with DSI devices because the system compliances are too low. Even for stiffer

polymers (E > 1 GPa), producing indents with both lateral and depth dimensions much less than 1 μm is rather difficult.

This difficulty is related to the load resolution, typically not better than ± 100 nN, and the inability of most DSI systems to detect initial contact loads less than 1 μN. Thus, although DSI systems are capable of applying maximum loads on the order of 1 μN, the smallest maximum loads applied in practice are typically tens of micronewtons to reduce the relative uncertainties in load and penetration depth. Finally, current analysis of DSI data is based on elasticity, which when applied to viscoelastic materials, could lead to large uncertainties in the calculated values of E. Thus, current DSI methods have limited capabilities for studying polymer thin films, polymer composites, and other important polymer systems for which obtaining property information with nanometer spatial resolution is often desired. Further, other calibration and procedural issues persist with regard to modulus measurements that must be addressed prior to the application of these methods to visco-elastic materials. For example, current calibration procedures used in DSI rely on indentation of a reference material with known modulus. Recent studies, including an inter-laboratory comparison, have shown the calibration results to have poor reproducibility and large uncertainties.

In this chapter, an overview of nanoindentation and its application to polymeric materials is given. First, traditional analyses of load-penetration data are presented followed by a discussion of uncertainty issues related to the determination of elastic modulus. The application of depth-sensing indentation to measurements of polymer response is then reviewed in chapters 7 and 8.

5.1 OVERVIEW OF NANOINDENTATION-THE METHOD OF OLIVER AND PHARR

The analysis of indentation load-penetration curves produced by depth-sensing indentation systems are often based on work by Oliver and Pharr[116]. Their analysis was in turn based upon relationships developed by Sneddon[117] for the penetration of a flat elastic half space by different probes with particular axisymmetric shapes (e.g., a flat-ended cylindrical punch, a parabolic of revolution, and a cone). In general, the relationships between penetration depth, h, and load, P, for such indenter geometries can be represented in the form

$$P = \alpha (h - h_f)^m \qquad (1)$$

where α contains geometric constants, the sample elastic modulus, the sample Poisson's ratio, the indenter elastic modulus, and the indenter Poisson's ratio, h_f is the final unloading depth, and m is a power law exponent that is related to the geometry of the indenter; for a flat-ended cylindrical punch, m = 1, for a parabolic of revolution, m = 1.5, and for a cone, m = 2. In applying Equation 1 to the calculation of modulus, Oliver and Pharr) made two significant realizations. First, the slope of the unloading curve changes constantly due to a constantly changing contact area. In prior research, the high load portion of the unloading curve was approximated as linear, which incorrectly assumes that the contact area remains constant for the initial unloading of the material. This practice created a dependence of calculated modulus values on the number of points used in the linear fit. Second, if the unloading curve can be fit by a power law expression (i.e., Equation 1), then a derivative, dP/dh, applied at the maximum loading point (h_{max}, P_{max}) should yield information about the state of contact at that point. This derivative was termed the contact stiffness, S, and is given by

$$S = 2aE_r = \frac{2\beta}{\sqrt{\pi}} E_r \sqrt{A} \qquad (2)$$

where *a* is the contact radius and A is the projected area of tip-sample contact. The reduced modulus, E_r, accounts for deformation of both the indenter and the sample and is given by

$$\frac{1}{E_r} = \frac{(1 - \nu^2)}{E} + \frac{(1 - \nu_i^2)}{E_i} \qquad (3)$$

where E and ν are the sample elastic modulus and Poisson's ratio, respectively, and E_i and ν_i are the elastic modulus and Poisson's ratio, respectively, of the indenter material. β is used to account for the triangular and square cross sections of many indenters used in nanoindentation studies. For β = 1, the cross section of the indenter is assumed to be circular, as the contact radius, *a*, is replaced by $(A/\pi)^{1/2}$, and Equation 2 (with β = 1) is valid for any indenter that has a shape described by a solid body of revolution of a smooth function. However, the values of β, as determined by King[118] using numerical

analysis, are only small corrections (e.g., β = 1.034 for a triangular punch) and are not often used in practice. Another correction factor has recently been suggested due to unrealistic boundary conditions used by Sneddon[117] and also Hertz[119]. This correction factor, γ, which depends upon the sample Poisson's ratio, ν, and tip geometry ranges from approximately 1.05 to 1.10 for ν between 0.1 and 0.4 and a conical indenter with an opening angle of 70.32°.

In Figure 5.1, an indentation load-displacement curve is illustrated along with several important parameters used in the Oliver and Pharr analysis. The stiffness, S*, is the slope of the tangent line to the unloading curve at the maximum loading point (h_{max}, P_{max}) and is given by

$$S^* = \left(\frac{dP}{dh}\right)_{(h_{max}, P_{max})} = \alpha m \left(h_{max} - h_f\right)^{m-1} \qquad (4)$$

where the parenthetic subscript denotes that the derivative is evaluated at the maximum loading point. When the displacement, h, is the total measured displacement of the system, S* is the total system stiffness. After successful calibration and removal of the load-frame compliance, the displacement of the load frame is removed so that h represents only the displacement of the tip into the sample. In this case, S* = S and the tangent line represents an unloading path for which the contact area does not change. Thus, the contact area, A, calculated using S (please see the Equation 2) should be the actual contact area at maximum load. Also, extrapolating this line down to P = 0 yields an intercept value for depth, h_i, which should be related to the contact depth, h_c, associated with the maximum loading point. However, h_c is related to the deformation behavior of the material and the shape of the indenter, as illustrated in Figure 2. In fact, $h_c = h_{max} - h_s$, where h_s is defined as the elastic displacement of the surface at the contact perimeter and can be calculated for specific geometries using displacement equations from Sneddon's analyses. For each of three specific tip shapes (flatened punch, parabolic of revolution, and cone), $h_s = \varepsilon P_{max}/S$ where ε is a function of the particular tip geometry, as summarized in Table 1. Thus, h_c is given by

$$h_c = h_{max} - \frac{\varepsilon P_{max}}{S} \qquad (5)$$

The nanoindentation procedures include calibration of the load-frame compliance, C_{lf}, and the tip shape area function, $A(h_c)$. Prior to the load-frame compliance calibration, the measured displacement, h_{total}, is a combination of displacement of the load frame, h_{lf}, and displacement of the sample, h_{samp}. Treating the system as two springs (the load frame and the sample) in series under a given load, P,

$$h_{total} = h_{lf} + h_{samp} \quad (6)$$

Dividing both sides by P,

$$C_{total} = C_{lf} + C_s = C_{lf} + \frac{\sqrt{\pi}}{2E_r}\frac{1}{\sqrt{A}} \quad (7)$$

where the total compliance $C_{total} = 1/S^*$ and the sample compliance $C_s = 1/S$. A number of possible methods exist for determining C_{lf} using a reference sample that is homogeneous and isotropic and for which both E and ν are known. Typically, a series of indentation measurements are made on the reference sample. Oliver and Pharr suggested using an iterative technique to calibrate both the load-frame compliance and the tip shape with one set of data from a single reference sample, as both C_{lf} and A are unknown in Equation 7. While this method has the advantage of not requiring an independent measurement of the area of each indent, its use has been limited, perhaps because it is mathematically intensive.

The use of the AFM with indentation measurements provides a method of high-resolution imaging of the plastic impression, which should have approximately the same projected area as the contact area at maximum load, particularly for a highly plastic reference material such as aluminum. Using this type of an approach, the measured compliance, C_{total}, can be plotted as a function of $1/\sqrt{A}$. A linear curve fit to the data can then be used to determine the load frame compliance, C_{lf}, which will be the value of the y-intercept. A third method and the one used in the present research is to assume that not only is E independent of penetration depth but also hardness, $H = P_{max}/A$. Thus, if H is constant, C_{total} can be plotted as a function of $1/\sqrt{P_{max}}$, and again the y-intercept of the fitted linear curve yields C_{lf}. In this method, aluminum is often replaced by fused silica, because oxide formation on aluminum can create variations in E and H with penetration depth.

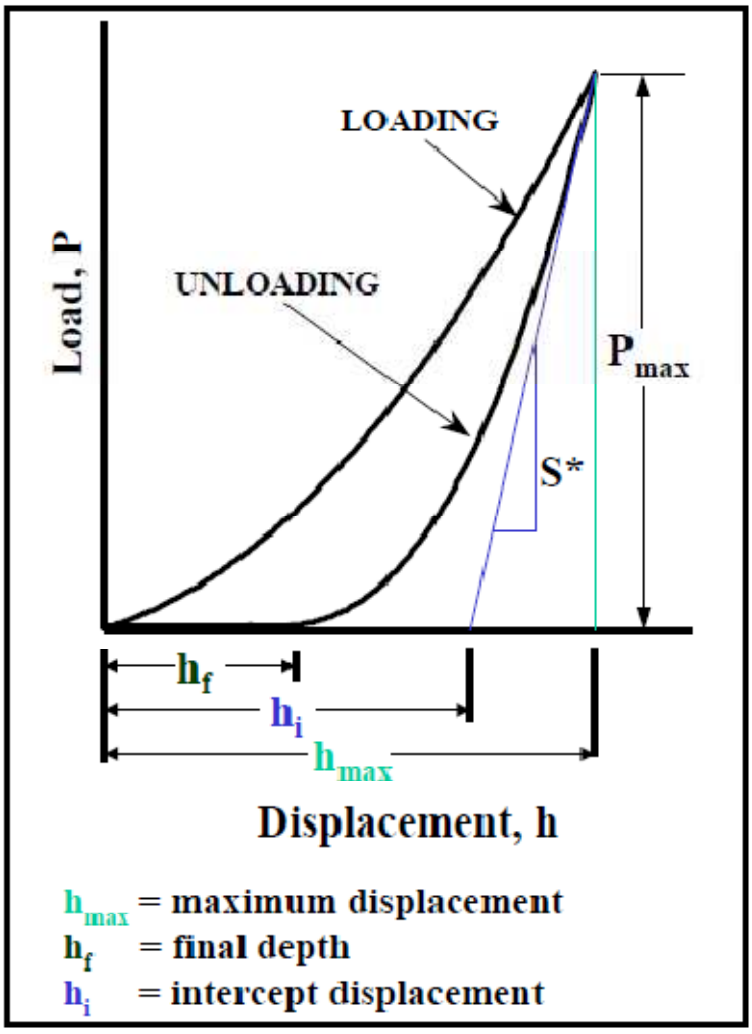

Figure 5.1 An indentation load-displacement curve in which several important parameters used in the Oliver and Pharr analysis are illustrated[120].

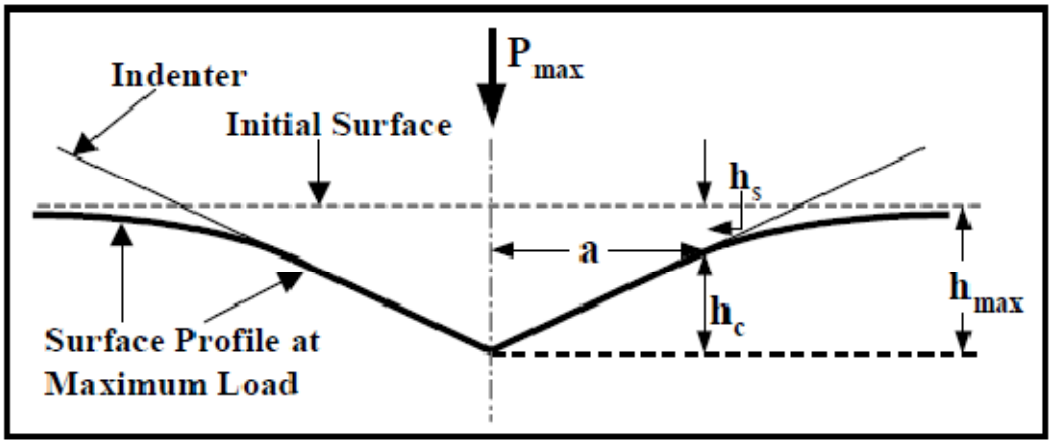

Figure 5.2 Illustration of the indentation geometry at maximum load for an ideal conical indenter[121]

Table 5.1. Theoretical values of m and ε for three axisymmetric tip shapes.

Tip Geometry	m	ε
Flat-ended cylindrical punch	1	1
Paraboloid of revolution	1.5	0.75
Cone	2	$2(\pi-2)/\pi$

For the load-frame compliance calibration, relatively large indentation loads and depths are applied to a reference material that exhibits significant plastic deformation (e.g. aluminum) so that the contact stiffness is large (C_s is small) and thus C_{total} is dominated by C_{lf}. For the tip shape calibration, the series of indents applied to a reference material typically covers a larger range of maximum load and maximum penetration depth. The objective of tip shape calibration is to measure the cross-sectional area of the indenter tip as a function of distance from the apex. In Figure 5.2, the indentation geometry for a conical indenter is illustrated in two dimensions. At a given load, P, the contact area, A, which is related to the contact radius, *a*, is the cross-sectional area of the indenter tip at a distance, h_c (the contact depth), from the tip apex. From measurements of h_{max}, P_{max}, and S, Equations 2 and 5 can be used to calculate A and h_c, respectively, for each indentation. A tip shape function, $A(h_c)$, is determined, given a sufficient number of measurements over a range of hc values, by fitting the A vs. h_c data, typically using a multiterm polynomial fit of the form:

$$A(h_c) = B_0 h_c^2 + B_1 h_c + B_2 h_c^{1/2} + B_3 h_c^{1/4} + \ldots \qquad (8)$$

where B0, B1,...,Bn are constant coefficients determined by the curve fit. Oliver and Pharr suggested using up to 9 terms (n = 8) with $B_0 = 24.5$, stating that the area function of a perfect Berkovich indenter, which was the type of indenter they used, is $A(h_c) = 24.5h_c^2$. The additional terms account for deviations from ideal geometry, such as blunting of the tip. Once the load frame compliance and tip shape calibrations have been performed, either separately or iteratively, measurements of elastic modulus for samples of interest can be made from indentation data. The unloading curves are again fit to a power law function (see Equation 1), and the fitting parameters are used to calculate S* (see Equation 4), which is equal to S assuming a correctly determined value of C_{lf}. S is then used to calculate h_c (see Equation 5), and h_c is used to calculate A from the tip shape area function. Finally, S and A are used to calculate E using Equation 2.

6. DYNAMIC MECHANICAL ANALYSIS OF DENTAL POLYMER COMPOSITES

Recent dental research has focused on making the physical properties of dental composite resins similar to those founded in tooth structure. However, variations still exist between composites and teeth, despite tremendous advances since the first generation of macrofilled composites. Basically, there are three main differences between the physical properties of tooth and composite: polymerization shrinkage, coefficient of thermal expansion and elastic modulus[122].

The elastic modulus is a very sensitive parameter for evaluating and ranking particle reinforced dental composites[123]. These restorative materials are being increasingly used in load-bearing areas of the posterior dentition[124] and are therefore inevitably subject to masticatory forces. When these forces stress the material below its elastic limit no plastic or permanent deformation occurs. However, when the elastic limit is exceeded, permanent damage starts. Typically, dental composites with low modulus will more readily elastically deform under functional stresses. Excessive elastic deformation of dental restorative material under functional stresses may result in catastrophic fracture of the surrounding brittle tooth structures, or alternatively, increased microleakage may result[125,126]. In such cases, enamel and dentin will be forced to carry more forces than originally intended, increasing the risk of cusp fracture. Additionally, the occlusal stresses generated during clinical service, whether intermittent or otherwise, also tend to disrupt the interfacial bonding between the deformed resin restoration and the restored teeth[127]. It may lead to interfacial gap formation and can contribute to microleakage, secondary caries and post-operative sensibility.

Conversely, composite materials with extremely high elastic modulus are unable to absorb occlusal vertical loading stresses. Consequently, masticatory stresses will be almost totally transmitted to the cavity walls, which can have a potential destructive effect on the prepared brittle tooth structure. Ausiello et al. showed that 90 GPa inlay ceramic restorations were unable to absorb occlusal vertical loading stresses that we totally transmitted to the cavity walls. On the other side, 50 GPa composite inlays

partially absorbed and partially transferred the stresses to the cavity walls. This indicates a greater stress-dissipating effect of the material with greater compliance, in this case the composite, thus minimizing the risks of tooth catastrophic fracture[128].
Moreover, extremely rigid materials cannot flow and compensate for the volumetric contraction stresses developed during polymerization, putting at risk the integrity of the adhesive interface between the composite and the tooth, and also increasing the risk of cusp fracture[129,130]. A possible solution to this problem may be the application of restorative materials that render the restoration sufficiently flexible to compensate for that part of the shrinkage that challenges the bond. As a result, the adhesive bond will remain intact, and marginal integrity will be preserved.

Ideally, the elastic properties of dental composites should be matched to those of the dental tissue they are supposed to replace[131,132]. It would minimize the differential movement between the restoration and the tooth during mastication, thus avoiding catastrophic failures. However, since enamel and dentin have distinct elastic properties and generally must be simultaneously replaced, two distinct restorative materials should be combined. Then, a more realistic concept would be choosing one of either, enamel or dentin, as a standard.

Many dental materials are visco-elastic, including the wide range of polymeric-based materials[133]. Logically, therefore, dental composite resins should be expected to exhibit some visco-elastic response. This gives a mismatch with the behavior of enamel at body temperature, but a closer match to that of dentine that has been shown to exhibit visco-elastic properties[134,135]. Consequently, the dental tissue to be chosen as standard - should be preferably the dentine. Thus, in order to survive in stress bearing areas in the oral environment, the elastic modulus of dental composites should be at least as high as dentin modulus[136], which is about 18 GPa[137], and preferably higher[138]. This corresponds to an imaginary volume percentage of filler of 60%[139]. Such composites would then be able to provide support at the interface with the tooth enamel, protecting the enamel rods at the margin from fracturing.

Ideally, materials would behave either entirely elastic and obey Hooke's Law, which states the stress in the sample is a function of deformation only and not a function of time, or entirely viscous and obey Newton's law of viscosity, which states the stress in the sample is a function of the rate of deformation[140]. Although these basic concepts

exist theoretically and in some very simple materials, such as steel and water, most materials such as polymers do not behave entirely as one of these two ideal classes of materials Such materials that behave neither as perfectly elastic solids, nor as completely viscous materials are described as visco-elastic materials[141].

In essence visco-elasticity defines how a material responds gradually to an applied stress reaching an ultimate value after a time lag. The phenomenon is caused by the chains of molecules within a polymer requiring time to fully adjust to the applied stress. Thus the more rapidly a stress is applied the shorter the time available for the molecules to relax and accommodate that stress.

A purely elastic material such as a spring retracts to its original position when stretched and released, whereas a viscous fluid retains its extended shape when pulled. A visco-elastic material combines these two properties - it returns to its original shape fter being stressed, but it does slowly enough to oppose the next cycle of vibration.
We could also say purely elastic materials are able to store all the energy applied during loading that is used for them to return to their original shape, while purely viscous materials do not return any of the energy applied during loading that is completely lost. On the other hand, visco-elastic materials, when deformed, store part of the loading energy within the material (elastic response), while some of the energy is dissipated as heat (viscous response). Once the load is removed, part of the material, corresponding to its elastic portion, returns to its original shape, while the other part, corresponding to material's viscous portion, undergoes permanent deformation.

The degree to which a material behaves either viscously or elastically depends on environmental temperature, vibration frequency, dynamic strain rate, static pre-load, time effects such as creep and relaxation, aging, and other irreversible effects. The most important parameters are temperature and frequency effects.

Dynamic tests such as dynamic mechanical analysis (DMA) are particularly well suited for visco-elastic materials, since they can determine both the elastic and viscous responses of a sample in one experiment[142]. This test works basically in the linear visco-elastic range, revealing fundamental properties over time, temperature and strain rate. This technique also allows the re-examination of the samples following particular treatments[143], which can be a valuable tool specially when monitoring the efficiency of polymerization during curing studies.

Since dental composites are exposed to dynamic loading rather than static loading, dynamic tests have become increasingly relevant[144]. While static tests obtain data related to a longer time scale than that of mastication[145], which can be a source of misleading results; dynamic tests better mimic the cyclic masticatory loading to which dental composites are clinically subjected. This might be extremely valuable to predict the clinical performance of biomaterials when working under the cyclic solicitations generated by the human body physiological movements.

6.1 THEORY ABOUT DYNAMIC MECHANICAL ANALYSIS

Dynamic Mechanical Analysis (DMA) is a method that has been used to acquire useful information about visco-elastic properties of dental composite resins as a function of time, temperature, and frequency.

With this technique a sample with well-defined dimensions is exposed to a sinusoidal mechanical deformation (strain) at fixed frequency or range of frequencies over a specific temperature range and also isothermally as a function of time and the corresponding forces measured[146]. This can be done in tensile, compression, shear, flexural and bending modes of operation. In an opposite way, the sample can be subjected to pre-selected force amplitude and the resulting deformation (strain) is measured. The more delayed the response, the more viscous the material while less delayed responses are characteristic of more elastic materials[147].

Briefly, the strain is a measure of the change in length of a material after a force is applied, and the stress is an internal force in a material equal and opposite to the applied load. When a sinusoidal stress is applied to a perfectly elastic solid the deformation occurs exactly in phase with the applied stress, hence the modulus is not time dependent. A completely viscous material will respond with the deformation lagging 90° behind the applied stress. However, when the stress is applied to a visco-elastic material, it will behave neither as a perfectly elastic nor as a perfectly viscous body and the resultant strain will lag behind the stress by some angles, where $s < 90°$ ([28; 40)]. The magnitude of the loss angle is dependent upon the amount of internal motion occurring in the same frequency range as the imposed stress[148].

The stress that is in phase with the applied strain is used to determine the elastic or storage modulus (*E'*), which is an indicator of elastic behavior and reveals the ability of the material to store elastic energy associated with recoverable elastic deformation. The stress that is out of phase with the applied strain is used to calculate the viscous or loss modulus *(E'')*. It is an indication of energy absorbed by the resin that is not returned elastically. Instead, this energy is used to increase segmental molecular vibration or to translate chain positions[149].

The loss tangent (*tan* δ) or mechanical damping is the phase angle between the dynamic strain and stress in the oscillating experiment. It is dimensionless and is given by the ratio of the viscous modulus to the elastic modulus[150]. This visco-elastic property is a measure of the mechanical energy dissipation or "loss" within the material in the form of heat. A perfectly elastic solid has *tan* $\delta = 0$[151]. Characteristically, the loss tangent reaches a maximum, or peak value, at the condition of temperature and/or frequency where the internal rate of molecular motion corresponds to the external driving frequency applied to the bulk specimen. The maximum of the loss tangent is frequently associated to the glass transition temperature (T_g) and the location of such "loss peaks" provides information about internal molecular mobility. The lower the loss tangent the quicker the material will respond to load (more elastic like), returning faster to its original shape, whereas the higher it is the higher the amount of energy lost as heat (more viscous like).

In the present study, the dynamic mechanical analysis of the composite materials was carried out using a DMA Q800 (TA Instruments, New Castle, USA) (Figure 6.1, left) linked to a Dell computer. The DMA Q800 consists of a temperature–controlled mechanical testing chamber that includes a furnace, a specimen holder, a motor-driven mechanical testing apparatus and a displacement measuring system. The computer is responsible for controlling experimental parameters and recording results. The DMA was set up for single cantilever mode (Figure 6.1, right) of flexural loading. This non-tensioning clamp contains two arms, a fixed and a moveable one which provides an oscillatory force using a non-contact direct driver motor, deforming the sample material. This instrument is designed to apply a reproducible force in the range of 0.0001-18 N, over a temperature range of -145 to 600 °C, using nitrogen as coolant. The oscillation amplitudes that can be selected by the operator in a dynamic experiment range from ±

0.5 to 10.000 μm. Due to instrument limitations the stiffness of the material must be considered during the selection of the test amplitude, since high amplitudes may not be accessible due to the high forces required to attain them.

The possible cooling rates range from 0.1 to 10 °C/min and the heating rates from 0.1 to 50 °C/min, although temperature ramp rates of more than 5 °C/min are not recommended for DMA experiments. This concern avoids the sample to lag the actual temperature and the transitions to be pushed to higher temperatures. However, the choice of ramp rate will depend on sample size, desired degree of accuracy in transitions and frequency or frequencies of interest, which can range from 0.01 to 200 Hz. This is the frequency range that the instrument's motor is capable of driving; however, the upper frequency that can be applied is dependent on the stiffness of the sample. The higher the sample stiffness the easier it will be to drive the sample at higher frequencies.

Figure 6.1 DMA Q800 (left) and single/double cantilever (right) simulating sample deformation.

7. THE EFFECT OF ALUMINA NANOFILLERS SIZE AND SHAPE ON MECHANICAL BEHAVIOR OF PMMA MATRIX COMPOSITE

Poly (methyl metacrylate) (PMMA) – has been used in a wide range of fields and applications such as: rear-lights and instrument clusters for vehicles, appliances and lenses for glasses. PMMA in the form of sheets affords panels for building windows, skylights, signs, displays, sanitary ware, LCD screens, furniture and many other applications where the transparency is an important factor[152]. Preparation of PMMA is an addition reaction that requires the presence of an initiator such as benzoyl peroxide which is decomposed either by heating or by the addition of a chemical activator such as dimethyl-p-toluidine that can serve in autopolymerization reaction.[153,154] PMMA polymer based materials are used as bone cement. Pure resin does not have enough strength and is reinforced using oxide particles or other fillers in order to obtain the material that can be used in load bearing conditions[155,156]. Another use of PMMA based resins is in dentistry for different applications such as denture basis, orthodontic appliances, and provisional restorations.[157]

Addition of fillers, in the form of alumina spherical nanoparticles having different shape and size, into the polymer, which serves as a matrix, improves the mechanical behavior of the obtained composite material. The addition of nanoparticles encounters the main problem of mixing and even distribution of nanoparticles in the matrix material because nanoparticles tend to agglomerate[158,159,160,161,162]. There were several techniques of enabling the good dispersion of nanoparticles and they include: direct mixing of polymer and nanoparticles, in-situ polymerization in the presence of nanoparticles, and simultaneous in-situ polymerization and nanoparticles formation[163]. Ultrasonication was reported to be the effective way to make a homogeneous dispersion of nanofillers in the monomer[164]. The main candidate materials for addition as nanofillers into polymer matrix are the fine nanoparticles of oxides such as silica[16513], titania[166], zirconia[167] and alumina[168]. Additions of oxide nanoparticles in the polymer matrix for preparation of bulk composites and films are the topic of a large number of research publications[169].

The shape of the fillers has also influenced the improvement of the composite mechanical properties[170,171,172].It is well known that the shape is very important when

describing the flow properties of the powder particles[173,174,175].As much the particle shape is important in flow characteristics of the fillers, it is important in the interaction with the composite matrix that results in the performance of the composite material on the macro scale.

The focus of this research was to study the influence of the shape and quantity of the alumina nanofillers addition in the PMMA polymer matrix on mechanical properties of the obtained composite material. Composites based on PMMA matrix with the addition of alumina nanofilers having different shape – spherical alumina nanoparticles and alumina whiskers were prepared. The mechanical behavior of the obtained composite was studied using the dynamic mechanical analysis (DMA) and nanoindentation techniques. The shape of the fillers and their distribution in the composite were studied using the scanning electron microscopy analysis. The dimensions of the reinforcements were measured using the image analysis techniques.

7.1 EXPERIMENTAL

The aluminum oxide spherical nanoparticles declared to have less than 50 nm diameter were produced by Aldrich. Alumina whiskers were also commercially available from Aldrich, and they were characterized by diameter 2 – 4 nm and length 200 – 400 nm. This enabled the use of very different alumina fillers having spherical alumina nanoparticles, with the length to diameter ratio of 1, and alumina whiskers having the length to diameter ratio of approximately 100.

Mecaprex KM, PRESI (Grenoble, France) autopolymerizing acrylic resins consisted of KM powder (PMMA powder containing dibenzoyl peroxide (DBPO) initiator) and of KM liquid monomer (methylmetaacrylate monomer - MMA with N, N-dimethyl-p-toluidine used as an activator). Alumina spherical nanoparticles or alumina whiskers were added to KM liquid. The mixture was sonicated for 60 min and KM powder was dispersed in the mixture. The mixing was done by hand during 2 min and the mixture was poured out in the form having dimensions suitable for DMA and nanoindentation testing. The form was covered using the glass cover to ensure that the surface of the specimen remains smooth. PMMA/MMA mass ratio of 0.75 was used as this ratio enables minimization of shrinkage as suggested by the manufacturer (PRESI)

and as previously reported in the literature. The polymerization of the monomer was done at a temperature of 25 °C. The instruction for use given by the producer says that the polymerization is complete at temperature between 20 and 23 °C for 20 min. The obtained composites were then exposed to a temperature of 37 °C during 30 days before they were mechanically tested in order to obtain the stabile composition of the polymer matrix of the composite. Table 7.1 summarizes the compositions of the composites PMMA/alumina whiskers and PMMA/alumina spherical nanoparticles prepared for analysis in this paper. The samples prepared using the alumina spherical nanoparticles as fillers are annotated as P1, P3 and P5 for the addition of 1 wt. %, 3 wt. % and 5 wt. % of the filler respectively. The samples using alumina whiskers as fillers were annotated as W1, W3 and W5 for the addition of 1 wt. %, 3 wt. % and 5 wt. % alumina whiskers respectively.

Table 7.1 The compositions of composite specimens prepared using the PMMA as the matrix and alumina spherical nano particles and alumina whiskers as fillers.

Sample description	Sample identification	Quantity of particles/whiskers, g	Mass MMA+initiator, g	Mass PMMA, g
PMMA without filler	PMMA	-	2.290	1.710
PMMA with 1 wt. % alumina spherical nanoparticles	P1	0.045	2.540	1.910
PMMA with 3 wt. % alumina spherical nanoparticles	P3	0.135	2.540	1.870
PMMA with 5 wt. % alumina spherical nanoparticles	P5	0.225	2.440	1.830
PMMA with 1 wt. % alumina whisker	W1	0.045	2.540	1.910
PMMA with 3 wt. % alumina whisker	W3	0.135	2.540	1.870
PMMA with 5 wt. % alumina whisker	W5	0.225	2.440	1.830

The mechanical behaviors of neat polymer and PMMA/alumina fillers nanocomposites were studied by dynamic mechanical analysis (DMA) - cantilever-bending and force control nanoindentation. The scanning electron microscopy was used to study the morphology of the alumina spherical nanoparticles and alumina whiskers prior to incorporation into the polymer and to study the distribution of the alumina spherical nanoparticles and alumina whiskers in the matrix after polymerization.

7.2 METHODS OF CHARACTERISATION

DMA analyses

Dynamic mechanical analysis was used to examine the performance of the PMMA matrix composite reinforced using alumina spherical nanoparticles or alumina whiskers and to measure the influence of alumina fillers shape on the behavior of the resulting materials. The data obtained from this analysis include: the storage modulus (*E'*), tangent delta (tan δ) and glass transition temperature (T_g). The storage modulus reveals the ability of the composite to store elastic energy associated with recoverable elastic deformation. Together with tangent delta the storage modulus describes the behavior of the composite under stress in the defined temperature range. Dynamic mechanical analysis (DMA) was performed by (DMA Q800, TA Instruments) under a nitrogen atmosphere and single cantilever mode. Storage modulus (*E'*) and loss factor (tan δ) were calculated for rectangular specimens of the size 35 mm × 13 mm × 3 mm at frequency ω = 1 Hz. Temperature range was changed from room temperature to 160 °C with a heating rate of 3 °C/min.

Nanoindentation

The nanoindentation test was performed using a Hysitron TI 950 TriboIndenter equipped with in-situ SPM imaging (Hysitron, MN). The Berkovich indenter has an average radius of curvature of about 100 nm. Tests were performed in force-controlled feedback mode. The indentation maximum load was set at 4 mN for each tested sample. The loading and unloading times as well as the hold time at the peak force were set to

25 s each. For each loading/hold/unloading cycle, the applied load value is plotted with respect to the corresponding position of the indenter. The resulting load/displacement curves provides data specific to the mechanical nature of the material under examination. All the results are obtained with the Oliver & Pharr method and using a supposed sample Poisson's ratio of 0.36 for reduced elastic modulus calculation. Established models are used to calculate quantitative indentation hardness (*H*) and reduced elastic modulus values (*E*) for such data.

The specimens were polished using the alumina paste having the abrasive grains up to 0.02 μm until flat surface was obtained. The specimens were about 1 mm thick, having dimensions 3 × 3 × 2 mm and were placed on the specimen holder in the nanoindenter. Loads of 4 mN were used for the tests. In order to obtain reliable results, 9 indentations were made for each type of sample on random locations.

Analysis of the morphology of the specimens

The morphology of the alumina spherical nanoparticles was examined using a field emission scanning electron microscope (FESEM), MIRA3 TESCAN, operated at 20 kV. The morphology of the samples was examined using a scanning electron microscope (SEM), Jeol JSM 5800, operated at 20 kV.

7.3 RESULTS AND DISCUSSION

Very fine alumina spherical nanoparticles and alumina whiskers tend to agglomerate and they are delivered in their agglomerated form from the producer. Figure 1 shows, field emission scanning electron microscopy (FESEM) micrographs of alumina spherical nanoparticles and alumina whiskers, which were agglomerated prior to sonication. The mean diameter of alumina spherical nanoparticle agglomerates as received from producer was 87 μm and that for alumina whiskers was of 1.1 μm. Those values were obtained using image analysis tools applied to the images shown in Figure 7.1.

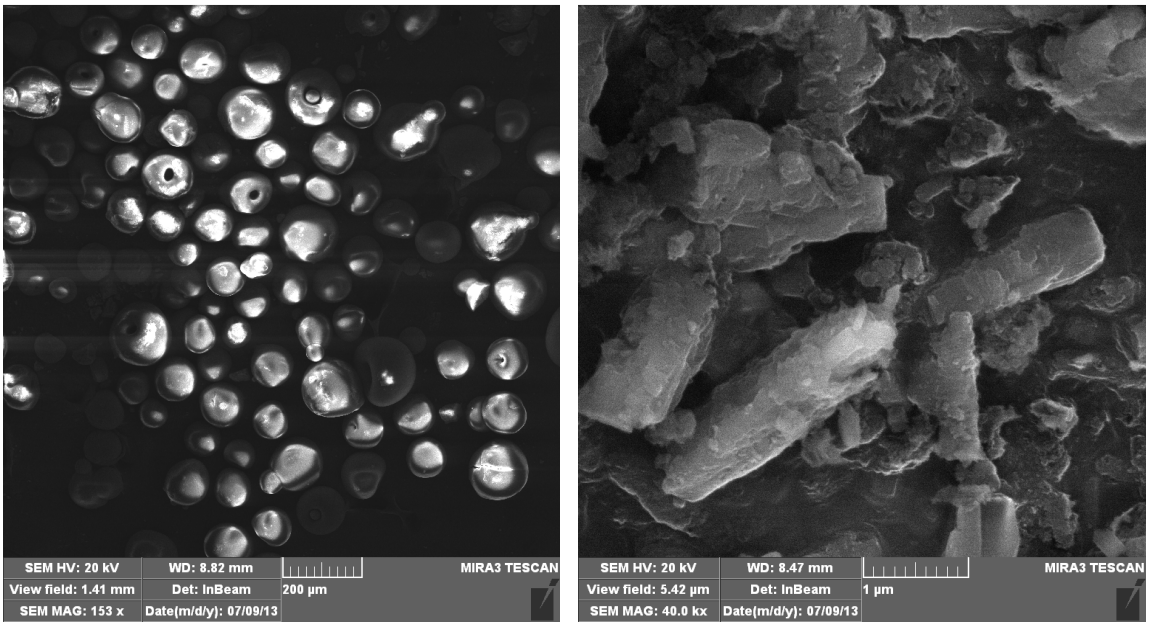

a) **b)**

Figure 7.1 The FESEM micrographs of alumina nanoparticles and whiskers, agglomerated prior to sonication, as received from the producer a) particles agglomerates having a mean diameter of 87 µm b) whiskers having a mean diameter of 1.1 µm.

The morphology of the samples having 3 wt. % of alumina spherical nanoparticles and 3 wt. % of alumina whiskers and of the polymer without reinforcement were examined using a scanning electron microscope (SEM), Jeol JSM 5800, operated at 20 kV, Figure 7.2. In Figure 7.2b the micrograph of the sample having 3 wt. % of alumina whiskers is given and in Figure 7.2c the micrograph of the composite having 3 wt. % of alumina spherical nanoparticles is presented. Those images were used to measure the diameters of the alumina spherical nanoparticles agglomerates still visible in the micrograph. The measurements made on the Figure 7.2c show that the mean diameter of alumina spherical nanoparticle agglomerates decreased to 0.47 µm in the composite containing 3 wt. % spherical alumina nanoparticles. The main length of alumina whiskers agglomerates visible in the composite was reduced to 0.27 µm. The sensible reduction in visible alumina spherical nanoparticle agglomerates sizes, as well as the reduction in visible alumina whiskers agglomerates sizes indicate that the agglomerates dimensions were reduced and that the alumina spherical nanoparticles and

alumina whiskers that were not in agglomerates were well distributed in the polymer giving the improvement of mechanical properties.

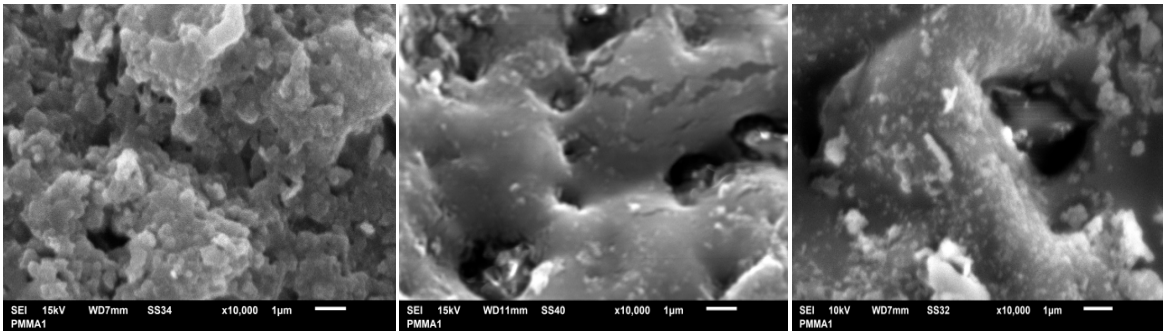

a) **b)** **c)**

Figure 7.2 The SEM micrographs of a) PMMA without the addition of reinforcement, b) composite having PMMA matrix and 3 wt. % of alumina whiskers and c) composite having PMMA matrix 3 wt. % of alumina spherical nanoparticles

DMA was used to compare the behavior of the pure PMMA to the behavior of the composites with additions of alumina fillers. It was observed that incorporation of both spherical alumina nanoparticles and alumina whiskers results in an increase in storage modulus values for the composite in the range of temperatures measured, Figure 7.3.

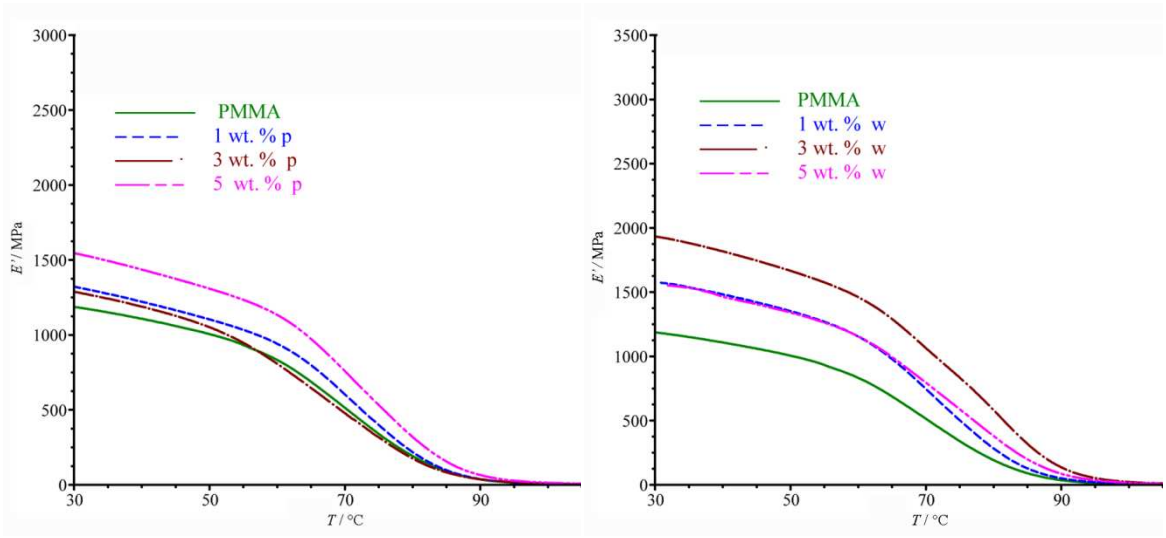

a) **b)**

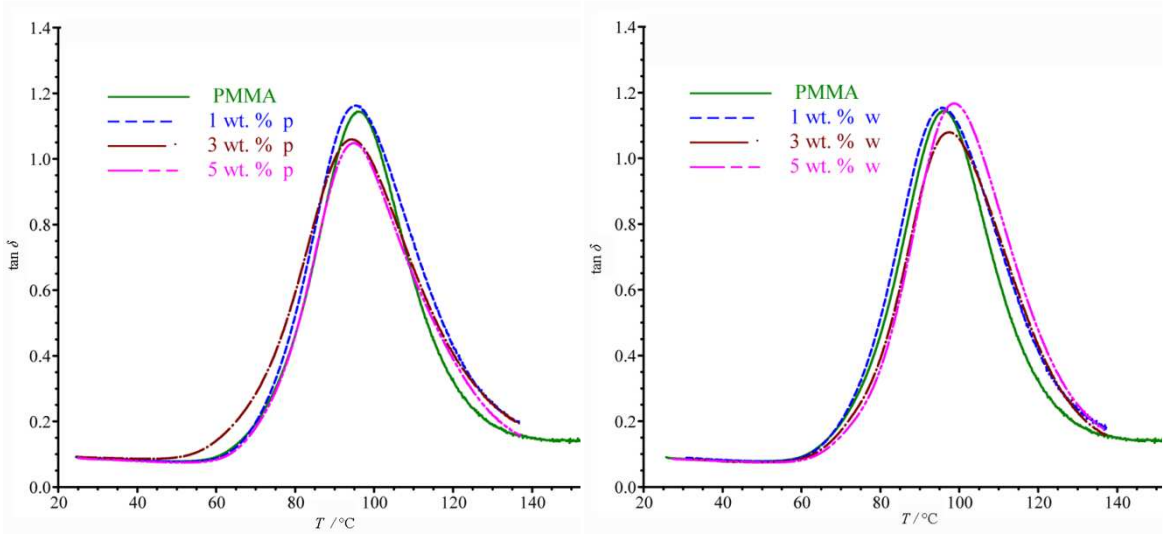

c) **d)**

Figure 7.3 The thermomechanical spectra of PMMA matrix/alumina spherical nanoparticles and PMMA matrix alumina whisker composites. a) Storage modulus of the PMMA matrix composite reinforced using alumina spherical nanoparticles changes vs. temperature. b) Storage modulus changes vs. temperature for the PMMA matrix composite reinforced using alumina whiskers. c) Dependence of tan δ on temperature for composites reinforced using alumina spherical nanoparticles. d) Dependence of tan δ on temperature for PMMA matrix composites reinforced using alumina whiskers.

The glass transition temperature T_g can be determined from the DMA results as the maximum of the curve showing the dependence of tan δ vs. temperature. In Figure 7.4 the changes of T_g are shown depending on the type and quantity of additives. Composites having 3 wt. % of added alumina whiskers show that the increase of the T_g value is of 3 °C which is the maximum increase observed in specimens prepared in the scope of this research. For samples where the addition of spherical alumina nanoparticles was tested the highest value of T_g increase is also observed in the composite with 3 wt. % of added alumina spherical nanoparticles, but this increase is less significant. This proves that both the alumina spherical nanoparticles as well as alumina whiskers were in good contact with the matrix.

In Figure 7.3 the storage modulus for composites having PMMA matrix and alumina spherical nanoparticles or alumina whiskers as reinforcements were compared to the values for the polymer PMMA. The composite having the addition of 3 wt. % of

spherical alumina nanoparticles shows the largest increase of the storage modulus value among the composites prepared with spherical alumina nanoparticles, this increase was of 23 %. All the composites having the alumina whiskers as reinforcements show the increase in storage modulus compared to pure PMMA. The addition of 3 wt. % alumina whiskers gives an increase of 63%. The addition of 5 wt. % of alumina whiskers did not improve the storage modulus value more than the addition of 3 wt. % of alumina whiskers and this could be explained by the difficulty of mixing and agglomerate braking when the concentration of alumina whiskers is larger than 3 wt. %. Values of tan δ presented in Figure 7.6 are in accordance with observations made for the storage modulus.

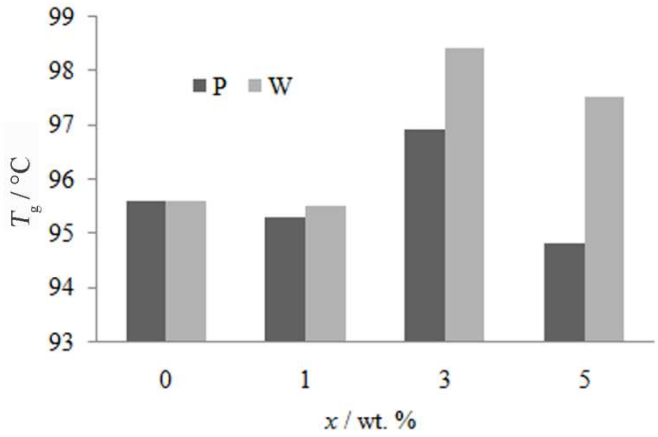

Figure 7. 4 The changes of T_g of the PMMA matrix composite materials having spherical alumina nanoparticles or alumina whiskers as additives.

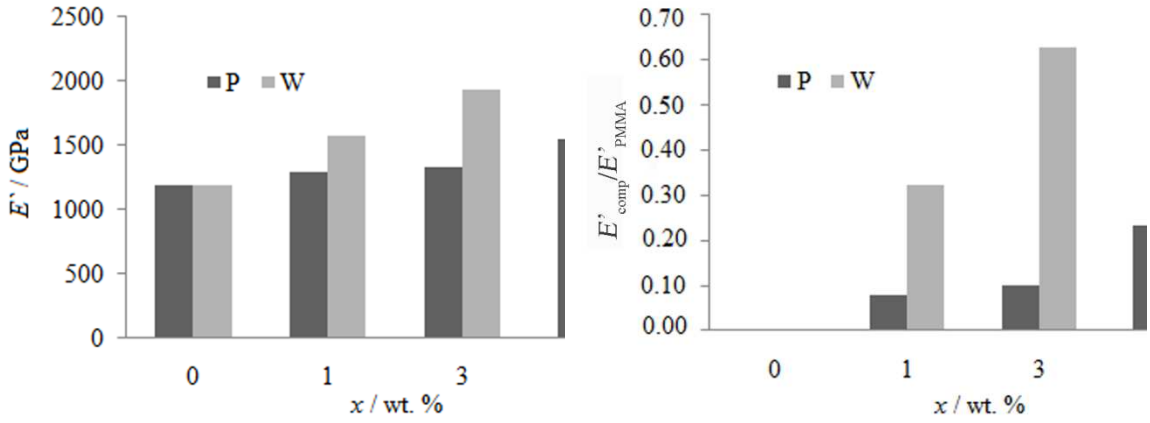

Figure 7.5 The dependence of E' of the composites having PMMA matrix composite materials having spherical alumina nanoparticles or alumina whiskers as additives.

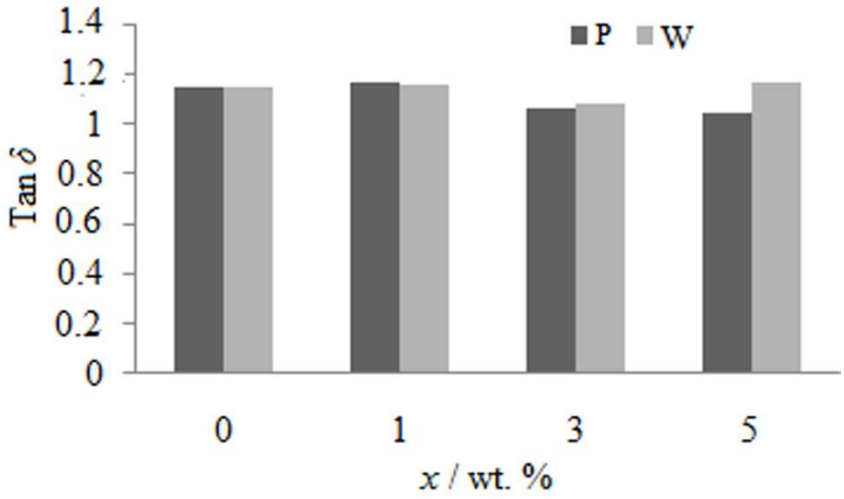

Figure 7.6 Dependance of tan δ on the quantity and morphology of added reinforcement into the PMMA matrix composite materials having spherical alumina nanoparticles or alumina whiskers as additives.

DMA gave the characteristics of the composite at the macro - level and those properties are describing the entire specimen behavior under load at different temperatures. The nanoindentation gives the possibility to study properties of the composite at the nano and micro level. From nanoindentation results it is possible to study if the properties have even values in all parts of the specimen in the composite and to discuss the possible inhomogeneity of the distribution of the reinforcement in the composite.

The obtained results gave the insight about the influence of the alumina fillers shape and the amount of alumina fillers added to the obtained mechanical properties of PMMA matrix composite. In figure 5 the data showing the changes of modulus of elasticity of the PMMA matrix/alumina spherical nanoparticles and PMMA matrix/alumina whisker composites depending on the type and amount of alumina fillers added are given. It could be seen that both the alumina spherical nanoparticles and alumina whiskers are making the composites stiffer compared to the PMMA polymer, even if only 1 wt. % of alumina spherical nanoparticles is added. Addition of alumina spherical nanoparticles into the composition did not dramatically change the

values of mechanical properties, modulus and hardness, of the obtained composite. Addition of 3 wt. % alumina spherical nanoparticles resulted in the composite material having the properties that had higher values of modulus of elasticity and hardness as measured using the nanoindentation method. Addition of 5 wt. % of alumina spherical nanoparticles did not improve additionally the mechanical properties of the PMMA matrix composite. The improvement of mechanical properties obtained using 1 wt. % of alumina whiskers gave better properties than the PMMA matrix composite with the addition of the same quantity of alumina spherical nanoparticles. The addition of 3 wt. % of whiskers gave maximum stiffness improvement of the PMMA matrix composite material and the obtained composite had the maximum value of the modulus of elasticity that was improved by 56 % compared to the polymer without reinforcement. The addition of 5 wt. % of alumina whiskers did not further improve the values of mechanical properties measured using nanoindentation method. From the data presented the addition of 3 wt. % of alumina whiskers is giving the material having the best modulus of elasticity and this is a considerable reinforcement for a small addition of alumina spherical nanoparticles.

The results of hardness measurement have the same trend as those for the modulus of elasticity for PMMA matrix/alumina spherical nanoparticle composites. The addition of 1 wt. % of alumina spherical nanoparticles gives a slight deterioration of the hardness of the material. The PMMA matrix composite with 3 wt. % of alumina spherical nanoparticles gave the best performance concerning hardness of the PMMA/alumina spherical nanoparticles composite. Addition of 5 wt. % of alumina whiskers did not improve additionally the hardness of the PMMA matrix composite. The addition of 3 wt. % of alumina whiskers gives the increase in hardness of the material that is a 40 % improvement compared to the PMMA polymer without the addition of the fillers.

The comparison of the nanoindentation curves for the PMMA polymer without the addition of reinforcement and for composites having 3 wt. % of alumina spherical nanoparticles and 3 wt. % alumina whiskers are given in Figure 7.7.

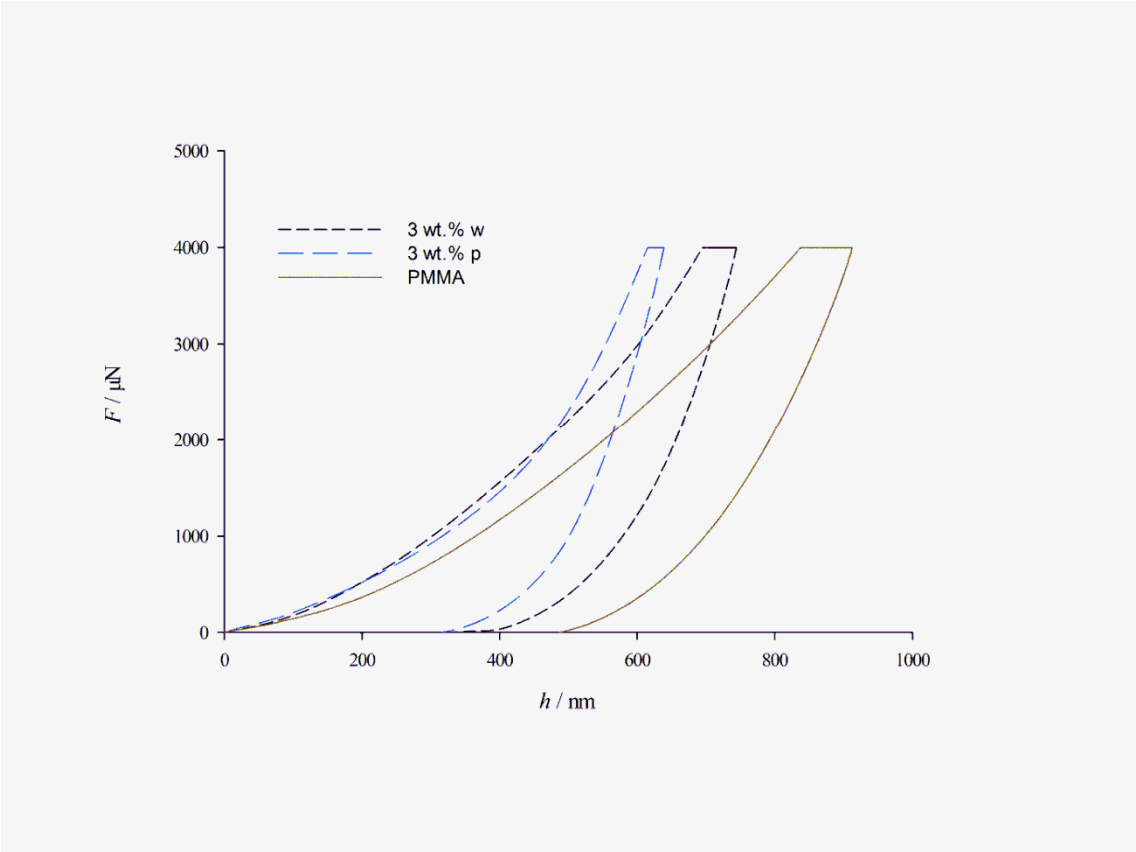

Figure 7.7 Nanoindentation curves showing the dependence of the force on displacement for the PMMA polymer and the composite having 3 wt. % of alumina spherical nanoparticles and alumina whiskers.

Comparison of DMA and nanoindentation results

Both the nanoindentation measurements of modulus of elasticity and hardness and the DMA measurement of the storage modulus prove that the composite having 3 wt. % of alumina whiskers is having the best mechanical properties among the composites studied. The nanoindentation (Figures 7.8 and 7.9) and DMA (Figure 7.5) results are in accordance proving that the addition of alumina spherical nanoparticles is less efficient compared to the addition of alumina whiskers having a very high value of length to diameter ratio.

When comparing the obtained results, reinforcing the PMMA matrix of a composite using alumina spherical nanoparticles, to those obtained from reinforcing the same PMMA polymer using functionalized silica particles, it could be observed that the

improvement of the properties obtained using the functionalized silica particles gives better values of the mechanical properties, modulus of elasticity and hardness, than the values in this study[176]. The preparation of the samples in this study was done using the instructions obtained from the producer and the specimens were left at a temperature of 37 °C for 30 days. In the other study the specimens were heated at 60 °C after the preparation and later up to 110 °C in order to eliminate stress and residual monomer. It is possible that the conditions that include heat treatment of the specimen eliminate completely the monomer from the composition and that in the case when only the temperature of 37 °C during 30 days was applied did not enable the complete monomer conversion. This could be the reason that the small amount of left monomer was present and it served as a plasticizer in the composite. The content of the residual monomer and allergic or cytotoxic effect of denture base acrylic resins may be related to powder to liquid ratio, storage time, temperature, polymerization method and it will be the subject of our next study. In this paper, basic research has focused on the influence of nanoparticle size, shape and nanoparticle loading on mechanical properties of acrylic polymers.

As it is shown alumina nanofillers have the possibility to improve the values of mechanical properties of the polymer when added in a very small amount. Similar improvements of values of mechanical properties could be obtained using very high loadings of functionalized microparticles of alumina. In order to obtain the improvement of the mechanical properties in the same range as those obtained with the addition of 3 wt. % of alumina whiskers 30 % of functionalized microparticles were added to a polymer matrix.

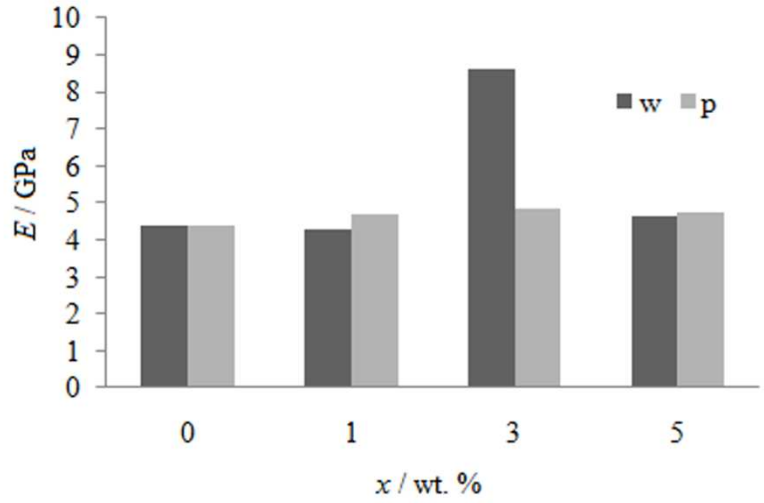

Figure 7. 8 Dependence of modulus of elasticity measured during nanoindentation tests for PMMA matrix composite materials having spherical alumina nanoparticles or alumina whiskers as additives.

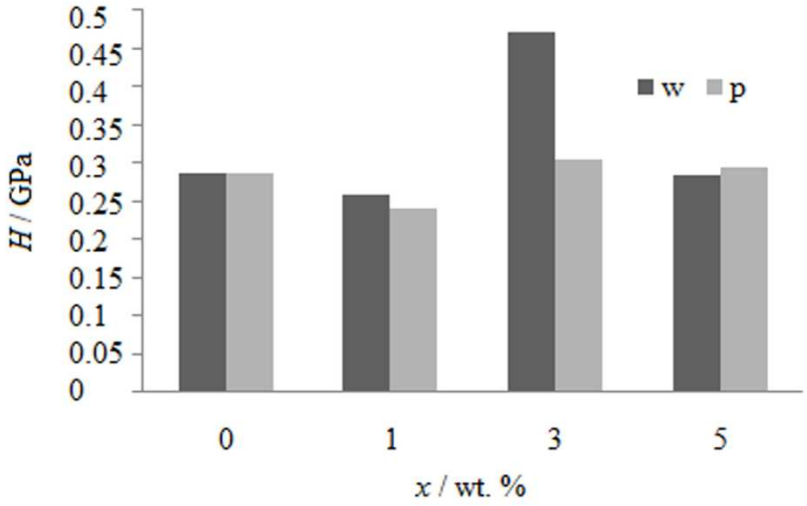

Figure 7.9 The summary of results from naniondentation testing of PMMA matrix composite materials having spherical alumina nanoparticles or alumina whiskers.

8. PREPARATION AND CHARACTERIZATION OF POLY (VINYL BUTYRAL) ELECTROSPUN NANOCOMPOSITE FIBERS REINFORCED BY ULTRASONICALLY IRRADIATED SEPIOLITE

Electrospinning offers a simple method for production of micro and nanocomposite fibers. Nanocomposite fibers constitute a new class of materials in which the polymeric nanofibers are reinforced by dispersed inorganic fillers with at least one dimension in nanometer-scale. In addition, electrospinning has following advantages: (a) the diameters of fibrous materials are reduced from micrometers to nanometers (b) it can produce nanofibrous mats with large surface area to mass ratio for better bonding and excellent mechanical strength of the matrix material; (c) it allows the nanoparticles to disperse in the spin solution; and (d) it does not compromise the chemical stability of the nanoparticles during spinning and composite fabrication. Electrospun fibers have also found increased uses in many other applications, including multifunctional membranes, biomedical structural elements (scaffolding used in tissue engineering, wound dressing and drug delivery), composite reinforcement and high surface area fabrics for protective clothing and sensors[177]. In particular, thick patterned nanofibrous mats are more valuable in scaffolds, drug carriers, and filters[178].

Nanoparticle-based materials have been attracting a growing interest in the different fields. However, the main difficulty in working with nanoparticles is their undesirable tendency to form larger particles by agglomeration. To prevent formation of aggregates, silane coupling agents have been extensively used. Silane bonding is one of the most popular surface modifications of silica, which also has silanol groups on the surface[179] . In the case of sepiolite, a number of chemical modifications of surfaces have been published in scientific papers: modifications with quaternary ammonium salts or amines, or with organosilane, usually in toluene[180,181,182]. There is very strong limitation of all the silane modification processes, impregnation or suspension in organic solvents, in that the surface modification is not produced on the surface of individualized sepiolite fibers but on the external surface of the sepiolite aggregates, since highly

hydrophilic sepiolite is not finely dispersed in these solvents. The surface modification in the form of thixotropic aqueous gel is better than surface grafting in toluene[183]. It is possible to modify almost-individual sepiolite fibers by carrying out surface modification reactions in the form of thixotropic aqueous gels, which makes possible the separation of sepiolite aggregates into individual fibers[184].

A wide range of applications may be expected from such functional nanocomposite fibers. Various types of inorganic nanofillers such as silica, alumina, carbon nanotubes, titania and clay have been used to produce polymer/inorganic nanofibers and to improve thermo-mechanical properties. Composite nanofibrous mats was prepared from thermoplastic polyurethane/silica nanoparticles, which gold nanoparticles adsorbed using further treatment with 3-aminopropyltriethoxysilane, demonstrating that the composite fibers could be used as functional fibers[185]. Nanofibers having α-alumina structure are excellent candidates to be used as reinforcement for polymer matrix composites, as well as to prepare the non-woven products having good chemical stability[186],[187]. Well-dispersed multiwalled carbon nanotube (MWNT)/PVB nanocomposite fibers were prepared by electrospinning, with enhanced electrical, mechanical, and thermal properties[188]. Photocatalyst TiO_2 nanotubes were obtained by calcination of precursor nanofibers of poly (vinyl alcohol) (PVA)-titanium compound hybrids [189]. The incorporation of clay nanolayers increases the dimensional stability, thermal and mechanical properties of the functional fibers compared with other fillers due to their layered structure. Most functional clay nanofibers exhibit these improvements in performance at relatively low loadings, which caused a decrease in the mean diameter of the nanocomposite fibers[190].

The approach that has been adopted in this study is to include neat and modified sepiolite fibers directly into electrospun fibers from PVB solutions, thus circumventing the problem of fibers aggregation. In the present study, the ultrasonic irradiation technique has been used for modification and dispersion of sepiolite fibers into large surface area composite nanofibrous mats. Furthermore, the incorporation of sepiolite nanofibers can change the thermo-mechanical properties of patterned nanofibrous mats. Up to our knowledge, the selected sepiolite/PVB nanocomposite system is not previously reported in the literature.

8.1 MATERIALS AND METHODS

PVB is a resin usually used for applications that require strong binding, optical clarity, adhesion to many surfaces, toughness and flexibility. It is prepared from poly (vinyl alcohol) by reaction with butyraldehyde. PVB (Mowital B75H, dynamic viscosity of 5 wt% solution in ethanol 160–260 mPa·S) was purchased from Kuraray. The experiments were carried out with the PVB solution in concentration of 10 wt% where ethanol was used as the solvent[191].

The natural sepiolite (Tolića kosa, Serbia) with a specific surface area of 292 m^2/g (BET surface area measurements), has been used as reinforcement filler for nanocomposite fibers in order to influence its fibrous morphology and low production cost. Sepiolite was ultrasonicated (Sonics Vibra Cell, VCX 750, 19 mm Ti horn, 20 kHz) for 20 min in water to disintegrate bundles and dried for two hours in the oven at 100 °C. The isolated fibers were treated with γ-aminopropyltriethoxysilane (Dynasylan®AMEO, Evonik-Degussa). Modification of sepiolite fibers with AMEO silane (5.4 g/4.0 g Sep) was carried out by ultrasonic irradiation (20 min) of the sepiolite aqueous gel in water. Modified sepiolite fibers were dried in the oven at 100 °C overnight, centrifuged (3000 rpm, 15 min), washed with dichloromethane at least five times to remove the excess of AMEO silane and, finally, dried under vacuum at 100 °C for 12 h. The neat and the modified sepiolite fibers were put into the PVB/ethanol solution and ultrasonically irradiated for 15 min and then stirred continuously for 24 hours.

Subsequently, sepiolite filled composite fibers have been produced by electrospinning technique. Electrospinning apparatus (Electrospinner CH-01, Linari Engineering) consisted of a 20 ml plastic syringe with a metallic needle of 0.8 mm inner diameter placed on the syringe pump (R-100E, RAZEL Scientific Instruments) and the high-voltage power supply (Spellman High Voltage Electronics Corporation, Model: PCM50P120). A set of experiments was carried out when the applied voltages were V = 16, 20, 24, 28 and 30 kV while the flow rate was Q = 0.2, 0.5 and 1 mL/h with the content of neat sepiolite 3 wt. %. Another experimental set was performed with flow rates valued Q = 0.5 mL/h, while the voltage was held at V = 24 kV, with the content of the neat and modified sepiolite nanofibers 3 wt. %, 30 wt. %, and 50 wt. %. The tip-to-

collector distance was h = 15 cm in all cases. Tip was set up vertically above the collector. Fibers were electrospun at room temperature with deposition time of 2 h. The electrospun fibrous mats of the PVB/Sep fibers were collected on alkaline-resistant fiberglass mesh in the form of a patterned nanofibrous mats and kept in air for 15 h to dry out.

The following instruments were used for characterization of the neat, modified sepiolite and electrospun nanofibrous mats. Fourier transform infrared (FTIR) spectra of the neat, modified sepiolite fibers and AMEO silane in KBr pellets were obtained in transmission mode between 400 and 4000 cm^{-1} with a resolution of 4 cm^{-1} using a BOMEM spectrophotometer (Hartmann & Braun, MB-series). Nitrogen-adsorption-desorption isotherms were determined using Micromeritics ASAP 2020. The sepiolite samples were degassed at 150 ºC for 10 h under reduced pressure. The specific surface area of samples was calculated using the Brunauer-Emmett-Teller (BET) method from linear part of the nitrogen adsorption isotherms. The morphology of as-spun fibers was investigated both by optical microscopy (OLYMPUS CX41) and field emission scanning electron microscopy (FESEM) on a MIRA3 TESCAN electron microscope at 20 kV. The fiber diameter distributions of the electrospun fibers were measured using Image-Pro Plus analysis software. Dynamic mechanical analysis (DMA, Q800 TA Instruments) was conducted in a dual cantilever mode (using the stainless still sample holder) at a frequency of 1 Hz where the temperature ranged from 30 °C to 100 °C with a heating rate of 3 °C/min for the determination of normalized complex modulus, (E_n*), loss tangent (*tan* δ) and the ratio between *E''* and *E'* (*Cole-Cole* plot).

8.2 RESULTS AND DISCUSSION

Fourier transform infrared measurement

Figure 8.1 (a) shows the typical infrared spectra of neat sepiolite fibers. The Mg-OH bands are assigned at 3686 cm^{-1} and 644 cm^{-1}. The Si-O-Si vibrations are present at 1014 cm^{-1} and the vibrations from bonded water occur at 1659 cm^{-1}, a shoulder from the Si-O group appears at 1219 cm^{-1}. There is a broad extended band at 3431 cm^{-1} (zeolitic water) with smaller band at 3572 cm^{-1} (structural bound water), which suggests that the

surface of the sepiolite fibers is covered by a compact layer of zeolitic and adsorbed water. Figure 8.1 (b) shows the infrared spectra of the modified sepiolite fibers. After sepiolite is modified by AMEO silane, the IR spectrum shows that the new characteristic absorption bands of 2932 cm^{-1} and 2850 cm^{-1}, which are assigned to ν_{as} and ν_s of the C–H bond of $–CH_2–$ group, respectively. In addition, in IR spectrum of modified sepiolite fibers the intensity of absorption bands from bonded water and structural OH groups decreases. The decrease in the OH bonds in modified fibers is assigned to covalent bonding between the sepiolite silanol groups and AMEO silane[192].

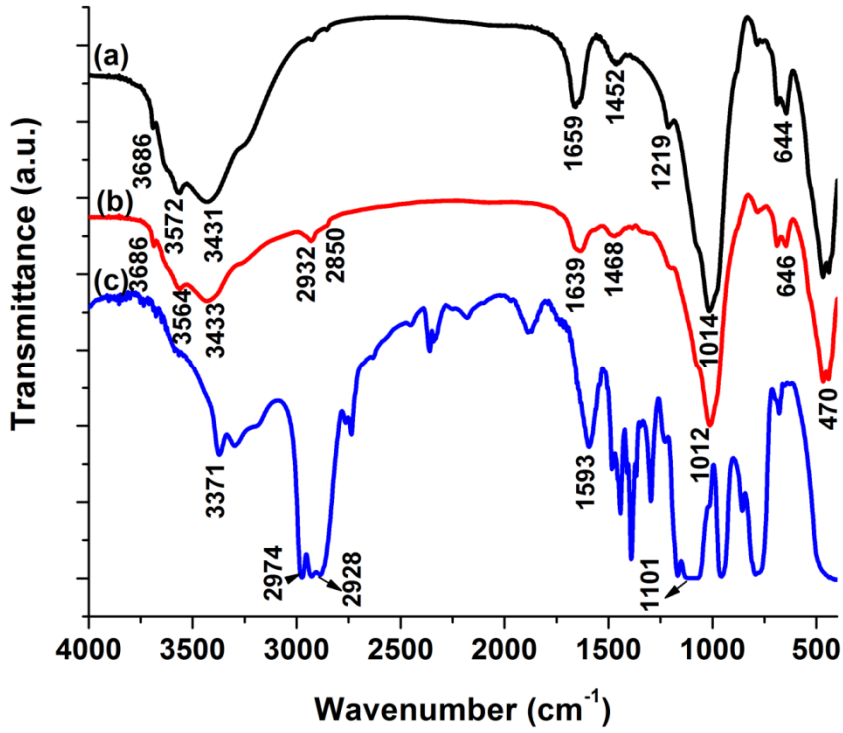

Figure 8.1 FTIR spectra of (a) neat sepiolite fibers, (b) modified sepiolite fibers and (c) AMEO silane

Fiber dimension and morphology

Sepiolite is a magnesium hydrated silicate of fibrous morphology, with fine microporous channels of dimensions 0.37–1.06 nm running parallel to the length of the fibers, with the ideal formula $Si_{12}0_{30}Mg_8(OH)_4–(H_2O)_{4.8}H_{20}$. Sepiolite has the highest

specific surface area of all the clay minerals, with a high density of silanol groups (Si-OH) of the sepiolite surface[193] [194]. The suspension of sepiolite in water (4 wt. %) obtained by ultrasonic irradiation (20 min), gives a stable-in-time thixotropic aqueous gel [8], characterized by the formation of a 3D network of sepiolite fibers which has the highest specific surface area (330 m^2/g, BET surface area measurements) (Figure 8.2).

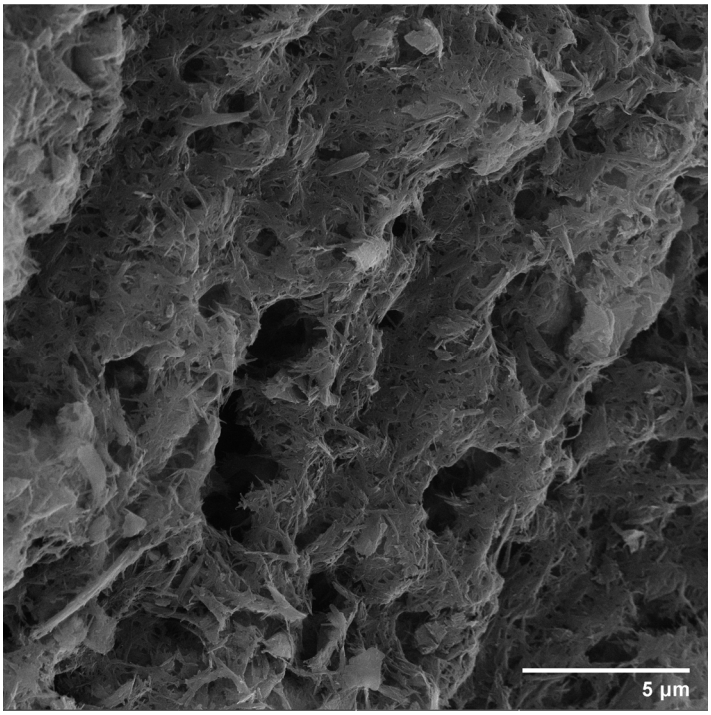

Figure 8.2 Sepiolite thixotropic aqueous gel as seen by FESEM

The diameter and morphology of PVB/Sep nanocomposite fibers were studied by optical and scanning electron microscopy (please see Figures 8.3 and 8.4) to evaluate the relationship of different flow rate, applied voltage, and weight content of neat and modified sepiolite fibers on the fiber diameter and fiber network morphology. Figure 8.3 shows the optical microphotograph of the neat PVB and PVB/Sep fibers containing 3 wt. % of neat sepiolite. It is evident from the pictures in the Figure 8.3. (a-f) that the higher implied voltage of V = 24 kV (28 kV and 30 kV) leads to the twisting of fibers under the same conditions of flow rate Q =1 ml/h and sepiolite content of 3 wt. %.

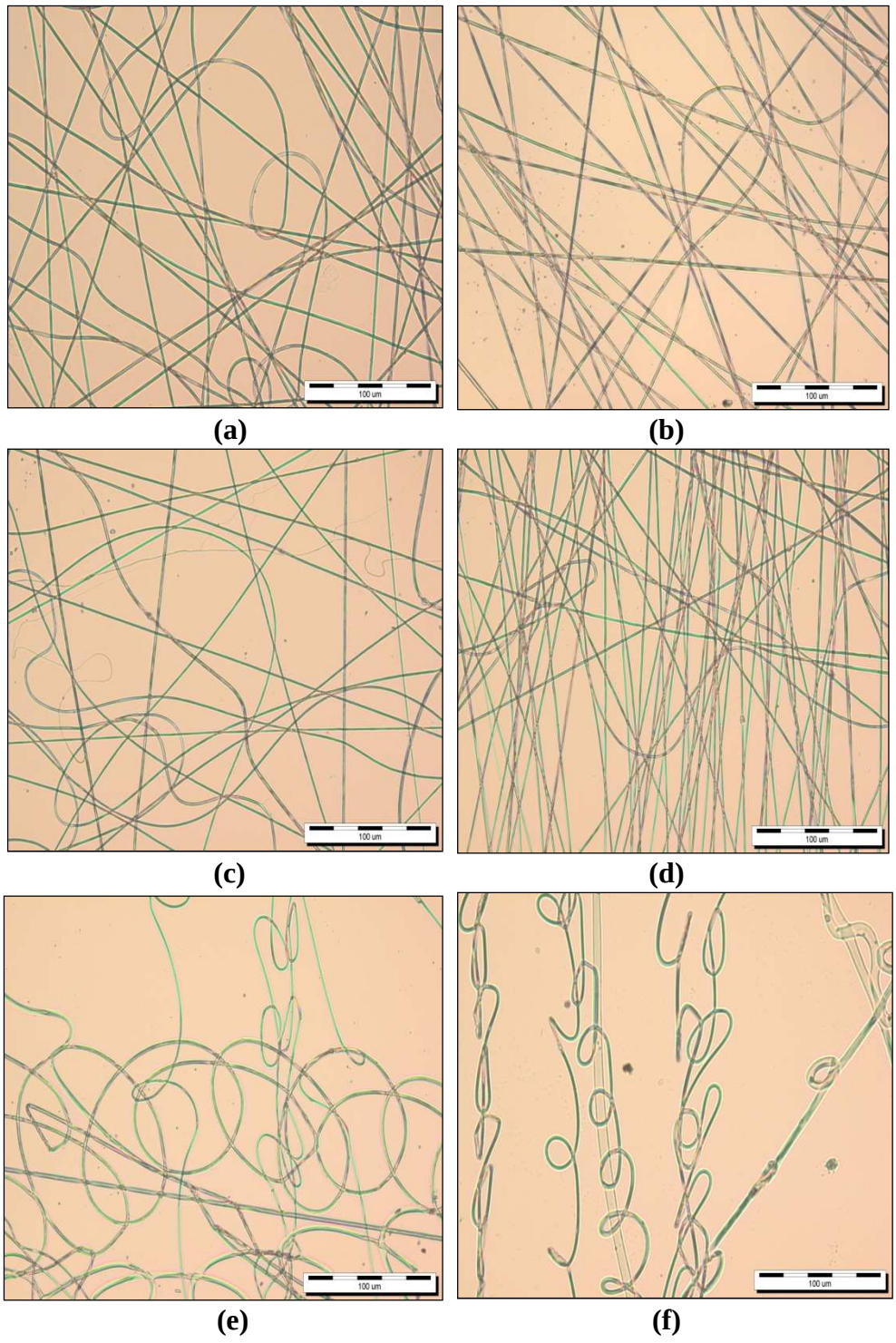

Figure 8.3 Optical microscopy image of the PVB fibers with 3 wt. % neat sepiolite fibers by the collector distance of h = 15 cm (scale bar 100 μm): (a) (Q = 0.2 mL/h, V = 20 kV); (b) (Q = 0.5 mL/h, V = 20 kV); (c) (Q = 1 mL/h, V = 16 kV); (d) (Q = 1 mL/h, V = 24 kV) ; (e) (Q = 1 mL/h, V = 28 kV); (f) (Q = 1 mL/h, V = 30 kV).

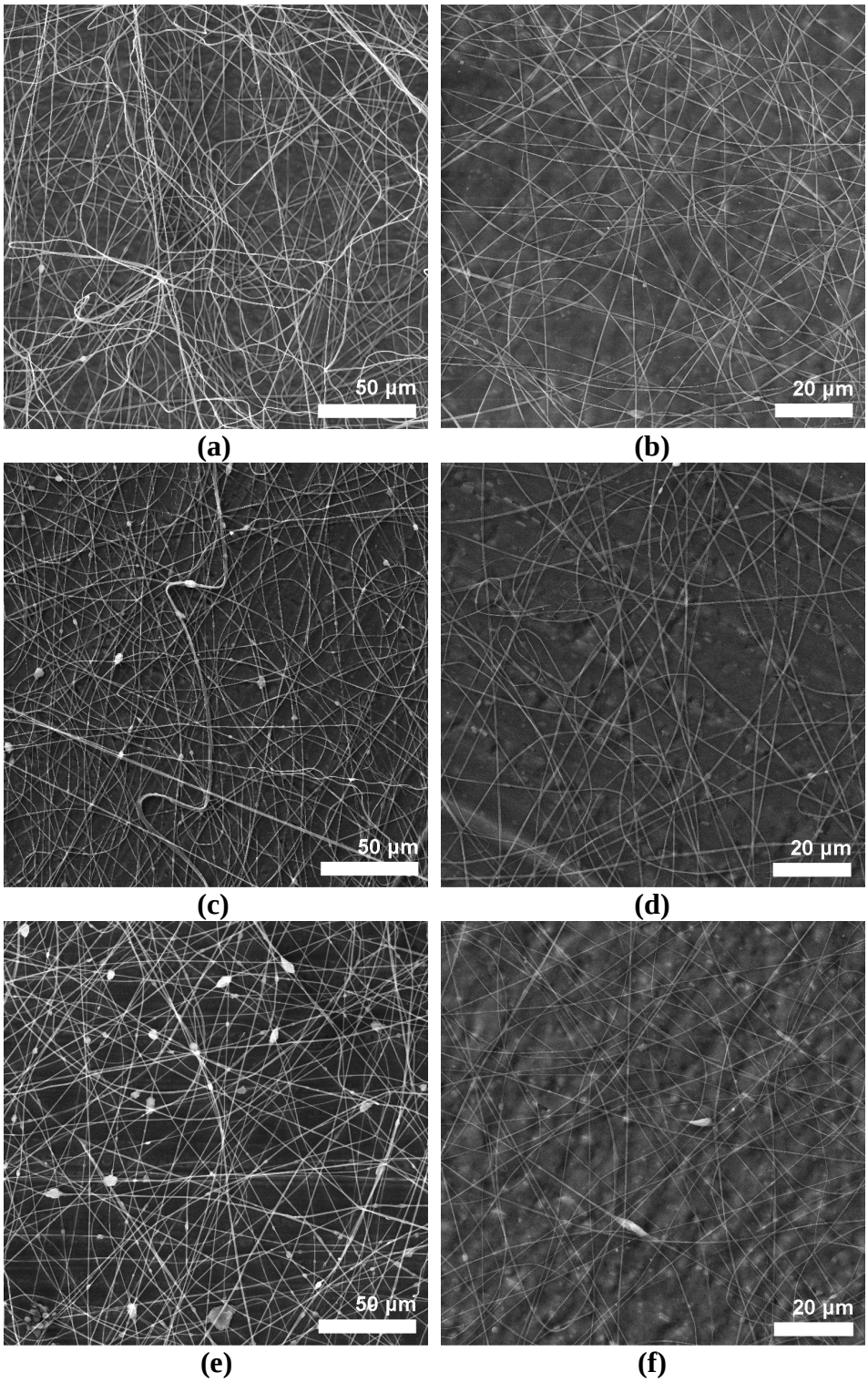

Figure 8.4 FESEM images of PVB/Sep composite fibers with different content of the sepiolite fibers (a, b) 3 wt. % neat and modified sepiolite fibers; (c, d) 30 wt. % neat and modified sepiolite fibers; (e, f) 50 wt. % neat and modified sepiolite fibers

Figure 8.4 shows the FESEM images of as-spun PVB/Sep composite fibers from the following solutions with the content of the sepiolite fibers: (a) 3 wt. %, (b) 30 wt. %, (c) 50 wt. % for electrospun PVB 10 wt% solution by the collector distance of h = 15 cm, flow rate of Q = 0.5 mL/h, and a constant applied voltage of V = 24 kV. For the PVB/Sep fibers containing 30-50 wt. % of neat sepiolite fibers, we found that some beaded structure was formed by the large agglomerates of the sepiolite (see Figure 8.4 (c, e)).

Figures 8.4 and 8.5 show the influence of the sepiolite content on the increase of mean diameter and the modification with AMEO silane decreases the mean diameters of nanocomposite fibers.

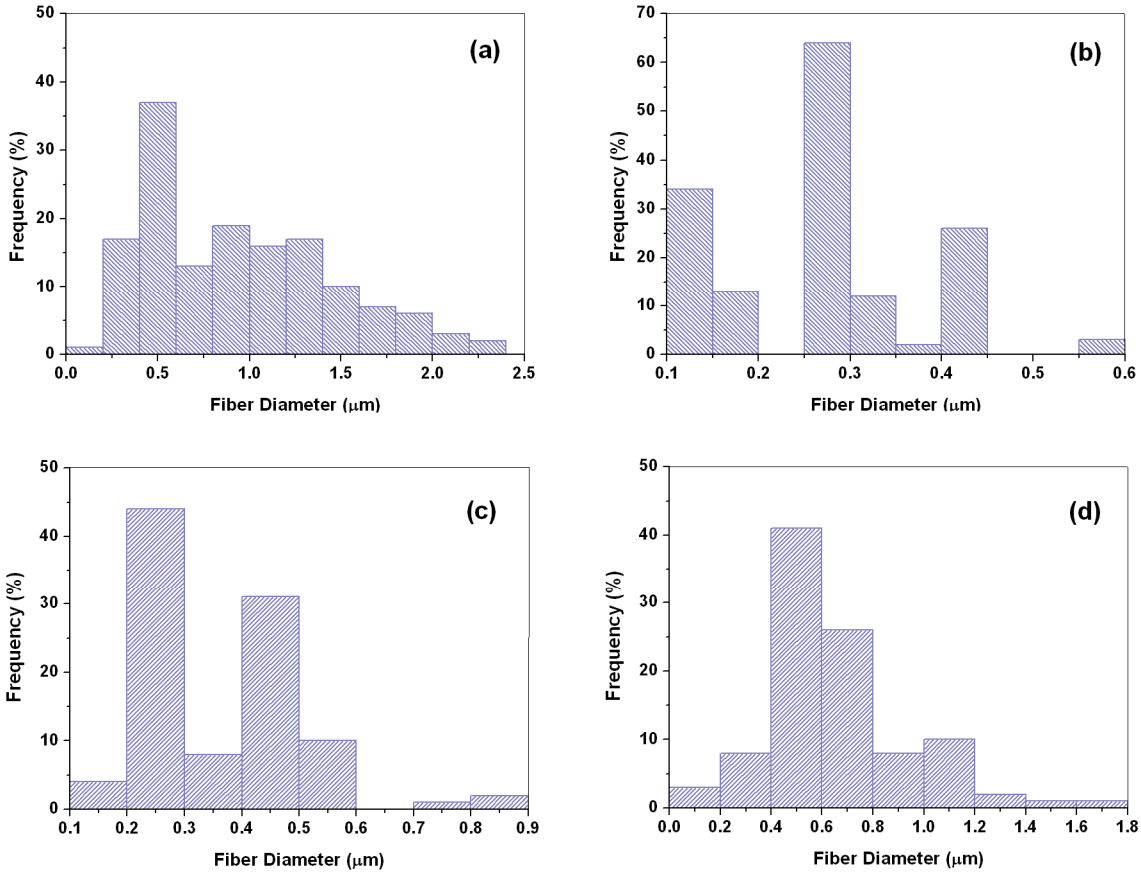

Figure 8.5 Histogram of the fibers diameter for electrospun (a) neat PVB fibers and PVB/Sep fibers containing (b) 3 wt. %, (c) 30 wt. %, (d) 50 wt. % of modified sepiolite by the collector distance of h = 15 cm, flow rate of Q = 0.5 mL/h, and applied voltage of V = 24 kV.

The fiber diameters of neat PVB fibers are in range of 0.149 to 2.202 μm (Table 8.1, Figures 8.5(a)), while the nanocomposite fibers containing 3 wt. % of modified sepiolite have the diameters in range of 0.140 μm to 0.599 μm (Fig. 8.5 (b). The mean diameters of the fibers are 0.928 μm for neat fibers and 0.230 μm for silane modified 3 wt.% sepiolite nanocomposite fibers. The fiber diameters of the modified fibers containing 30 wt. % and 50 wt. % sepiolite have the diameters in range 0.897 to 0.143 μm and 1.809 to 0.144 μm, respectively (see Figures 8.5 (c, d) and Table 8.1).

Table 8.1. Statistical parameters characterising the measurement of fiber diameter

Parameter	PVB fibers	PVB/Sep (3 wt%)	PVB/Sep/ AMEO (3 wt%)	PVB/Sep (30 wt%)	PVB/Sep/ AMEO (30 wt%)	PVB/Sep (50 wt%)	PVB/Sep/ AMEO (50 wt%)
Mean (μm)	0.928	0.777	0.230	0.795	0.368	0.882	0.652
Minimum (μm)	0.149	0.284	0.140	0.284	0.143	0.286	0.144
Maximum (μm)	2.202	1.270	0.599	2.572	0.897	2.020	1.809
Stand. Dev. (μm)	0.506	0.232	0.108	0.339	0.129	0.337	0.274
Count	150	155	158	156	150	154	150

Statistical parameters characterizing fibers diameter distribution are given in Table 8.1. About 50 fibers were selected for the diameter measurement (using Image-Pro Plus analysis software) from three experiments. A significant decrease of the mean fiber diameter of sepiolite composite fibers was shown, which appear for all modified sepiolite fiber contents (see Figure 8.5). Most polymer/clay nanofibers exhibit decrease of mean diameter at relatively low loadings, usually less than 5 wt. %. The diameter decrease of nanocomposite fibers may be due to the increase of PVB solution conductivity caused by clay-nanomaterials[195].

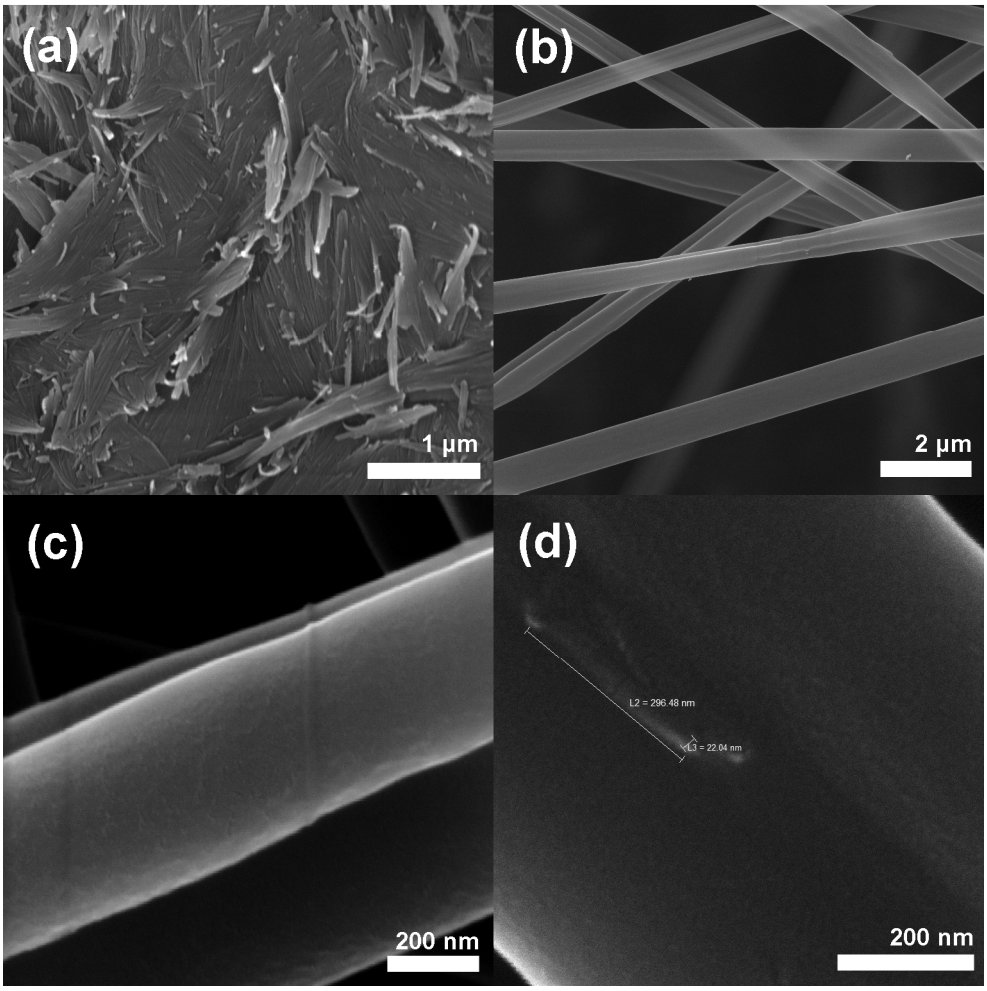

Figure 8.6 The morphology of (a) neat sepiolite and (b-d) electrospun PVB/Sep fibers containing 3 wt. % of modified sepiolite

As shown in Figure 8.6 (a), neat sepiolite formed aggregates by surface interaction between individual fibers. The as-spun PVB/Sep fibers containing 3 wt. % of modified sepiolite fiber had a smooth fibrous structure without beads (Figure 8.6 (c, d)), which suggested that the modified sepiolite fibers were well-dispersed in the spinning solution. It is shown that the diameter of composite nanofibers is highly dependent on the sepiolite modification technique as well as on electrospinning process. The technique of electrospinning could be also used in order to improve the dispersion of sepiolite aggregates. It was found that the sepiolite fibers were well-dispersed within the composite fibers and were oriented along the fiber axis (Figure 8.6 (d)) with the fiber length and diameter of 296 nm and 22 nm, respectively).

Dynamic mechanical analysis (DMA)

Dynamic mechanical analysis is a method that measures the mechanical properties of a material as a function of the oscillatory frequency and the temperature. For the DMA characterization, the strength values are in the form of complex modulus which can be written as follows: $E^* = E' + iE''$, where E^* is the complex modulus, E' is the storage modulus $(E' = |E^*| \cos \delta)$ and E'' $(E'' = |E^*| \sin \delta)$ is the loss modulus. Since the samples have viscoelastic properties containing both elastic part and viscous part, the complex modulus is the sum of moduli from those two parts. The complex modulus E^* is calculated from the measured data and the sample geometry:

$$E^*_{dual\cdot cantilever} = \frac{l^3}{16 \cdot b \cdot h^3} \cdot \frac{F}{A} \quad (1)$$

where: l – sample length, b – sample width, h – sample thickness, F – force, and A – deflection[196] .The ratio between E' and E'', the so called Tan Delta ($\tan \delta$) shows the loss of energy in the heat form resulting from the viscoelastic properties of the samples. The loss factor (Tan Delta) obtained from:

$$\tan \delta = \frac{E''}{E'} \quad (2)$$

Structural changes of patterned nanofibrous mats after sepiolite addition to polymeric matrices can be studied using the *Cole-Cole* method. The dynamic mechanical properties when examined as a function of the oscillatory frequency and the temperature are represented on the *Cole-Cole* complex plane[197] :

$$E = f(E') \quad (3)$$

In this case, DMA was used to determine the E_n^*, $\tan \delta$ and *Cole-Cole* plot of patterned nanofibrous mats consisted of multiple layers of a nanofibers pattern.

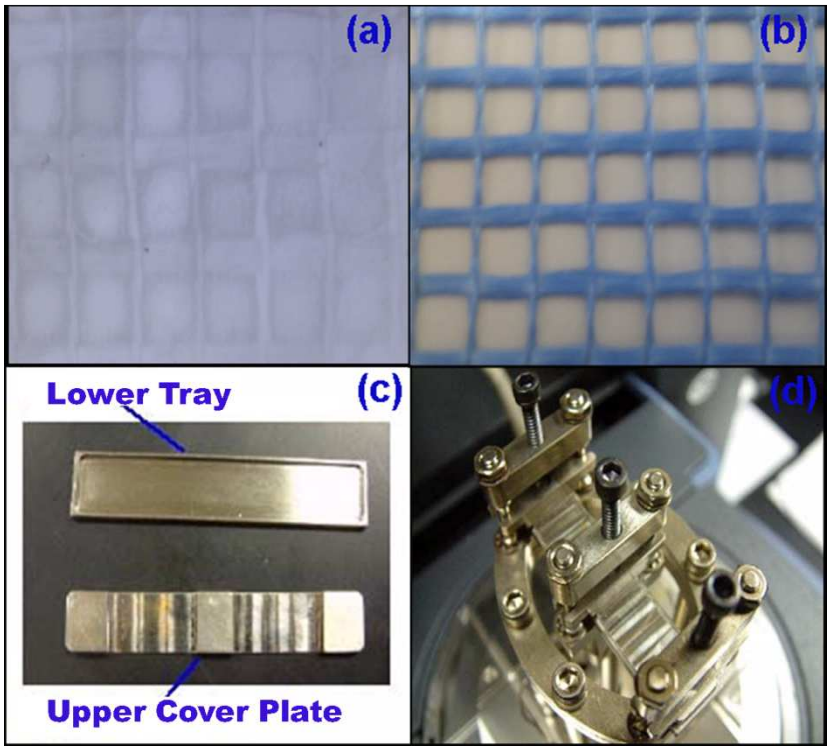

Figure 8.7 Photograph of patterned nanofibrous mats (a) collected on fiberglass mesh (b) using a stainless steel sample holder (c) in dual cantilever mode (d)

DMA has previously been used to investigate the glass transition temperature (T_g) of the pharmaceutical powdered materials[198,199]. The present study however is the first study we are aware of to apply DMA to analyse complex nanofibrous materials. DMA of patterned nanofibrous mats was established with the stainless steel sample holder loaded in the DMA Q800[200] . The sample holder is a uniquely designed lower tray and upper cover plate assembly for containing patterned nanofibrous mats. The clamp was used in conjunction with the 35 mm dual cantilever clamp (adapted from TA Q800 operator's manual). The patterned mats were cut for dimensions of sample holder (approximately 60 mm × 13 mm × 1 mm, about ~100 mg) (see Figure 8.7). The using of stainless steel sample holder enabled the characterization of the glass transition temperature with temperature change by observing the signal change of the calculated normalized complex modulus, (E_n*) (Figure 8.8 (a)).

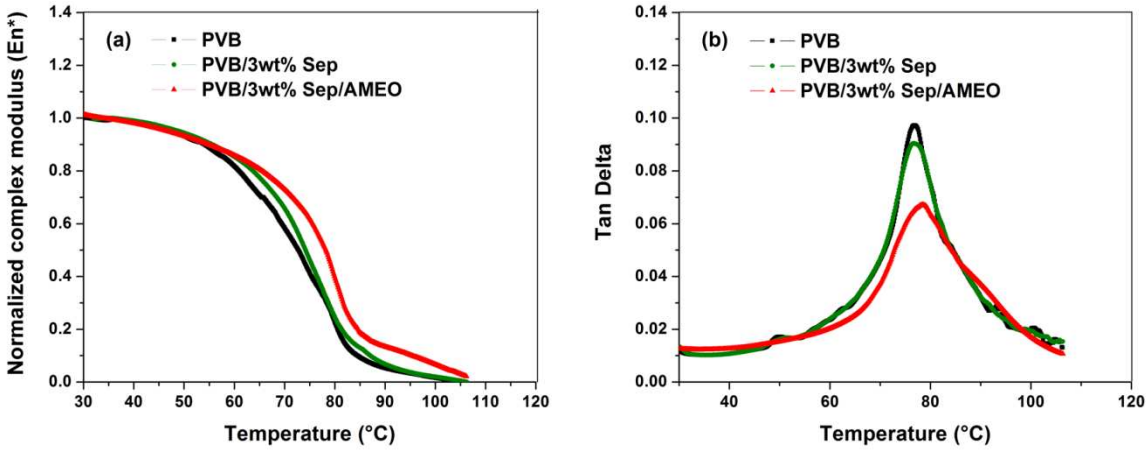

Figure 8.8 (a) E_n and (b) Tan Delta vs. temperature curves for patterned nanofibrous mats*

This normalized complex modulus, presents the ratio of the complex modulus within a sample set to the value of the maximum modulus in the same data set. However, it should be noted that the value of the *E'* and *E''* obtained using a sample holder accessory is only qualitative (adapted from TA Q800 operator's manual), but the ratio between *E''* and *E'*, (*Cole-Cole* plot) is quantitative. Since *tan δ* is geometry-independent, the structural information at corresponding temperatures could be obtained using this accessory.

The E_n* of the electrospun nanofibrous mats and composite nanofibrous mats as a function of temperature is shown in Figure 8.8 (a). It shows a significant reduction in the modulus with temperature. The E_n* of the composite nanofibrous mats showed an increase at higher temperatures compared to pure polymer nanofibrous mats (in Figure 8.8 (a) and Table 8.2).

Table 2. E_n*, T_g and *tan* δ peak temperature of patterned nanofibrous mats obtained from DMA

Sample	E_n* (at 75 °C)	T_g (°C) (from E_n*)	T_g (°C) (from *tan* δ)	Tan Delta (*tan* δ)
PVB	0.416	69.3	76.9	0.097
PVB/3wt.%Sep	0.466	70.2	77.4	0.090
PVB/3wt.%Sep/AMEO	0.601	72.9	79.1	0.067

The composite nanofibrous mats with AMEO modified sepiolite showed significant increase in E_n* at 75 °C (around the T_g temperature of pure PVB)[201]. This indicates the efficient stress transfer between the polymer matrix and modified sepiolite fibers in the composite nanofibrous mats. Glass transition temperature was defined as the onset temperature from the E_n* and *tan* δ peak temperature. Figure 8.8 (b) shows T_g and *tan* δ versus temperature plots of curves for patterned nanofibrous mats. The incorporation of neat sepiolite had modest effect on the T_g and *tan* δ values. Increase of the T_g and addition of neat sepiolite fibers reduced the *tan* δ values of patterned nanofibrous mats by restricting the movement of polymer molecules and established hydrogen bonding with the silanol groups of the sepiolite surface and OH groups of PVB. The *tan* δ values of the composite nanofibrous mats were significantly lowered with AMEO silane grafting (0.067). The decrease of the *tan* δ value is a measure of enhanced interfacial bond strength and the adhesion between polymer matrix and modified sepiolite fibers.

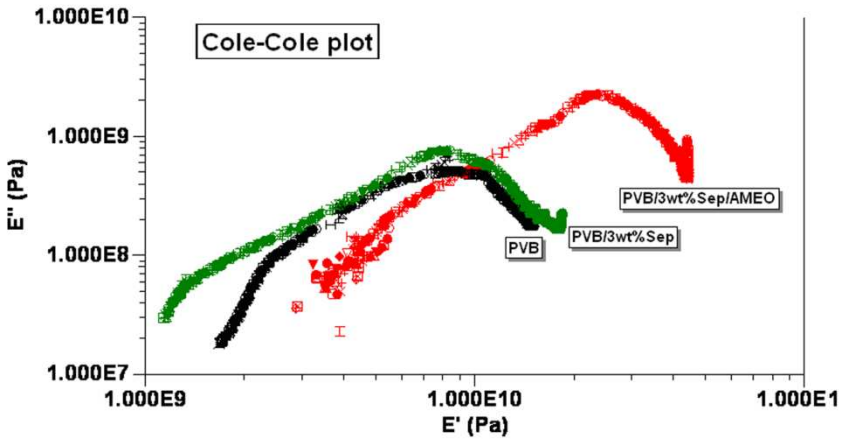

Figure 8.9 Cole-Cole plot for patterned nanofibrous mats

The effect of interface modification between sepiolite fibers and polymer matrix was also confirmed by *Cole-Cole* plot. Figure 8.9 shows *Cole-Cole* plot, where the loss modulus data *log E"* are plotted as a function of the storage modulus data *log E'*. It is used to examine the structural changes occurring in neat PVB nanofibrous mats and composite nanofibrous mats before and after incorporation of modified sepiolite into polymeric matrices. The imperfect circles indicate heterogeneity of the hybrid system and favorable amino modified fibers/polymer bonding.

9. CONCLUSION

The PMMA matrix composites were prepared using the addition of alumina spherical nanoparticles and alumina whiskers as reinforcement. The ultrasonication was used to mix the ingredients and to break the agglomerates of alumina spherical nanoparticles and alumina whiskers prior to polymerization of the matrix material. The DMA and nanoindentation were used to characterize the mechanical behavior of the obtained composites. The DMA results show that the alumina spherical nanoparticles are able to increase the storage modulus of the composite up to 30 % compared to PMMA while the alumina whiskers are able to improve the storage modulus values by 62 %. The T_g of the composite increases up to 1.2 °C with the addition of alumina spherical nanoparticles while the increase in T_g is of 3 °C when alumina whiskers are added. Among the composites studied having 1 wt. %, 3 wt. % and 5 wt. % of added alumina spherical nanoparticles and 1 wt. %, 3 wt. % and 5 wt. % of added alumina whiskers to the PMMA matrix the best results in increasing the T_g were obtained using the 3 wt. % of added alumina whisker reinforcement. The nanoindentation results, for the same set of composite materials containting alumina fillers of different shape and PMMA matix, for the modulus of elasticity and hardness favors the specimen having 3 wt. % of alumina whiskers added as reinforcement to PMMA matrix.

When the influence of the morphology of the reinforcement is concerned, better results were obtained using the alumina whisker reinforcement where the length to diameter is much more important than in the alumina nanoparticles which were declared as spherical. The increase of all properties: storage modulus, T_g, measured using the DMA, and modulus of elasticity and hardness measured using the nanoindentation, are better when the alumina whiskers are added than in the case of alumina spherical nanoparticles. The use of ultrasonic bath for the homogenization of the composite was satisfactory for the purpose of the production of the specimens and this is proved by the increase of the mechanical properties measured using the presented techniques.

The effects of operating parameters including applied voltage, flow rate and tip-target distance on the morphology of electrospun PVB/Sep nanocomposite fibers were systematically evaluated. The modification of the sepiolite thixotropic gel with the AMEO silane led to a better dispersion and deagglomeration of sepiolite inside the

nanocomposite fibers. The composite nanofibers with 3 wt. % sepiolite had a mean diameter of 230 nm. Presented dynamic mechanical analysis of patterned nanofibrous mats is a new method for characterization and determination of thermo-mechanical properties. The future research will be focused on preparation of composite nanofibrous mats with higher sepiolite content and their application in antiballistic protection.

BIOGRAPHY

Somaya Ahmed Ben Hassan was born 04.07.1980. in Zliten-Libya. She received the bachelor degree in physics 2005. in Al-Fateh University, Libya. Master degree in Material Science and Engineering has received 2009. in Department of Physics& Material Scinece & Engineering, Jaypee Institute of Information Technology University Noida, India. She has been enrolled to PhD studies on University of Belgrade, Faculty of Technology and Metallurgy 2010. The title of PhD Thesis ``Structure and the physical and mechanical properties of dental hybrid composite materials`` was approved by University Council 25. 04. 2012.

Appendix 1.

Изјава о ауторству

Потписани-а Somaya Ahmed Ben Hassan
број индекса _____

Изјављујем

да је докторска дисертација под насловом

″ STRUCTURE AND THE PHYSICAL AND MECHANICAL PROPERTIES OF DENTAL HYBRID COMPOSITE MATERIALS ″

- резултат сопственог истраживачког рада,
- да предложена дисертација у целини ни у деловима није била предложена за добијање било које дипломе према студијским програмима других високошколских установа,
- да су резултати коректно наведени и
- да нисам кршио/ла ауторска права и користио интелектуалну својину других лица.

Потпис докторанта

У Београду, _____

_____

Appendix 2.

Изјава о истоветности штампане и електронске верзије докторског рада

Име и презиме аутора: Somaya Ahmed Ben Hassan

Број индекса _____

Студијски програм Инжењерство материјала

Наслов рада **″ STRUCTURE AND THE PHYSICAL AND MECHANICAL PROPERTIES OF DENTAL HYBRID COMPOSITE MATERIALS ″**

Ментор _____

Потписани/а др Радослав Алексић, ред. проф.

Изјављујем да је штампана верзија мог докторског рада истоветна електронској верзији коју сам предао/ла за објављивање на порталу **Дигиталног репозиторијума Универзитета у Београду.**

Дозвољавам да се објаве моји лични подаци везани за добијање академског звања доктора наука, као што су име и презиме, година и место рођења и датум одбране рада.

Ови лични подаци могу се објавити на мрежним страницама дигиталне библиотеке, у електронском каталогу и у публикацијама Универзитета у Београду.

Потпис докторанта

У Београду, _____

_____

Appendix 3.

Изјава о коришћењу

Овлашћујем Универзитетску библиотеку „Светозар Марковић“ да у Дигитални репозиторијум Универзитета у Београду унесе моју докторску дисертацију под насловом:

″ STRUCTURE AND THE PHYSICAL AND MECHANICAL PROPERTIES OF DENTAL HYBRID COMPOSITE MATERIALS ″

која је моје ауторско дело.

Дисертацију са свим прилозима предао/ла сам у електронском формату погодном за трајно архивирање.

Моју докторску дисертацију похрањену у Дигитални репозиторијум Универзитета у Београду могу да користе сви који поштују одредбе садржане у одабраном типу лиценце Креативне заједнице (Creative Commons) за коју сам се одлучио/ла.

1. Ауторство

2. Ауторство - некомерцијално

3. Ауторство – некомерцијално – без прераде

4. Ауторство – некомерцијално – делити под истим условима

5. Ауторство – без прераде

6. Ауторство – делити под истим условима

(Молимо да заокружите само једну од шест понуђених лиценци, кратак опис лиценци дат је на полеђини листа).

Потпис докторанта

У Београду, _____

_____

1. Ауторство - Дозвољавате умножавање, дистрибуцију и јавно саопштавање дела, и прераде, ако се наведе име аутора на начин одређен од стране аутора или даваоца лиценце, чак и у комерцијалне сврхе. Ово је најслободнија од свих лиценци.

2. Ауторство – некомерцијално. Дозвољавате умножавање, дистрибуцију и јавно саопштавање дела, и прераде, ако се наведе име аутора на начин одређен од стране аутора или даваоца лиценце. Ова лиценца не дозвољава комерцијалну употребу дела.

3. Ауторство - некомерцијално – без прераде. Дозвољавате умножавање, дистрибуцију и јавно саопштавање дела, без промена, преобликовања или употребе дела у свом делу, ако се наведе име аутора на начин одређен од стране аутора или даваоца лиценце. Ова лиценца не дозвољава комерцијалну употребу дела. У односу на све остале лиценце, овом лиценцом се ограничава највећи обим права коришћења дела.

4. Ауторство - некомерцијално – делити под истим условима. Дозвољавате умножавање, дистрибуцију и јавно саопштавање дела, и прераде, ако се наведе име аутора на начин одређен од стране аутора или даваоца лиценце и ако се прерада дистрибуира под истом или сличном лиценцом. Ова лиценца не дозвољава комерцијалну употребу дела и прерада.

5. Ауторство – без прераде. Дозвољавате умножавање, дистрибуцију и јавно саопштавање дела, без промена, преобликовања или употребе дела у свом делу, ако се наведе име аутора на начин одређен од стране аутора или даваоца лиценце. Ова лиценца дозвољава комерцијалну употребу дела.

6. Ауторство - делити под истим условима. Дозвољавате умножавање, дистрибуцију и јавно саопштавање дела, и прераде, ако се наведе име аутора на начин одређен од стране аутора или даваоца лиценце и ако се прерада дистрибуира под истом или сличном лиценцом. Ова лиценца дозвољава комерцијалну употребу дела и прерада. Слична је софтверским лиценцама, односно лиценцама отвореног кода.

REFERENCES

[1] Söderholm KJM and Roberts MJ, Influence of water exposure on the tensile strength of composites, Journal of Dental Research, 69 (1990) 1812-1816.

[2] Beun, S., Glorieux, T., Devaux, J.,Vreven, J., and Leloup, G., "Characterization of nanofilled compared to universal and microfilled composites", Dent. Mater., Vol. 23(2007), pp. 51-61.

[3] Mitra, S. B., Wu, D., and Holmes, B. N., "An application of nanotechnology in advanced dental materials", J. Am. Dent. Assoc., Vol. 134 (2003), pp. 1382-1391.

[4] Zhang, H., Zhang, Z., Friedrich, K., and Eger, C., "Property improvements of in situ epoxy nanocomposites with reduced interparticle distance at high nanosilica content", Acta Mater., Vol. 54 (2006), pp. 1833.

[5] Tian, M., Gao, Y., Liu, Y., Liao, Y., Hedin, N. E., and Fong, H., "Fabrication and evaluation of Bis-GMA/TEGDMA dental resins /composites containing nano fibrillar silicate", Dent. Mater., Vol. 24 (2008), pp. 235-244.

[6] Ferracane J L, Resin Composite-State of the art, Dental Materials, 27 (2011), 29–38.

[7] Klapdohr S, Moszner N., New inorganic components for dental filling composites, Monatsh. Chem., 136 (2005):21–45.

[8] Chen MH. Update on dental nanocomposites, J Dent Res., 89 (2010):549–560.

[9] Jandt KD, Sigusch BW, future perspectives of resin-based dental materials, Dent. Mater., 8 (2009):1001–1006.

[10] Peutzfeldt A. Resin Composites In Dentistry: The Monomer Systems, Eur. J. Oral. Sci.,105 (1997): 97-116.

[11] Stansbury JW. Curing Dental Resins And Composites By Photopolymerization, J. Esthet. Dent., 12 (2000):300–8.

[12] Park YJ, Chae KH, Rawls HR. Development Of A New Photoinitiation System For Dental Light-Cure Composite Resins, Dent. Mater.,15 (1999):120–127.

[13] Neumann MG, Miranda Jr WG, Schmitt CC, Rueggeberg FA, Correa IC. Molar Extinction Coefficients And The Photon Absorption Efficiency Of Dental Photoinitiators And Light Curing Units, J. Dent., 33 (2005):525–532.

[14] Shin DH, Rawls HR. Degree Of Conversion And Color Stability Of The Light Curing Resin With New Photoinitiator Systems, Dent Mater; 25 (2009):1030–1038.

[15] Bayne SC, Thompson JY, Swift Jr EJ, Stamatiades P,Wilkerson M, A Characterization Of First-Generation Flowable Composites, J. Am. Dent. Assoc., 129 (1998):567–577.

[16] Choi KK, Ferracane JL, Hilton TJ, Charlton D. Properties Of Packable Dental Composites, J. Esthet. Dent., 12 (2000):216–226.

[17] Ferracane J L, Resin Composite-State Of The Art, Dental Materials, 27 (2011):29–38.

[18] Bayne SC, Heymann HO, Swift Jr EJ. Update on dental composite restorations, J. Am. Dent. Assoc.,125 (1994):687–701.

[19] Ilie N, Hickel R. Investigations On Mechanical Behavior Of Dental Composites, Clin. Oral. Invest., 13 (2009):427–438.

[20] Ilie N, Hickel R. Macro-, Micro-And Nano-Mechanical Investigations On Silorane And Methacrylate-Based Composites, Dent. Mater., 25 (2009):810–819.

[21] Curtis AR, Palin WM, Fleming GJ, Shortall AC, Marquis PM, The Mechanical Properties Of Nanofilled Resin-Based Composites: The Impact Of Dry And Wet Cyclic Pre-Loading On Bi-Axial Flexure Strength, Dent. Mater., 25 (2009):188–197.

[22] Hahnel S, Henrich A, Bürgers R, Handel G, Rosentritt M. Investigation Of Mechanical Properties Of Modern Dental Composites After Artificial Aging For One Year, Oper. Dent., 35 (2010):412–9.

[23] Blackham JT, Vandewalle KS, Lien W. Properties Of Hybrid Resin Composite Systems Containing Prepolymerized Filler Particles, Oper. Dent., 34 (2009): 697–702.

[24] Ernst CP, Brandenbusch M, Meyer G, Canbek K, Gottschalk F, Willershausen B, Two-Year Clinical Performance Of A Nanofiller Vs A Fine-Particle Hybrid Resin Composite, Clin. Oral. Invest., 10 (2006):119–125.

[25] Kramer N, Reinelt C, Richter G, Petschelt A, Frankenberger R. Nanohybrid Vs. Fine Particle Composite In Class II Cavities: Clinical Results And Margin Analysis After Four Years, Dent Mater;25 (2009):750–759.

[26] Scougall-Vilchis RJ, Hotta Y, Hotta M, Idono T, Yamamoto K. Examination Of Composite Resins With Electron Microscopy, Microhardness Tester And Energy Dispersive X-Ray Microanalyzer, Dent. Mater. J., 28 (2009):102–212.

[27] Wolter H, Glaubitt W, Rose K. Multifunctional (Meth) Acrylate Alkoxysilanes-A New Type Of Reactive Compounds, Mat. Res. Soc. Symp. Proc., 271 (1992):719–24.

[28] Soh MS, Yap AUJ, Sellinger A. Physicomechanical Evaluation Of Low-Shrinkage Dental Nanocomposites Based On Silsesquioxane Cores, Eur. J. Oral. Sci., 115 (2007): 230–238.

[29] Xu HH, Sun L, Weir MD, Antonucci JM, Takagi S, Chow LC, et al, Nano DCPA-Whisker Composites With High Strength And Ca And PO(4) Release. Dent. Res., 85 (2006):722–727.

[30] Xu HHK, Moreau JL, Sun L, Chow LC, Novel Caf2 Nanocomposite With High Strength And Fluoride Release, J. Dent. Res., 89 (2010):739–45.

[31] Lee TY, Cramer N, Hoyle C, Stansbury J, Bowman C, (Meth) Acrylate Vinyl Ester Hybrid Polymerizations, J. Polym. Sci. A Polym. Chem., 47 (2009):2509–2517.

[32] Leung D, Spratt DA, Pratten J, Gulabivala K, Mordan NJ, Young AM. Chlorhexidine-Releasing Methacrylate Dental Composite Materials, Biomaterials, 26 (2005):7145–7153.

[33] Sevinc BA, Hanley L. Antibacterial Activity Of Dental Composites Containing Zinc Oxide Nanoparticles, J. Biomed. Mater. Res B: Appl. Biomater., 94B (2010):22–31.

[34] Beyth N, Yudovin-Farber I, Bahir R, Domb AJ, Weiss EI. Antibacterial activity of dental composites containing quaternary ammonium polyethylenimine nanoparticles against Streptococcus mutans, Biomaterials, 27 (2006):3995–4002.

[35] Ebi N, Imazato S, Noiri Y, Ebisu S. Inhibitory Effects Of Resin Composite Containing Bactericide-Immobilized Filler On Plaque Accumulation, Dent. Mater., 17 (2001):485–91.

[36]Wiegand A, BuchallaW, Attin T. Review on fluoride-releasing restorative materials—fluoride release and uptake characteristics, antibacterial activity and influence on caries formation, Dent. Mater., 23 (2007):343–62.

[37] Schmalz G, Arenholt-Bindslev D.,Biocompatibility of Dental Materials, Springer-Verlag Berlin Heidelberg, 2009

[38] Schmalz G, Arenholt-Bindslev D.,Biocompatibility of Dental Materials, Springer-Verlag Berlin Heidelberg, 2009.

[39] Sanchez, C. Beatriz J.,Belleville P and Popall M., Applications of hybrid organic–inorganic nanocomposites, J. Mater. Chem. , 15 (2005):3559–3592.

[40] Bauer, C.M., Kunzelmann, K-H., and Hickel, R., Simulierter Nahrungsabrieb von

Kompositen und Ormoceren®, Dtsch. Zahnärztl. Z., 50 (1995):635–338.

[41] Manhart, J., Hollwich, B., Mehl, A., Kunzelmann, K-H., and Hickel, R., Randqualität

von Ormocer- und Kompositfüllungen in Klasse-II-Kavitäten nach künstlicher Alterung,

Dtsch. Zahnärztl. Z., 54 (1999):89–95.

[42] Haller, B. and Schuster, P., Randqualität eines Ormocers (Admira) und eines Feinhybridkomposites (Arabesk Top) in Klasse-II-Kavitäten, Dtsch. Zahnärztl. Z., 55 (2000): 331–335.

[43] Schmalz G, Arenholt-Bindslev D.,Biocompatibility of Dental Materials, Springer-Verlag Berlin Heidelberg, 2009.

[44] Schmalz G, Arenholt-Bindslev D.,Biocompatibility of Dental Materials, Springer-Verlag Berlin Heidelberg, 2009.

[45] Stansbury J and Bowman B, The Progress in Development of Dental Restorative Materials , Material Matters, 2010, 53, 73.

[46] Stansbury, J. W.; Trujillo-Lemon, M.; Lu, H.; Ding, X.; Lin, Y.; Ge, J. Dent. Mater., 2005, 21, 56-67.

[47] Lu, H.; Lovell, L. G.; Bowman, C. N. Macromolecules 34, (2001):8021-8025.

[48] V. Yong and H. T. Hahn, Nanotechnology, 2004, 15, 1338

[49]J. J. Mack, L. M. Viculis, A. Ali, R. Luoh, G. Yang, H. T. Hahn,

F. K. Ko and R. B. Kaner, Adv. Mater., 2005, 17, 77.

[50] A. D. Pool and H. T. Hahn, Int. SAMPE Symp. Exhib., 2003, 48, 1617.

[51] A. Panda and E. J. Podlaha, Electrochem. Solid-State Lett., 2003, 6, C149.

[52] E. J. Podlaha and D. Landolt, J. Electrochem. Soc., 1997, 144, L200.

[53] F. Mammeri, E. L. Bourhis, L. Rozes and C. Sanchez, J. Mater. Chem., 2005, 15, 3787.

[54] C. Sanchez and F. Ribot, New J. Chem., 1994, 18, 1007.

[55] P. Judeinstein and C. Sanchez, J. Mater. Chem., 1996, 6, 511.

[56] X. Zhang and L. C. Simon, Macromol. Mater. Eng., 2005, 290, 573.

[57] S.-L. Gao and E. Mader, Composites, 2002, 33A, 559.

[58] Sanchez, C. Beatriz J.,Belleville P and Popall M., Applications of hybrid organic–inorganic nanocomposites, J. Mater. Chem., 15 (2005), 3559–3592.

[59] R. Shenhar, T. B. Norsten and V. M. Rotello, Adv. Mater., 2005, 17, 657.

[60] Thorat S, Diaspro A, Salerno M. Effect of alumina reinforcing fillers in BisGMA-based resin omposites for dental applications, Adv. Mater. Lett., 4 (2013):15-21.

[61] D. J. Kim, P. H. Kang and Y. C. Nho, J. Appl. Polym. Sci., 2004, 91, 1898.

[62] B. J. Ash, R. W. Siegel and L. S. Schadler, J. Polym. Sci., 2004, B42, 4371.

[63] K. A. DeFriend, M. R. Wiesner and A. R. Barron, J. Membr. Sci., 003, 224, 11.

[64] B. J. Ash, R. W. Siegel and L. S. Schadler, Macromolecules, 2004, 37, 1358.

[65] M. Zhang and R. P. Singh, Mater. Lett., 2005, 58, 408.

[66] F. Bauer, H.-J. Glasel, U. Decker, H. Ernst, A. Freyer,E. Hartmann, V. Sauerland and R. Mehnert, Prog. Org. Coat., 2003, 47, 147.

[67] M. Pourbaix, Atlas of Electrochemical Equilibria In Aqueous Solutions, Cebelcor, Houston, TX, 1974.

[68]Z. Guo, T. Pereira, O. Choi, Y. Wang and H. Thomas Hahn, J. Mater. Chem., 16 (2006) 2800-2808.

[69] L. González, A. Rodríguez, A. Marcos-Fernández, A. del Campo, J. Appl. Polym. Sci., 2001, 79, 714.

[70] Brauner, K. and Preisinger, A. (1956) Stluktur mid Entstehmlg des Sepioliths : Tsunger. Miner. u. Petrogr. Mittlgn., Bd. 6, pp. 120-140.

[71] J.E. Kogel, N.C. Trivedi, J.M. Barker, S.T. Krukowsk, Industrial Minerals & Rocks:

Commodities, Markets, and Uses, 7th ed., SME Inc., 2006.

[72] E. Ruiz-Hitzky, Molecular access to intracrystalline tunnels of sepiolite, J. Mater. Chem. 11 (2001) 86–91.

[73] H. Du, J.D. Miller, A molecular dynamics simulation study of water structure and adsorption states at talc surfaces, Int. J. Miner. Process., 84 (2007) 172–184.

[74] Chen, H.; Zheng, M.; Suna, H.; Jia, O., Mater. Sci. Eng. A, 2007, 15, 725.

[75] Bokobza, L.; Burr, A.; Garnaud, G.; Perin, M. Y.; Pagnotta, S. J. Polym. Int., 2004, 53, 1060.

[76] Santiago, F.; Mucientes, A. E.; Osorio, M.; Poblete, F. J. Polym. Int., 2006, 55, 843.

[77] Darder, M.; Lopez-Blanco, M.; Aranda, P.; Aznar, A. J.; Bravo, J.; Ruiz-Hitzky, E. Chem. Mater., 2006, 18, 1602.

[78] Zheng, Y.; Zheng, Y. J. Appl. Polym. Sci., 2006, 99, 2163.

[79] Toldy, A.; Toth, N.; Keglevich, Gy.; Kiss, K.; Marosi, Gy. Polym. Adv. Technol., 2006, 17, 778.

[80] Deneuborg, F.-X.; Beigbeder, A.; Degee, Ph.; Viville, P.; Dubois, Ph. Silicone-Based Nanocomposites: New Materials for Antifouling Coatings. Available at: http://morris.umh.ac.

[81] Bokobza, L., J. Appl. Polym. Sci., 2004, 93, 2095.

[82] Xie, S.; Zhang, S.; Wang, F.; Yang, M.; Seguela, R.; Lefebvre,J.M., Compos. Sci. Technol., 2007, 67, 2334.

[83] Ma, J.; Bilotti, E.; Peijs, T.; Darr, J. A. Eur. Polym. Sci., 2007, 43, 4931.

[84] Bilotti, E.; Fischer, H. R.; Peijs, T. J. Appl. Polym. Sci., 2008, 107, 116.

[85] Combe E. C., Notes on Dental Materials, Churchill Livingstone, Edinburgh, UK, 1972

[86] Reese A. and Thomas M. V., Restorative Dental Materials: An Overview. Vol. 1, Quintessence, London, UK, 1985.

[87]. Van Noort R, Introduction to Dental Materials, Elsevier, Sheffield, UK, 2nd edition, 2002.

[88] Wang L.,. D'Alpino P. H. PLopes, L. G., and. Pereira J. C, "Mechanical properties of dental restorative materials: relative contribution of laboratory tests," Journal of Applied Oral Science, vol. 11, no. 3, pp. 7–162, 2003.

[89]. Wei Y,. Jin D,. Wei G, Yang D., and Xu J., "Novel organic-inorganic chemical hybrid fillers for dental composite materials," Journal of Applied Polymer Science, vol. 70, no. 9, pp. 1689–1699, 1998.

[90] Pettersson B., "Hyperbranched polymers: unique design tools for multi-property control in resins and coatings," Pigment & Resin Technology, vol. 25, no. 4, pp. 4–14, 1996.

[91] Moszner N.and Klapdohr S., "Nanotechnology for dental composites," International Journal of Nanotechnology, vol. 1, no. 1-2, pp. 130–156, 2004.

[92] Wei Y., Jin D., Xu J., Baran G., and Qiu K.-Y., "Mechanical properties of interface-free polyacrylate-silica hybrid sol-gel materials for potential dental applications," Polymers for Advanced Technologies, vol. 12, no. 6, pp. 361–368, 2001.

[93] H. Dodiuk-Kenig, Y. Maoz, K. Lizenboim, I. Eppelbaum, B. Zalsman, and S. Kenig, "The effect of grafted caged silica (polyhedral oligomeric silesquioxanes) on the properties of dental composites and adhesives," Journal of Adhesion Science and Technology, vol. 20, no. 12, pp. 1401–1412, 2006.

[94] Dodiuk-Kenig H., Lizenboim K., Eppelbaum I., Zalsman B., and Skenig S., "The effect of hyper-branched polymers on the properties of dental composites and adhesives," Journal of Adhesion Science and Technology, vol. 18, no. 15-16, pp. 1723–1737, 2004

[95] Grafe T. H. and Graham K. M., "Nanofiber webs from electrospinning," in Proceedings of the 5th International Conference on Nonwovens in Filtration, pp. 1–5, Stuttgart, Germany, March 2003.

[96] Ramakrishna S., An Introduction to Electrospinning, World Scientific, Singapore, 2005.

[97] Jung Y. H., Kim H. Y., Lee D. R., Park S. Y., and. Khil M. S, "Characterization of PVOH nonwoven mats prepared from surfactant-polymer system via electrospinning," Macromolecular Research, vol. 13, no. 5, pp. 385–390, 2005.

[98] Zhang C., Yuan X., Wu L., Han Y., and Sheng J., "Study on morphology of electrospun poly(vinyl alcohol) mats," European Polymer Journal, vol. 41, no. 3, pp. 423–432, 2005.

[99] Ziabicki, A. Fundamentals of fiber formation, John Wiley and Sons, London, (1976).

[100] Kim, J-S. & Reneker, D. H., Polymer Eng. & Sci., May, 39(5), 849 (1999).

[101] Fang, X. & Reneker, D. H., J. Macromol. Sci-Phys., B36(2), 169 (1997).

[102] Doshi, J & Reneker, D.H., J. of Electrostat., 35, 151 (1995).

[103] Taylor, G. I., Proc. Roy. Soc. London, A313, 453 (1969)

[104] Shin, Y.M., Hohman, M. M., Brenner, M. P. & Rutledge, G. C., Polymer, 42, 9955 (2001)

[105] Stitzel, J. D., Bowlin, G. L., Mansfield, K., Wnek, G. E. & Simpson, D. G., Proc. 32nd SAMPE Meeting, Boston, Nov (2000).

[106] Yarin A. L., Zussman E., ”Electrospinning of Nanofibers from Polymer Solutions”, XXI ICTAM, 15-21 August 2004, Warsaw, Poland

[107] A. L. Yarin et al., ”On bending instability in electrospinning of nanofibers”, Journal of Applied Physics, v. 89, no. 5, 3018-3026 (2001)

[108] A. L. Yarin et al., ”On bending instability in electrospinning of nanofibers”, Journal of Applied Physics, v. 89, no. 5, 3018-3026 (2001)

[109] D. Li, Y. Xia, ”Electrospinning of Nanofibers: Reinventing the Wheel?”,

Advanced Materials, v. 16, no. 14, 1151-1170 (2004)

[110] A. L. Yarin, E.Zussman, ”Electrospinning of Nanofibers from Polymer Solutions”, XXI ICTAM, 15-21 August 2004, Warsaw, Poland.

[111] A. L. Yarin, E.Zussman, ”Electrospinning of Nanofibers from Polymer Solutions”, XXI ICTAM, 15-21 August 2004, Warsaw, Poland.

[112] Ziabicki, A. In Fundamentals of Fiber Formation.; Wiley Interscience: NY, 1976.

[113] http://en.wikipedia.org/wiki/Electrospinning

[114] http://www.che.vt.edu/Faculty/Wilkes/GLW/electrospinning/electrspinning.html

[115] VanLandingham M. R. , Villarrubia J.S., Guthrie W. F. , and Meyers G.F, Nanoindentation of Polymers: An Overview, Macromol. Symp., 2001, 167, 15-43.

[116] Oliver W. C., Pharr G. M., J. Mater. Res.**, 7**(6) 1564, (1992).

[117] Sneddon I. N., Int. J. Engng. Sci., 3 47,(1965).

[118] R. B. King, Int. J. Solids Structures 23(12) 1657, (1987).

[119] J. L. Hay, in: Proceedings of the SEM IX International Congress on Experimental

Mechanics, Society for Experimental Mechanics, Bethel, CT, 2000, p.665.

[120] VanLandingham M. R. , Villarrubia J.S., Guthrie W. F. , and Meyers G.F, Nanoindentation of Polymers: An Overview, Macromol. Symp., 2001, 167, 15-43.

[121] VanLandingham M. R. , Villarrubia J.S., Guthrie W. F. , and Meyers G.F, Nanoindentation of Polymers: An Overview, Macromol. Symp., 2001, 167, 15-43.

[122] Agosta C. and Estafan D., "Eliminating microleakage from the composite

resin system", General Dentistry, 2003, pp. 506-509.

[123] Braem, M., Lambrechts, P., Van Doren, V.E., and Vanherle G., "The impact of composite structure on its elastic response", J. Dent. Res., Vol. 65, 1986, pp. 648-653.

[124] Davis D.M. and Waters N.E., "An investigation into the fracture behavior of a particulte-filled bis-GMA resin", J. Dent. Res., Vol. 66, No. 6, 1987, pp. 1128- 1133.

[125] Jones, D. W., "Dental composite biomaterials", J. Can. Dent. Assoc., Vol. 64, 1998, pp. 732-734.

[126] Jones, D. W. and Rizkalla, A. S., "Characterization of experimental composite biomaterials", J. Biomed. Mater. Res., Vol. 33, No. 2, 1996, pp. 89-100.

[127] Watts, D. C., "Elastic moduli and visco-elastic relaxation", J. Dent., Vol. 22, No. 3, 1994, pp. 154-158.

[128] Ausiello P, Rengo S., Davidson C.L., and Watts D.C., "Stress distribution in adhesively cemented ceramic and resin-composite Class II inlay restorations: a 3D-FEA study", Dent. Mater., Vol. 20, 2004, pp. 862-872.

[129] Attar N., Tam L.E., and McComb D., "Flow, strength, stiffness and radiopacity of flowable resin composites", J. Can. Dent. Assoc., Vol. 69, No. 8, 2003, pp. 516-521.

[130] Davidson C.L. and Feilzer A.J., "Polymerization shrinkage and polymerization shrinkage stress in polymer-based restoratives", J. Dent., Vol. 25, 1997, pp. 435-440.

[131] Jones, D. W. and Rizkalla, A. S., "Characterization of experimental composite biomaterials", J. Biomed. Mater. Res., Vol. 33, No. 2, 1996, pp. 89-100.

[132] Nakayama, W. T., Hall, D. R., Grenoble, D. E., and Katz, J. L., "Elastic properties of dental resin restorative materials", J. Dent. Res., Vol. 53, No. 5, 1974, pp. 1121-1126.

[133] Clarke R.L. and Braden M., "Visco-elastic properties of some roomtemperature polymerizing resins", J. Dent. Res., Vol. 61, No. 8, 1982, pp. 997-1001.

[134] Duncanson M.G. and Korostoff E., "Compressive visco-elastic properties of human dentin: 1. Stress-relaxation behavior", J. Dent. Res., Vol. 54, 1975, pp. 1207-1212.

[135] Korostoff E., Pollack S.R., and Duncanson M.G., "Viscoelastic properties of human dentin", J. Biomed. Mater. Res., Vol. 9, 1975, pp. 661-674.

[136] Nakayama, W. T., Hall, D. R., Grenoble, D. E., and Katz, J. L., "Elastic properties of dental resin restorative materials", J. Dent. Res., Vol. 53, No. 5, 1974, pp. 1121-1126.

[137]Craig, R. G. and Peyton F.A., "Elastic and mechanical properties of human dentin", J. Dent. Res., Vol. 37, No. 4, 1958, pp. 710-718.

[138] Willems, G., Lambrechts, P., Braem, M., Celis, J. P., and Vanherle, G., "A classification of dental composites according to their morphological and mechanical characteristics", Dent. Mater., Vol. 8, No. 5, 1992, pp. 310-319.

[139] Braem, M., “An in vitro investigation into the physical durability of dental composites”, Ph.D. Thesis, Katholieke Universiteit te Leuven, Belgium.

[140] Colo, S. M., Hedman K., and Rudolph, B. K. S., "Rheological instrumentation for the characterization of polymers", American Laboratory, 1997, pp. 16-18.

[141] Saber-Sheikh, K., Clarke, R. L., and Braden, M., "Viscoelastic properties of some soft lining materials. I--Effect of temperature", Biomaterials, Vol. 20, No. 9, 1999, pp. 817-822.

[142] Colo, S. M., Hedman K., and Rudolph, B. K. S., "Rheological instrumentation for the characterization of polymers", American Laboratory, 1997, pp. 16-18.

[143] Jacobsen, P. H. and Darr, A. H., "Static and dynamic moduli of composite restorative materials", J. Oral. Rehabil., Vol. 24, No. 4, 1997, pp. 265-273.

[144] Yang, J. M., Li, H. M., Yang, M. C., and Shih, C. H., "Characterization of acrylic bone cement using dynamic mechanical analysis", J. Biomed. Mater. Res., Vol. 48, No. 1, 1999, pp. 52-60.

[145] Bates, J. F., Stafford, G. D., and Harrison, A., "Masticatory function - a review of the literature. III. Masticatory performance and efficiency", J Oral Rehabil, Vol. 3, No. 1, 1976, pp. 57-67

[146] Waters, M., Jagger, R., Polyzois, G., and Williams, K., "Dynamic mechanical thermal analysis of maxillofacial elastomers", J Prosthet Dent, Vol. 78, No. 5, 1997, pp. 501-505.

[147] Nahm S., "Use of dynamic mechanical analysis in thermoset resin development (for composite applications", Composites 2001 Convention and Trader Show, Tampa, Florida, USA.

[148] Harris, J. S., Jacobsen, P. H., and O'Doherty, D. M., "The effect of curing light intensity and test temperature on the dynamic mechanical properties of two polymer composites", J. Oral Rehabil., Vol. 26, No. 8, 1999, pp. 635-639.

[149] Tamareselvy, K. and Rueggeberg, F. A., "Dynamic mechanical analysis of two crosslinked copolymer systems", Dent. Mater., Vol. 10, No. 5, 1994, pp. 290- 297.

[150] Waters, M., Jagger, R., Williams, K., and Jerolimov, V., "Dynamic mechanical thermal analysis of denture soft lining materials", Biomaterials, Vol. 17, No. 16, 1996, pp. 1627-1630

[151] Saber-Sheikh, K., Clarke, R. L., and Braden, M., "Viscoelastic properties of some soft lining materials. I--Effect of temperature", Biomaterials, Vol. 20, No. 9, 1999, pp. 817-822.

[152] M. Kutz, Handbook of Materials Selection. John Wiley & Sons. USA (2002).

[153] P. K. Vallittu, V. Miettinen, P. Alakuijala, Dent. Mater., 11 (1995) 338.

[154] A. A. Del Bel Cury, R. N. Rached, S. M. Ganzarolli, J. Oral. Rehabil,. 28 (2001) 433.

[155] Nakamura, T. Kokubo, Y. Kitamura, J. Biomed. Mater. Res., 59 (2002) 225.

[156] H. Ying-Gev, S. Chun-Hsiung, J. Biomed. Mater. Res., 38 (1997) 143.

[157] J. A. Bartoloni, D. F. Murchison, D. T. Wofford, N. Sarkar, J. Oral Rehabil., 27 (2000) 488.

[158] F. Pervin, Y. Zhou, V. Rangari, S. Jeelani, Mat. Sci. Eng., A 405 (2005) 246.

[159] T. Adachi, M. Osaki, W. Araki, S. Kwon, Acta Mater., 56 (2008) 2101.

[160] H. Al -Turaif, Prog. Org. Coat., 38 (2000) 43.

[161] A. Omrani, L. Simon, A. Rostami, Chem. Phys., 114 (2009) 145.

[162] B. Ahmadi, M. Kassiriha, K. Khodabakhshi, E. Mafi, Prog. Org. Coat., 60 (2007) 99.

[163] P. M. Ajayan, P. V. Braun, L. S. Schadler, Nanocomposite Science and Technology, Wiley-VCH, Weinheim, Germany (2004) 77.

[164] M. Hussain, A. Nakahira, K. Niihara, Mater. Lett., 26 (1996) 185.

[165] D. Stojanovic, A. Orlovic, S. Markovic, V. Radmilovic, P. Uskokovic, R. Aleksic, J. Mater. Sci., 44 (2009) 6223.

[166] T. E. Motaung, A. S. Luyt, F. Bondioli, M. Messori, M. L. Saladino, A. Spinella, G. Nasillo, E. Caponetti, Polym. Degrad. Stabil., 97 (2012) 1325.

[167] H. Wang, P. Xu, W. Zhong, L. Shen, Q. Du, Polym. Degrad. Stabil., 87 (2005) 319.

[168] A. Omrani, L. C. Simon, A. A. Rostami, Mater. Chemi. Phys., 114 (2009) 145.

[169] A. Allahverdi, M. Ehsani, H. Janpour, S. Ahmadi, Progr. Org. Coat., 75 (2012) 543.

[170] B. Wetzel, P. Rosso, F. Haupert, K. Friedrich, Eng. Fract. Mech., 73 (2006) 2375.

[171] A. Chatterjee, M. S. Islam. Mater. Sci. Eng. A, 487 (2008) 574.

[172] T. Mahrholz, J. Stängle, M. Sinapius, Compos. Part A, 40 (2009) 235.

[173] M. S. Goyat, S. Ray, P. K. Ghosh, Compos. Part A – Appl. S., 42 (2011) 1421.

[174] X. Fu, D. Huck, L. Makein, B. Armstrong, U. Willen, T. Freeman, Particuology, 10 (2012) 203.

[175] J. Mellmann, T. Hoffmann, C. Fürll, Powd. Tech., 249 (2013) 269.

[176] K. Nakane, N. Shimada, T. Ogihara, N. Ogata, S. Yamaguchi, Formation of TiO_2 nanotubes by thermal decomposition of poly(vinyl alcohol)-titanium alkoxide hybrid nanofibers, J. Mater. Sci., 42 (2007) 4031–4035.

[177] S. Ramakrishna, K. Fujihara, W.E Teo, T.C. Lim & Z.Ma, Introduction to Electrospinning and Nanofibers, World Scientific, Singapore, 2005.

[178] Fabrication of patterned nanofibrous mats using direct-write electrospinning, J. Lee, S.Y. Lee, J. Jang, Y.H. Jeong, D.-W. Cho, Fabrication of patterned nanofibrous mats using direct-write electrospinning, Langmuir, 28 (2012) 7267–7275.

[179] D.. Stojanovic, A. Orlovic, S. Markovic, V. Radmilovic, P.S. Uskokovic, R. Aleksic, Nanosilica/PMMA composites obtained by the modification of silica nanoparticles in a supercritical carbon dioxide–ethanol mixture, J. Mater. Sci., 44 (2009) 6223–6232.

[180] J. Lemic, M. Tomaševic-Canovic, M. Djuricic, T. Stanic, Surface modification of sepiolite with quaternary amines, J. Colloid. Interf. Sci., 292 (2005) 11–19.

[181] G. Tartaglione, D. Tabuani, G. Camino, Thermal and morphological characterisation of organically modified sepiolite, Micropor. Mesopor. Mat., 107 (2008) 161–168.

[182] V. Marjanović, S. Lazarević, I. Janković-Častvan, B. Potkonjak, Đ. Janaćković, R. Petrović, Chromium (VI) removal from aqueous solutions using mercaptosilane functionalized sepiolites, Chem. Eng. J., 166 (2011)198–206.

[183] X. Liang, Y. Xua, G. Sun, L. Wang, Y. Sun, Y. Sun, X. Qin, Preparation and characterization of mercapto functionalized sepiolite and their application for sorption of lead and cadmium, Chem. Eng. J., 174 (2011) 436–444.

[184] N. García, J. Guzmán, E. Benito, A. Esteban-Cubillo, E. Aguilar, J. Santarén, P. Tiemblo, Surface modification of sepiolite in aqueous gels by using methoxysilanes and its impact on the nanofiber dispersion ability, Langmuir, 27 (2011) 3952–3959.

[185] X.C. Zhang, Y.Z. Chen, J. Yu, Z.X. Guo, Thermoplastic polyurethane/silica nanocomposite fibers by electrospinning, J. Polym. Sci. Pol. Phys., 49 (2011) 1683–1689.

[186] P. Milanović, M. Dimitrijević, R. Jančić Heinemann, J. Rogan, D.B. Stojanović, A. Kojović, R. Aleksić, Preparation of low cost alumina nanofibers via electrospinning of aluminium chloride hydroxide/poly (vinyl alcohol) solution, Ceram. Int., 39 (2013) 2131–2134.

[187] H. Yu, J. Guo, S. Zhu, Y. Li, Q. Zhang, M. Zhu, Preparation of continuous alumina nanofibers via electrospinning of PAN/DMF solution, Mater. Lett., 74 (2012) 247–249

[188] S. Imaizumi, H. Matsumoto, Y. Konosu, K. Tsuboi, M. Minagawa, A. Tanioka, K. Koziol, A. Windle,. Top-down process based on electrospinning, twisting, and heating for producing one-dimensional carbon nanotube assembly, ACS Appl. Mater. Inter., 3 (2011) 469–475.

[189] K. Nakane, N. Shimada, T. Ogihara, N. Ogata, S. Yamaguchi, Formation of TiO_2 nanotubes by thermal decomposition of poly(vinyl alcohol)-titanium alkoxide hybrid nanofibers, J. Mater. Sci., 42 (2007) 4031–4035.

[190] Y. Ji, B. Li, S. Ge, J.C. Sokolov, M.H. Rafailovich, Structure and nanomechanical characterization of electrospun PS/clay nanocomposite fibers, Langmuir, 22 (2006)1321–1328.

[191] D. Lubasova and L. Martinova, Controlled morphology of porous polyvinyl butyral

nanofibers, Journal of Nanomaterials, vol. 2011, Article ID 292516, 6 pages, 2011.

doi:10.1155/2011/292516.

[192] H. Chen, M. Zheng, H. Sun, Q. Jia, Characterization and properties of sepiolite/polyurethane nanocomposites, Mat. Sci. Eng. A-Struct., 445–446 (2007) 725–730.

[193] L. Lanotte, C. Bilotti, L. Sabetta, G. Tomaiuolo, S. Guido, Dispersion of sepiolite rods in nanofibers by electrospinning, Polymer, 54 (2013) 1295–1297.

[194] Y.P. Zheng, J.X. Zhang, L. Lan, P.Y. Yu, Sepiolite nanofluids with liquid-like behavior, Appl. Surf. Sci., 57 (2011) 6171–6174

[195]S. Zahed, S.S. Naser, The role of Na-montmorillonite on thermal characteristics and morphology of electrospun PAN nanofibers, Fiber. Polym. ,11 (2010) 695–699.

[196] W. Stark, M. Jaunich, Investigation of ethylene/vinyl acetate copolymer (EVA) by thermal analysis DSC and DMA, Polym. Test., 30 (2011) 236–242.

[197] M. Jawaid, H.P.S. Abdul Khalil, O.S. Alattas, Woven hybrid biocomposites: dynamic mechanical and thermal properties, Compos. Part A-Appl. S., 43 (2012) 288–293.

[198] P.G. Royall, C.-Y. Huang, S.-W.J. Tang, J. Duncan, G. Van de Velde, M.B. Brown, The development of DMA for the detection of amorphous content in pharmaceutical powdered materials, Int. J. Pharm., 301 (2005) 181–191.

[199] A. Pinheiro, J.F. Mano, Study of the glass transition on viscous-forming and powder materials using dynamic mechanical analysis, Polym. Test., 28 (2009) 89–95.

[200] M.G. Abiad, O.H. Campanella, M.T. Carvajal, Assessment of thermal transitions by dynamic mechanical analysis (DMA) using a novel disposable powder holder, Pharmaceutics, 2 (2010) 78–90.

[201]A.M. Torki, D.B. Stojanović, I.D. Živković, A. Marinković, S.D. Škapin, P.S. Uskoković, R.R. Aleksić, The viscoelastic properties of modified thermoplastic impregnated multiaxial aramid fabrics, Polym. Compos., 33 (2012) 158–168.